Dynamical Modelling of the effect of Insulin-like Growth Factor 1 on Human Cell Growth

A thesis presented in fulfilment of the requirements for the degree of

Master of Science
in Mathematics
at Massey University, Albany, New Zealand

Gemma Phillips

2013

Abstract

Insulin-like Growth Factor-1 (IGF-1) plays a vital role in human growth and development. Interactions with IGF-1 receptors and IGF-1 binding proteins (IGFBPs) regulate IGF-1 function. Boroujerdi et al. (1997) published a mathematical model describing dynamic regulation of IGF-1. We extended the Boroujerdi et al. (1997) model to evaluate the role of cyclic Gly-Pro (CGP) in dynamic regulation of IGF-1 function. Recent research from the Liggins Institute suggests that a metabolite of IGF-1, CGP, may have a role in regulating IGF-1 homeostasis, possibly through competitive binding to IGFBPs.

The goal of the research was to understand the kinetics of IGF-1, IGFBPs and CGP, along with their interactions with IGF-1 receptors. This goal and an understanding of how the kinetics mediate IGF-1 function was achieved through consideration of the nonlinear dynamics of the physiology using a modelling approach.

The resulting models were directly focused on three central theories. The first is that CGP can either inhibit, stimulate or maintain IGF-1 function based on the extent of receptor binding. The other theories are that CGP regulates IGF-1 through competitive binding to IGFBPs and that CGP does not directly interact with the IGF-1 receptors.

Four *in vitro* models were developed and fitted to experimental data. These included two implicit models which relied on two feedback terms in the equations. The second model was an alteration of the first to produce a reduction in cell number levels for high doses of CGP added to the system. The other two models were explicit models, the first of which could not express the IGF-1 dynamics well (it showed no CGP response). Although the models incorporated these theories, there are other mechanisms influencing the system which will have an effect on the data. Therefore the fourth model was introduced as a simplified version of the third. This was aimed at resembling cell culture situations more closely and was designed to have the receptor bound IGF-1 dependent on IGF-1 and CGP production rates.

The models can be used to predict cellular response in an *in vitro* situation, or as a basis for further research in this field.

Acknowledgements

I would like to thank my supervisors, Professor Graeme Wake and Dr Paul Shorten for their constant advice, encouragement and support throughout this project.

Prof. Wake and Dr. Shorten were funded to supervise this thesis via the Gravida National Centre for Growth and Development.

Thank you to Dr Jian Guan (Head Biologist at Liggins Institute) for her feedback, guidance and biological explanations.

In addition I would like to express my gratitude towards Mr Tony Pleasants and the Norman F Barry Foundation, Wake's Scientific Consulting and Dr Guan the head of Neuroscience from Liggins Institute (Ministry of Business and Employment, MIBIE) for funding this project.

Lastly I would like to express my appreciation to my family, Alistair Watt, and his family for their understanding, love and support.

List of Figures

List of Tables

Abbreviations

BSA	Bovine serum albumin
CGP	Cyclo-glycyl-proline or Cyclic Gly-Pro
DE	Differential equation
DKP	Diketopiperazine
EDTA	Ethylenediaminetetraacetic acid
GPE	Glycine-proline-glutamate
IGF-1	Insulin-like Growth Factor 1
IGF-1R	Insulin-like Growth Factor 1 Receptor
IGFBP	Insulin-like Growth Factor Binding Proteins
kDa	Kilo Dalton (Dalton is a unit of mass based on molecular mass)
nM	nmol L^{-1}
ODE	Ordinary Differential Equation
PBS	Phosphate Buffered Solution
PDE	Partial Differential Equation
RK4	Runge Kutta fourth order method
SDS	Sodium Dodecyl Sulfate
SSE	Sum of Squares of Errors
WST-1	Water Soluble Tetrazolium Salt-1

Contents

1 Introduction

The aim of this study is to describe the dynamic relationship between Insulin-like Growth Factor-1 (IGF-1), Insulin-like Growth Factor Binding Proteins (IGFBPs), Insulin-like Growth Factor-1 receptors and the Cyclic Gly-Pro complex (CGP), a metabolite of IGF-1, using a modelling approach. The models extend previous work by Boroujerdi, Jones, Sonksen, and Russell-Jones (1997) and Boroujerdi, Sonksen, and Jones (1994), where they looked at investigating the IGF-1 pharmacokinetics after infusion of recombinant IGF-1.

The main goal is to extend these models to describe data found by Dr Jian Guan and her Liggins team. This involves creating a model to demonstrate the role CGP plays in the activation of feedback (both positive and negative) to the IGF-1 receptors and binding proteins.

Since IGF-1 cannot be administered to specific locations in the body and since treatment with IGF-1 can result in negative effects on the body, the goal is to establish CGP as a regulating control over IGF-1 homeostasis. This regulation occurs through competitive binding between CGP and IGF-1 for the binding proteins.

An important part of creating these models is using the nonlinear dynamics of the physiology to represent the kinetics of IGF-1, IGFBPs, and CGP mediating IGF-1 function. These kinetics include IGF-1 interactions with the IGF-1 receptors via IGFBP and CGP influences. Once the model is established, it can then be tested against an independent data set to assess it's accuracy. The models will be used to predict cellular response and explore IGF-1 dynamics.

1.1 Objective of this Study

In this study, we consider the regulating effects of CGP on IGF-1 actions in the body and in cell cultures. The ultimate goal is to create a model which more accurately accounts for trends in current data being collected on IGF-1 dynamics. We hypothesise CGP can be used to tightly regulate IGF-1 activity to avoid the pathological states which result from excessive or insufficient levels of IGF-1 in the body.

1.2 Thesis Outline

Chapter one introduces the research and the goals to the reader. Chapter two explores the biological terms and roles. It explains how the data was collected (for both the *in vivo* and *in vitro* experiments) and the anticipated outcomes of the project. Chapter three gives an overview of some previous research on IGF-1 activity. Chapter four extends on from this research to include the previously omitted variable (CGP), and explores how this affects the system. Chapter five introduces the first two *in vitro* models: both implicit models use two nonlinear feedback terms to represent CGP/IGF-1 interactions. The final two *in vitro* models are explored in chapter six: these are explicit models showing the competitive binding between CGP/IGFBPs and IGF-1/IGFBPs. Required mathematical background knowledge can be found in the appendix along with bifurcation diagrams and previous model parameters and simulations.

2 Biological Background:

2.1 Introduction

Insulin-like Growth Factor-1 (IGF-1) plays a crucial role in growth and development. A deficiency in IGF-1 can cause metabolic disorders, delayed wound healing, growth retardation and developmental disorders. Since IGF-1 plays such an important role in regulating growth and development in normal tissues there has been links to raised IGF-1 levels being associated with certain pathological states including tumours (Werner, 2000). Highly elevated IGF-1 activity is linked to developmental cancer and autoimmune diseases. Treatment by either administering IGF-1 or blocking IGF-1 function can have a negative influence on normal tissue development and wound healing whilst potentially promoting pathological growth.

The effective route of administration is also problematic given the large size of IGF-1. Even though the restricted central uptake of IGF-1 is of concern, the metabolic and mitogenic effects of IGF-1 are even more troubling when treating neurological disorders (Guan & Gluckman, 2009).

The biological function of IGF-1 is mediated through the activation of IGF-1 receptors, located on the surface of human cells. IGF-1 receptors have been found in many dif-

ferent tissues and cells indicating that there are a vast amount of variety in the effects IGF-1 can have in the body (Werner, 2000). The structure of the IGF-1 receptor consists of two alpha subunits and two beta subunits (see Figure 1 below). The two alpha subunits are extracellular, outside the cell, which is where the ligand binding happens. The two beta subunits contain the tyrosine kinase enzymes which function as the on or off switches in certain cellular functions. These are important for communicating signals within the cell and regulating cellular activity. IGF-1 binding to these receptors causes a modification in the shape of the protein which is followed by one receptor subunit turning on or phosphorylating the other subunit (trans-autophosphorylation) thus changing the function and activity of IGF-1. The IGF-1 and its receptor binding is concentration (dose) related. The physiological role of IGF-1 is determined by the arrangement and concentration of the IGF-1 receptors. Studies have shown that an increased expression of IGF-1 receptors is correlated with tumours, hypertrophy, healing and wound repair, (Werner, 2000).

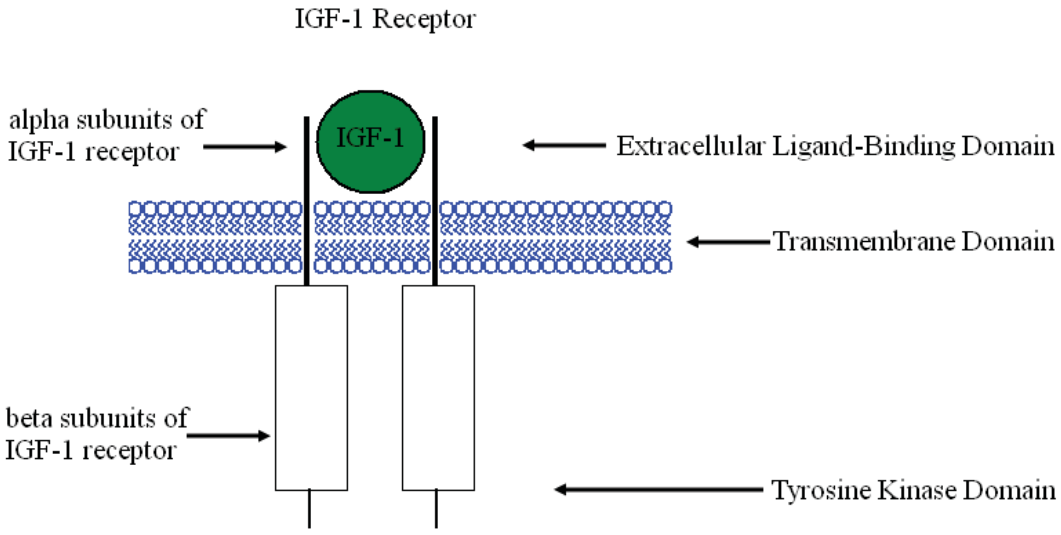

Figure 1: Schematic diagram of the IGF-1 receptor. The green circle represents IGF-1 attaching to the receptor outside the cell via the two alpha subunits (black thick lines). The blue symbols represent the cell wall. The two rectangles represent the beta subunits which contain the tyrosine kinase enzymes (on or off switches).

The majority of IGF-1 is produced in the liver and secreted into the blood circulation. Most of the circulating IGF-1 in the blood binds to Insulin-like Growth Factor Binding Proteins (IGFBPs), of which IGFBP-3 (150kDa molecular weight) makes up more than

75%. These binding proteins regulate IGF-1 binding to the receptors, and control the IGF-1 intended cell action by inducing or inhibiting the IGF-1 cell growth responses and metabolic actions (Clemmons, 1991). The unbound IGF-1 (free IGF-1) is enzymatically sensitive and can be rapidly metabolised in blood. In contrast, the binding of IGFBP-3 prevents IGF-1 degradation and prolongs the half life of IGF-1 while it circulates in the blood (Humbel, 1991). However, only free IGF-1 can bind and activate the IGF-1 receptors, thus IGFBP-3 also prevents IGF-1 from activating IGF-1 receptors. IGF-1 will be internalised after activating the receptors and then metabolised. One of the products of IGF-1 metabolism is Cyclic Glycine-Proline (CGP), which is enzymatically resistant with a stable half life before being eliminated from blood circulation. There is no evidence that CGP can directly interact with IGF-1 receptors.

As is the case for the IGF-1 receptors, the IGFBPs play an important role in controlling the expression of IGF-1. Their specific roles have been shown to be; transporting IGF-1 in blood, regulating the amount of IGF-1 being transferred, transporting IGF-1 to specific cells and tissues and regulating the binding of IGF-1 to its receptor. The affinity of IGF-1 for IGFBPs is much higher than it is for the receptors, therefore the way the binding proteins inhibit IGF-1 bioactivity is through inhibiting binding to the receptors (Moon, 2011).

IGF-1 naturally metabolises into des(1-3)IGF-1 and gly-pro-glut (GPE), a tri-peptide from the amino acid end of the IGF-1 polypeptide chain (N-terminal). GPE is rapidly further metabolised and forms the Cyclic Gly Pro complex (CGP). All three peptides (CGP, GPE and des(1-3)IGF-1) are therefore bioactive metabolites of IGF-1. "Glycine proline glutamate (GPE) is naturally cleaved from the IGF-1 N terminal" (Guan et al., 2007). GPE does not bind to the IGF-1 receptor nor does it affect the binding of IGF-1 or des(1-3)IGF-1 to this receptor. CGP is an "endogenous diketopiperazine (DKP)" meaning it is a cyclic compound formed from partial dehydrolysis of proteins growing from or on the inside of an organism. As it is not enzymatically stable, GPE could be an inter-median between IGF-1 and CGP.

To evaluate the mechanism of CGP Dr Guan's group has demonstrated the role of CGP in regulating IGF-1 function through either negative or positive pathways, in which CGP competes with IGF-1 in binding to IGFBP-3. Dr Jian Guan, the head of the research group at the Liggins Institute, proposes that CGP can decrease elevated levels of IGF-1 and increase low levels. The reason for this is believed to be the

competitive binding between CGP and IGF-1 with binding proteins. When there are low levels of CGP in the system, less binding proteins are bound by CGP and more are bound by IGF-1, this results in less free IGF-1 available to bind to the receptors. Since the majority of IGF-1 is inactive in the body we have less of a response from the receptors. When there are high levels of CGP, more of it will bind with the available binding proteins and, so there will be less of these to bind with IGF-1. This results in more free IGF-1 available to bind to receptors where they can be internalised. This hypothesis that competitive binding occurs between CGP and IGF-1 will be tested in the models in this research.

2.2 Data Collection Methods

To create a mathematical model demonstrating the dynamic interactions of IGF-1, IGFBPs and CGP interacting with IGF-1 receptors, previous research was reviewed. A seven compartment model by Boroujerdi et al. (1997) and a two compartment model by Mizuno et al. (2001) were examined to gain insight into the biological interactions. From here a new *in vivo* model (within the body) was created based on these previous models and was adapted to form four new *in vitro* models (outside the body) which fit with the hypothesis found from current *in vitro* research. The current data indicates competitive binding is present and that an omitted hormone (CGP) from previous models is crucial in the IGF-1 dynamical model. Once the models have been formed, the parameters can then be calibrated using the data. Two different methods of data collection were used: one involving infusion of recombinant IGF-1 into the body (*in vivo* experiments) and the other involving cell cultures (*in vitro* experiments). Both these data collection methods are described below.

2.2.1 *In vivo* data collection methods

The *in vivo* experiments carried out by Boroujerdi et al. (1997) used radioactive tracer bolus experiments to estimate the metabolic clearance rate of IGF-1 in the body. The experiment required a 3 hour infusion of recombinant IGF-1 (with radioactive tracer) intravenously through an antecubital vein on four humans. The blood was taken from a heated peripheral hand vein and the blood glucose was clamped at 5nM by variable infusion of 20% dextrose. Plasma fractionation (separating the components of the blood plasma), required the addition of ethanol-hydrochloric acid to the plasma pool.

Radioimmunoassay was used, after plasma fractionation in the molecular mass regions of 7 (free IGF-I), 50, and 150kDa to measure the mass of each complex. The 150kDa pool represents IGFBP-3 or IGF-1 bound to IGFBP-3, and the 50kDa pool represents the other IGFBPs or IGF-1 bound to the other IGFBPs. Each mass was computed in their assumed plasma volume (Boroujerdi et al., 1997).

The parameter estimates used in Mizuno et al. (2001) were found from data involving the infusion of recombinant IGF-1 into 30 healthy male volunteers. There were five treatment types these included: 5 μg h^{-1}kg^{-1} for 3 hours, 10 μg h^{-1}kg^{-1} for 3 hours, 20 μg h^{-1}kg^{-1} for 3 hours or 20 μg h^{-1}kg^{-1} for 6 hours. Blood samples were collected and the total blood plasma concentration of IGF-1 was measured by radioimmunoassay after using acid and ethanol extraction to separate the blood plasma from the binding proteins. The total amount of IGF-1 and the amount of free IGF-1 were both measured for this model.

2.2.2 *In vitro* data collection methods

The *in vitro* experiments used for parameter calibration were carried out at the Liggins Institute and involved the following processes. Cells are washed with Phosphate Buffered Solution (PBS) and then trypsin is added to the culture. Trypsin is a substance used to break proteins down into smaller peptides such that the smaller peptides can be hydrolysed into amino acids. The flasks containing these substances are then left to incubate for 3-5 minutes or until most of the cells have detached. After this the cells are washed and the contents are transferred to a sterile conical tube, which is then centrifuged at 1000 rpm for 5 min, to separate the immiscible liquids. Once the supernatant (liquid lying above the solid residue) is removed, the compressed substance remaining is then dispersed by gently tapping before being resuspended in complete medium. The cell culture work is performed within a laminar flow hood under sterile conditions (Moon, 2011). "The flasks and well plates are pre-coated with 0.1% gelatine solution. Each well is a 96-well plate which receives approximately 100 microliters of 0.1% gelatine. The gelatine solution is left to incubate at 37 °C for at least 30 minutes before being removed" (p. 45 Moon, 2011).

There are two common methods for testing the material for the release of toxic chemicals in large enough quantities to kill cells (cell culture assays). The first involves using the water soluble tetrazolium salt-1 (WST-1) reagent, and the second uses Alamar Blue.

WST-1 requires cells to be seeded (often in 96-well plates at 4000 cells per well with six replicates per sample) and left overnight in the complete medium. The medium is removed the next day and the wells are washed (with PBS). Then GPE/CGP or IGF-I in serum-free medium can be added. It is then left to incubate for between one and three days before the WST-1 is added. The absorbance is measured at 440nm and 650nm wavelengths and then analysed (Moon, 2011).

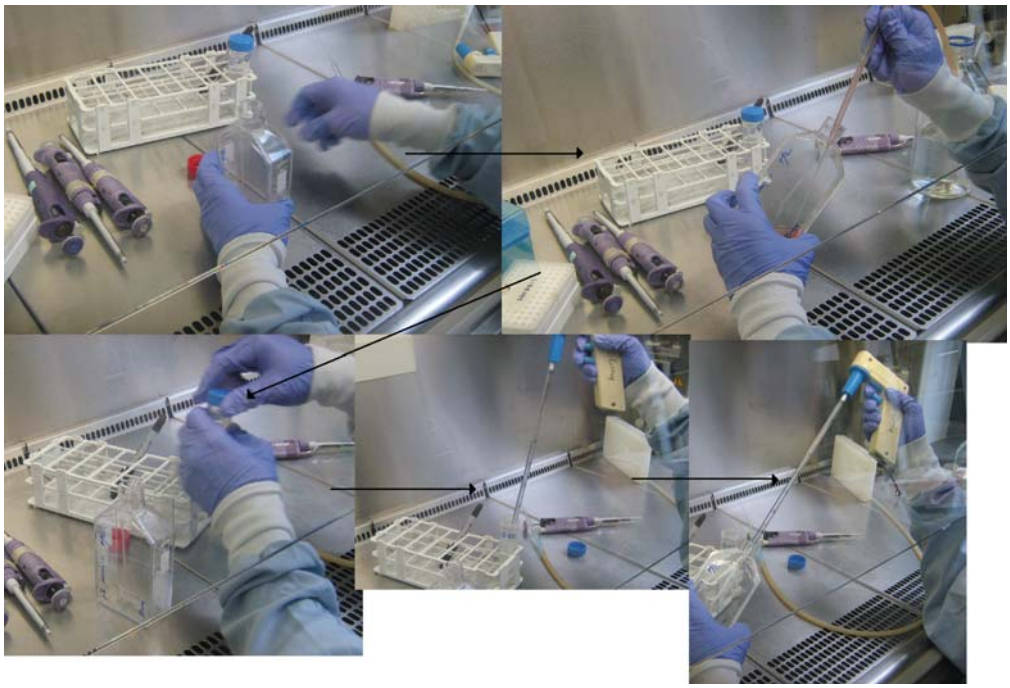

Figure 2: Lab pictures of Steve Moon at Liggins Institute, washing the cells

The Alamar Blue is used to verify the results obtained using WST-1. In this case the Alamar Blue is added to each well and incubated for 4 hours before measuring the 530nm excitation and 590nm emission. This Alamar Blue solution dyes all cells a blue colour so they can be seen easily under the microscope, the dead cells lose their colour so you can distinguish between the living and dead cells (Moon, 2011). Another way of confirming results from these methods is through a total cell count assay.

Another important procedure used for detecting proteins in samples of tissue is the Western blot. This separates proteins based on their size and charge, through gel electrophoresis. The sample is prepared in the manner described above. The wells are put into the gel, which has one lane reserved for a marker mixture (proteins with defined

molecular weights all of which are stained into coloured bands to distinguish them). Voltage is applied along the gel causing the proteins to become emerged with the negatively charged sodium dodecyl sulfate (SDS), so that they move towards the positively charged electrode. There is a mesh of gel the proteins need to travel through, this means that smaller proteins will move through faster. Hence the proteins are separated by their size from the different speeds the proteins move through the mesh.

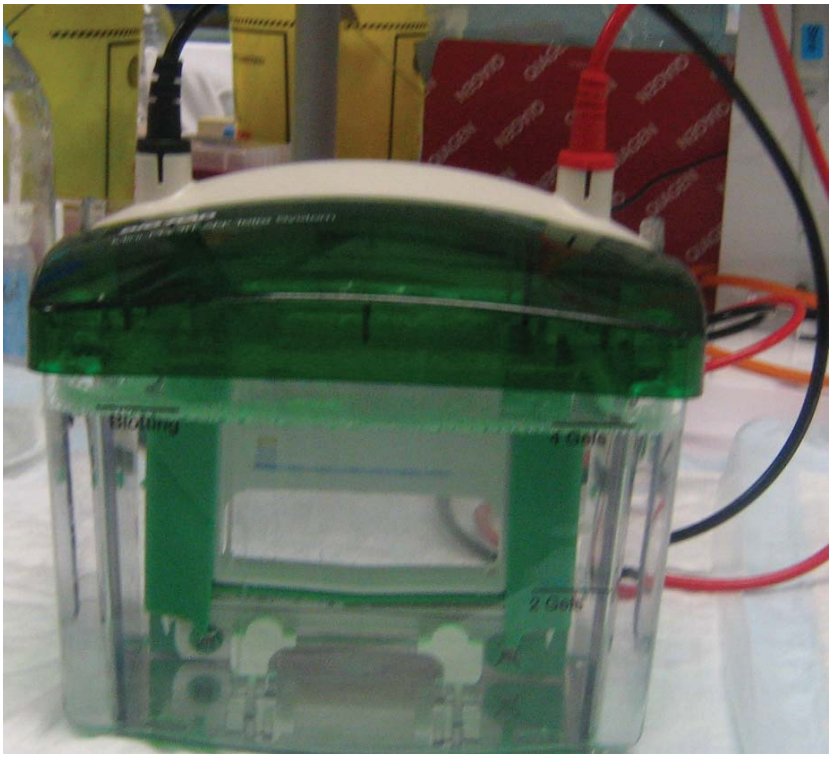

Figure 3: Mini-PROTEAN Tetra system used for western blotting

2.3 Types of Data Collected

Although there are *in vivo* experiments currently in progress involving the study of rats with strokes and tumours, the *in vivo* parameters are estimated using similarities to the parameters in the Boroujerdi et al. (1997) model. The *in vitro* data used was collected by Dr Jian Guan and her team (Liggins Institute) in a manner similar to the above explanation (see section 1.2). This data measured the absorbance percentages, which we assume to be proportional to the cell number used in the *in vitro* models. Cell culture data collected included control experiments, IGF-1 only treatments, CGP only treatments, combination of IGF-1 and CGP treatments and antibody treatments

(reduced IGFBPs available). The antibody treatment data was kept aside for validation of the model. See Tables 1-2 for the types of data used.

Type of Treatment	Level							
IGF only treatment (ng/ml):	0	1	10	20	50	100		
CGP only treatment (nM):	0	1	5	10	20	50	100	
Combination one treatment:								
IGF (ng/ml), note 10ng/ml=1.31nM):	10	10	10	10	10	10	10	10
CGP (nM):	0	0	1	5	10	20	50	100
Combination two treatment:								
IGF (ng/ml), note 50ng/ml=6.54nM):	50	50	50	50	50	50	50	50
CGP (nM):	0	0	1	5	10	20	50	100

Table 1: The four treatment types used in parameter calibration. Each experiment was run for six days and had six replicates (data not shown).

Type of Treatment	Level				
No Antibody (combination one):					
IGF(nM):	0	1	1	1	1
CGP (nM):	0	0	1	10	100
Antibody treatment (combination two):					
IGF(nM):	0	1	1	1	1
CGP (nM):	0	0	1	10	100

Table 2: The two treatment types used in validation (antibody treatment). The treatments were all run for six days. In the no antibody experiment the first two levels had six replications each and the last three levels had three replications each. The antibody treatment had six replications for the first level and three replications for each of the last four levels (data not shown).

The culture medium was completely changed before each new treatment to avoid any accumulating effects. *In vitro* solutions have proteases (enzymes which break down proteins and can convert IGF-1 to CGP) in them but only a minimal amount, we can therefore assume these are overridden by the treatment and can be ignored.

3 Previous Research:

3.1 Introduction

Previous IGF-1 research by Boroujerdi et al. (1997) and Mizuno et al. (2001) is explored in this chapter. The Boroujerdi et al. (1997) model consisted of seven compartments representing IGF-1 interacting with IGFBPs and receptors in the body. They used *in vivo* experiments to calculate parameter values for their mathematical model and compared the resulting curves with the data. The Mizuno et al. (2001) model consisted of two concentration compartments, free IGF-1 and IGF-1 bound to IGFBPs in the body. They also used *in vivo* experiments for parameter estimation and compared the resulting model curves to the data. For both models the results have been reproduced and further analysis has been done on the Boroujerdi et al (1997) model.

3.2 Boroujerdi et al. (1997) Model

The model in this project is an extension of that in Boroujerdi et al. (1997). They created a model to simulate IGF-1 interactions within the body by looking at the effects of infusing recombinant (synthetic) IGF-1 into human subjects. The research was aimed at showing that the binding proteins were what influenced IGF-1 via retaining IGF-1 in the vascular compartment or inhibiting their actions. The data used was obtained by infusing 4 healthy, adult, male volunteers for 3 hours at a rate of 43.7 pmol min^{-1} kg^{-1}, with recombinant IGF-1. Insulin-like Growth Factor Binding Proteins (IGFBPs) 1,2,4,5 and 6 were grouped into one compartment while IGFBP-3 had a separate compartment since this protein has the largest concentration and is the most influential of the binding proteins on IGF-1. The molecular mass of free IGF-1 is 7kDa and IGFBP-3 is taken as 150kDa. The remaining binding proteins have ranging masses from 24 to 43kDa and are taken to be 50kDa for this experiment.

Variable	Definition
q_1	Molar mass of IGFBPs 1,2,4,5,6 50kDa (nmol)
q_2	Molar mass of free IGF-1 in the plasma (nmol)
q_3	Molar mass of IGF-1/IGFBPs 1,2,4,5,6, 50kDa (nmol)
q_4	Molar mass of IGFBP 3, 150kDa (nmol)
q_5	Molar mass of IGF-1/IGFBP 3, 150kDa (nmol)
q_6	Molar mass of IGF-1 in interstitial fluid volume (nmol)
q_7	Receptor bound IGF-1 (nmol)

Table 3: Variable definitions reproduced from Boroujerdi et al. (1997). IGFBP-3 (in free and bound form) has a molecular weight of 150kDa, IGFBPs 1-6 excluding 3 are grouped together with a molecular weight of 50kDa (in free and bound form).

Parameter	Definition
k_{ij}	Rate constant, to compartment i from j, where zero is outside the system (min^{-1})
k_{+1a}	Binding constant of IGFBPs 1,2,4,5,6, 50kDa (nmol^{-1} min^{-1})
k_{+1b}	Binding constant of IGFBP 3, 150kDa (nmol^{-1} min^{-1})
k_{-1a}	Dissociation rate constant of IGFBPs 1,2,4,5,6, 50kDa (min^{-1})
k_{-1b}	Dissociation rate constant of IGFBP 3, 150kDa (min^{-1})
R	IGF-1 receptor number (nmol)
R_a	IGF-1 production rate (nmol min^{-1})
$R_{a,1}$	IGFBPs, 50-kDa production rate of IGFBPs 1,2,4,5,6 (nmol min^{-1})
$R_{a,2}$	IGFBPs, 150-kDa production rate of IGFBP-3 (nmol min^{-1})
$Infu$	IGF-1 infusion rate (nmol min^{-1})

Table 4: Parameter definitions reproduced from Boroujerdi et al. (1997)

The model consisted of seven variables, the first five occur in the plasma and the last two in the interstitial fluid within the body (see Figure 4).

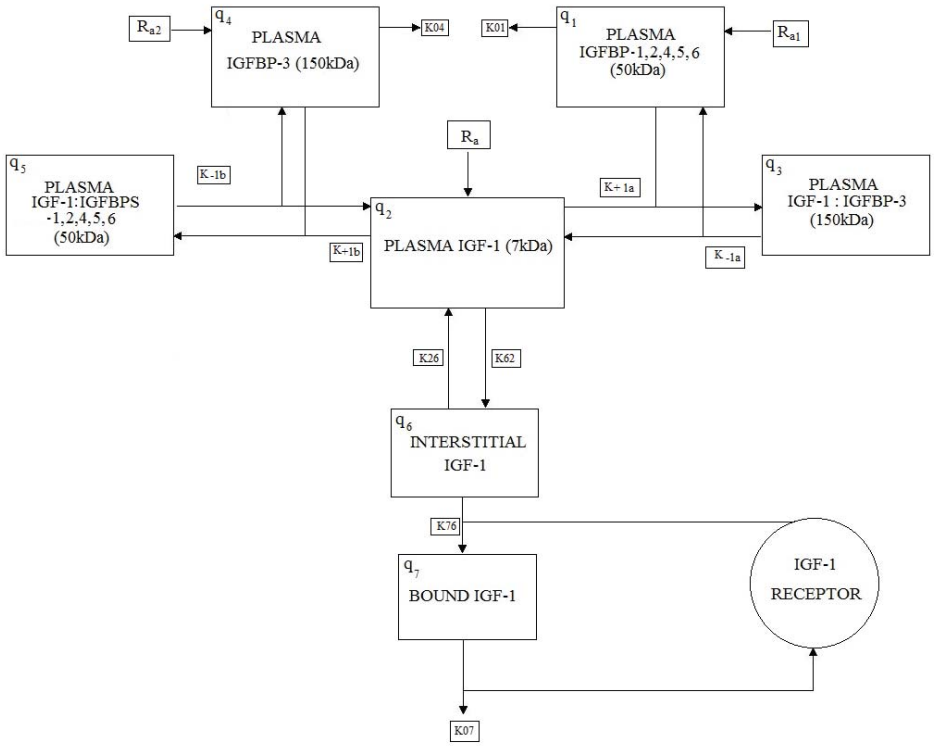

Figure 4: Schematic diagram of the seven compartments reprinted from Boroujerdi et al. (1997). Each box represents a compartment, and the arrows represent transport between compartments.

3.3 Boroujerdi et al. (1997) Equations

The differential equations Boroujerdi et al. (1997) used were:

$$\frac{dq_1}{dt} = -k_{01}q_1 - k_{+1a}q_1q_2 + k_{-1a}q_3 + R_{a,1} \tag{1}$$

$$\frac{dq_2}{dt} = -k_{+1a}q_1q_2 + k_{-1a}q_3 - k_{+1b}q_4q_2 + k_{-1b}q_5 - k_{62}q_2 + k_{26}q_6 + R_a + Infu \tag{2}$$

$$\frac{dq_3}{dt} = k_{+1a}q_1q_2 - k_{-1a}q_3 \tag{3}$$

$$\frac{dq_4}{dt} = -k_{04}q_4 - k_{+1b}q_4q_2 + k_{-1b}q_5 + R_{a,2} \tag{4}$$

$$\frac{dq_5}{dt} = k_{+1b}q_4q_2 - k_{-1b}q_5 \tag{5}$$

$$\frac{dq_6}{dt} = k_{62}q_2 - k_{26}q_6 - k_{76}q_6(1 - \frac{q_7}{R}) \tag{6}$$

$$\frac{dq_7}{dt} = k_{76}q_6(1 - \frac{q_7}{R}) - k_{07}q_7 \tag{7}$$

The majority of the equations are based on the law of mass action, however Equations 6 and 7 showed different interactions. Their simulations found that a nonlinear clearance rate for IGF-1 was necessary therefore a receptor-mediated clearance was included. Looking at differential Equations 6 and 7 we can see that for large receptor numbers (R), we have a negative effect on the interstitial IGF-1 (q_6) and a positive effect on the receptor bound IGF-1, q_7, from the $k_{76}q_6(1 - q_7/R)$ term. When we have a small receptor number the opposite occurs. When the receptor concentration is high more IGF-1 is moved from the interstitial IGF-1 (q_6) to the receptor bound form of IGF-1 (q_7). When there are fewer receptors there is less binding occurring (less q_7). This would indicate that the model uses the proportion of IGF-1 receptors to explain the clearance of IGF-1."Receptor mediated clearance adequately describes the reduction in metabolic clearance rate observed with increasing plasma free IGF-1 concentrations" (Boroujerdi et al., 1997, p. 438).

3.4 Results from the Boroujerdi et al. (1997) Model

To find an initial value for each variable there were a few assumptions made (Boroujerdi et al., 1997).

> "At steady state ($t0$), the initial condition for the binding model of IGF-1 with IGFBPs can only be set by providing an estimate of the total concentration of IGFBPs (nM) i.e. IGFBP plus IGF-1/IGFBP in a molecular band. The amount of measured IGF-1 in a molecular band at t0 is used to estimate IGF-1/IGFBP. The mean of IGFBP-3 estimates during the experiment is used as an estimate for the total IGFBP in the 150kDa band. During the IGF-1 infusion, the maximum of measured IGF-1 concentration (nM) in the 50kDa molecular band is used as an estimate for the initial concentration of total IGFBPs in that band (nM)" (p. 441).

The following formulae were used from the data in the table, at t0 (see Table 5):

q_3 = [%50kDa] [total (IGF-1) nM]

q_1= [mean of IGFBP]-[q_3 nM]

q_4= [%150kDa] [total (IGF-1) nM]

q_5= [maximal (IGF-1) in 50kDa nM]- [q_4 nM]

q_2= [%free] [total IGF-1 nM]

	Steady State			During IGF-I infusion		
Subj	%free	%50kDa	%150kDa	Total [IGF-I] nM	Max [IGF-I] in 50kDa nM	Mean IGFBP-3 nM
1	5.0	36.0	59.0	38.2	32	120
2	17.3	17.2	65.0	25.8	25	93
3	7.0	15.0	78.0	23.6	20	78
4	4.0	11.3	84.7	25.5	16	123

Table 5: "Distribution of IGF-I among IGFBPs at steady state and mean estimate of IGFBP-3 during IGF-I infusion" (Boroujerdi et al., 1997, p. 441).

Finally the q_6 and q_7, initial values were found by rearranging differential equations six and seven (Equations 6 and 7 respectively), using the quadratic formula to provide a value for one then substituting back in to find the other.

All the variables are however, worked out in nM (nmol L^{-1}), whereas the equation glossary states the $\boldsymbol{q}$ values used in the equations are in nmol, thus we multiply each $\boldsymbol{q}$ variable by V_2 (L) before plotting, where V_2 must first be converted into L by mul-

tiplying by the subject's weight and dividing by 1000. All solutions are converted into nM to express all variables in units of concentration instead of mass before plotting.

The subject one parameters and initial values from the Boroujerdi et al. (1997) article are shown in Table 6 and 7 (see Appendix A.1, Tables 35-37, for subjects 2-4 initial values and parameters).

Variable	Initial value	Converted To Correct Units
q_1	18.248 (nmol L^{-1})	64.74 (nmol)
q_2	1.910 (nmol L^{-1})	6.74 (nmol)
q_3	13.7520 (nmol L^{-1})	48.56 (nmol)
q_4	97.4620 (nmol L^{-1})	344.12 (nmol)
q_5	22.5380 (nmol L^{-1})	79.58 (nmol)
q_6	1.8487 (nmol L^{-1})	6.82 (nmol)
q_7	1.80167 (nmol L^{-1})	6.22 (nmol)

Table 6: Subject one initial values from Boroujerdi et al. (1997)

Parameter Name	Value	Converted To Correct Units
Infu (3hrs)	43.7 (pmol min^{-1} kg^{-1})	3.39986 (nmol min^{-1})
Weight	77.8 (kg)	77.8 (kg)
V_2	45.5 (ml kg^{-1})	3.501 (L)
V_6	150 (ml kg^{-1})	11.670 (L)
R	0.91 (nmol kg^{-1})	70.798 (nmol)
k_{01}	0.0058 (min^{-1})	0.0058 (min^{-1})
k_{04}	0.00144 (min^{-1})	0.00144 (min^{-1})
k_{07}	0.082 (min^{-1})	0.082 (min^{-1})
k_{76}	0.082 (min^{-1})	0.082 (min^{-1})
k_{52}	0.0374 (min^{-1})	0.0374 (min^{-1})
k_{32}	0.094 (min^{-1})	0.094 (min^{-1})
k_{62}	0.109 (min^{-1})	0.109 (min^{-1})
k_{26}	0.033 (min^{-1})	0.033 (min^{-1})
k_{+1a}	0.005151 ($nmol^{-1}$ min^{-1} L)	0.00146 ($nmol^{-1}$ min^{-1})
k_{+1b}	0.00384 ($nmol^{-1}$ min^{-1} L)	0.00109 ($nmol^{-1}$ min^{-1})
k_{-1a}	0.013056 (min^{-1})	0.0131 (min^{-1})
k_{-1b}	0.03169 (min^{-1})	0.0317 (min^{-1})
$R_{a,1}$	0.105838 (nmol min^{-1} L^{-1})	0.374 (nmol min^{-1})
$R_{a,2}$	0.140345 (nmol min^{-1} L^{-1})	0.496 (nmol min^{-1})
R_a	0.147345 (nmol min^{-1} L^{-1})	0.510 (nmol min^{-1})

Table 7: Subject one parameter values from Boroujerdi et al. (1997).

When the initial values in Table 6 and the parameter values in Table 7 are used we obtain simulations which are qualitatively the same to those in Boroujerdi et al. (1997).

Any error in the values may be due to rounding in the published parameter values or could be a result of the numerical integration method used to solve the equations. MATLAB's ode45 function, which is based on an explicit Runge-Kutta (4,5) formula, was used and the process was repeated using XPPaut (Runge-Kutta solver). "The models differential equations... are solved by numerical integration using the Runge-Kutta fourth order method with adjustable step size" (Boroujerdi et al., 1997, p. 440). Below are the graphs produced by Boroujerdi et al. (1997) for subject one (left), followed by the replicated graphs (right) using XPPaut (see Appendix B.1, Figures 55-56, for subjects 2-4).

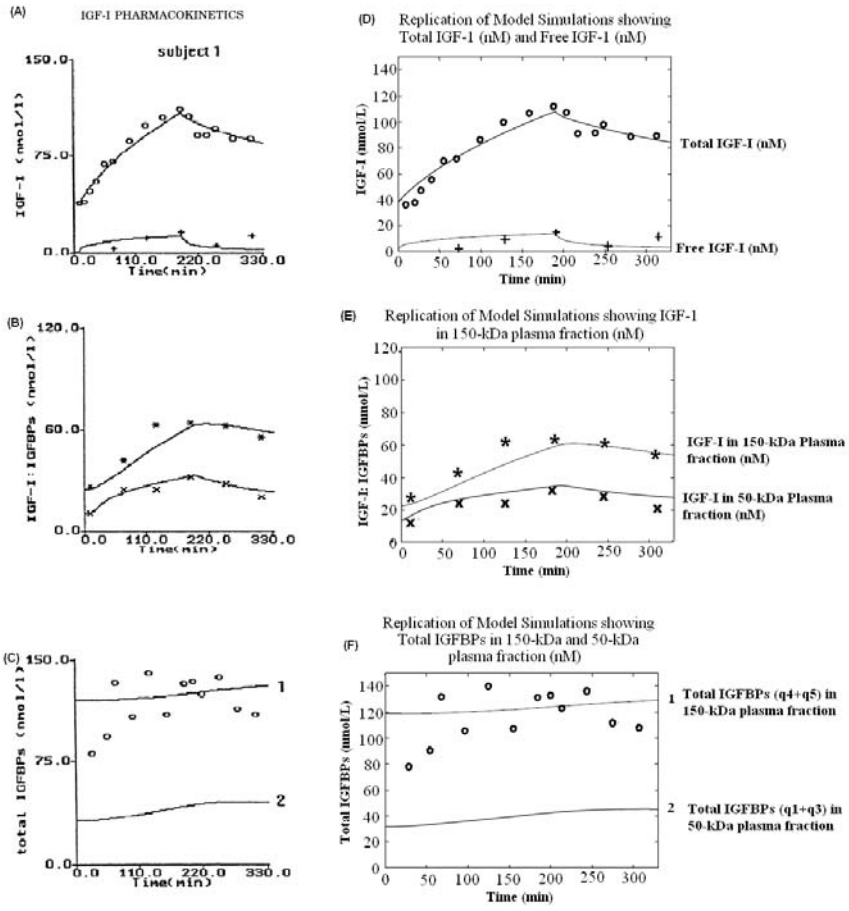

Figure 5: Model simulations for subject one reproduced from Boroujerdi et al. (1997) (left) along side the replicated model simulations (right). o, represents total IGF-1 (nM) and +, represents free IGF-1 (nM) in graphs (A) and (E). In graphs (B) and (E); *, represents IGF-1 in 150kDa plasma fraction (nM) and x, represents IGF-1 in 50kDa plasma fraction (nM). In (C) and (F); (1) represents total IGFBPs in 150kDa plasma fraction (q_4+q_5), (2) represents total IGFBPs in 50kDa plasma fraction (q_1+q_3), nM and o, represents measured IGFBP-3 (nM). The infusion starts at time=10min and is stopped at time=190min.

3.5 Extended Analysis of the Boroujerdi et al. (1997) Model

3.5.1 Bifurcation Analysis

We are able to solve the Boroujerdi et al. (1997) equations analytically, for the steady states and look at a bifurcation analysis of his results. The analytical solutions for the equillibrium points of the equations were:

$$q1 = \frac{R_{a,1}}{k_{01}} \tag{8}$$

$$q2 = \frac{R_a(k_{26}k_{07}R - R_a k_{76} + k_{07}Rk_{76})}{k_{76}k_{62}(-R_a + k_{07}R)} \tag{9}$$

$$q3 = \frac{k_{+1a}R_{a,1}R_a(k_{26}k_{07}R - R_a k_{76} + k_{07}Rk_{76})}{k_{01}k_{62}k_{-1a}k_{76}(-R_a + k_{07}R)} \tag{10}$$

$$q4 = \frac{R_{a,2}}{k_{04}} \tag{11}$$

$$q5 = \frac{k_{+1b}R_{a,2}R_a(k_{26}k_{07}R - R_a k_{76} + k_{07}Rk_{76})}{k_{04}k_{76}k_{62}k_{-1b}(-R_a + k_{07}R)} \tag{12}$$

$$q6 = \frac{k_{07}RR_a}{k_{76}(-R_a + k_{07}R))} \tag{13}$$

$$q7 = \frac{R_a}{k_{07}} \tag{14}$$

After calculating the steady state solutions, a bifurcation analysis (using XPPaut) was performed to investigate the change in long term solutions in the system as the production rate parameters were changed. This is done to look for potential long term periodic orbit solutions (e.g. from Hopf bifurcations), which cannot be found by calculating the steady state solutions. The parameters which were used were R_a (production rate of IGF-1), $R_{a,1}$ (production rate of IGFBPs 50kDa) and $R_{a,2}$ (production rate of IGFBP-3, 150kDa). All seven $\boldsymbol{q}$'s were graphed against each of these parameters and the same result was found throughout. Each graph showed no bifurcation occurring, all the results were stable equilibria throughout the feasible region. The bifurcation diagrams for R_a, $R_{a,1}$ and $R_{a,2}$ respectively are shown in Figures 6, 7 and 8 (note that red lines represent stable equilibria, black lines represent unstable equilibria), see Appendix B.2.1, Figures 57-59, for the other $\boldsymbol{q}$ variable bifurcation diagrams.

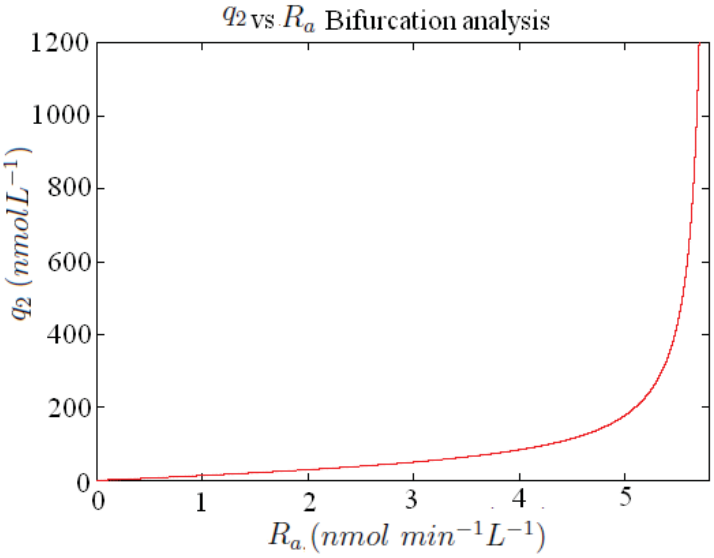

Figure 6: Bifurcation analysis showing the effect of IGF-1 produciton rate, R_a, on free plasma IGF-1, q_2, showing an asymptote occurring at R_a=5.79$nmol\ min^{-1}\ L^{-1}$. Red lines represent stable steady state solutions. (Boroujerdi et al. (1997) model).

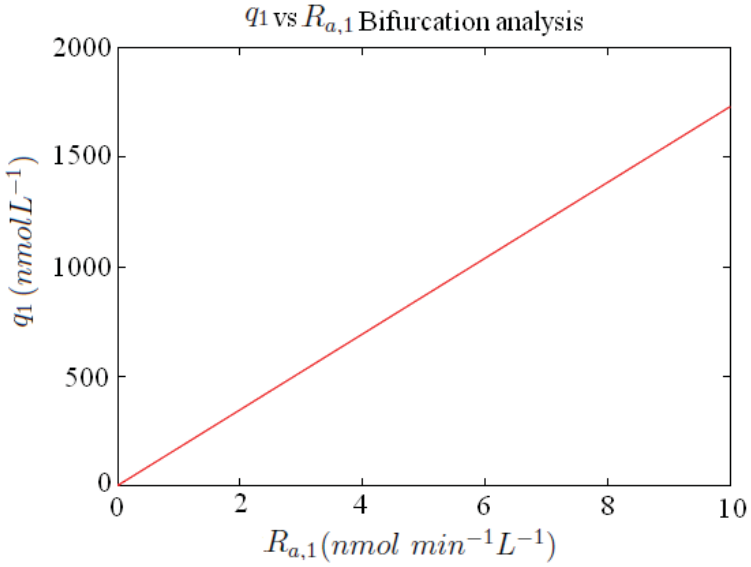

Figure 7: Bifurcation analysis showing the effect of IGFBP (50kDa) production rate, $R_{a,1}$, on the amount of free IGFBPs (50kDa), q_1. Red lines represent stable steady state solutions. (Boroujerdi et al. (1997) model).

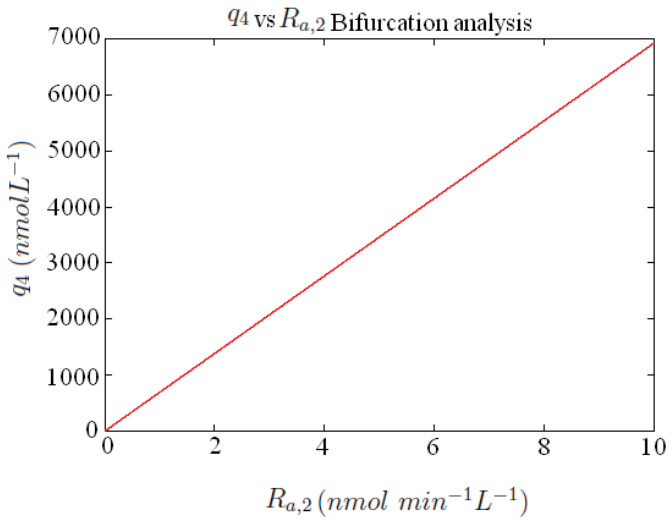

Figure 8: Bifurcation analysis showing the effect of IGFBP-3 (150kDa) production rate, $R_{a,2}$, on the amount of free IGFBP-3 (150kDa), q_4. Red lines represent stable steady state solutions. (Boroujerdi et al. (1997) model).

Here we can see in Equation 9 and Figure 6 that there is an asymptote at approximately R_a= 5.79 nmol min^{-1} L^{-1}. This means the equations would only be physiological for small values of R_a. Biologically speaking in this situation, the production rate must be small because it is unrealistic for IGF-1 levels in the body to rise to the physiologically infeasible values seen near R_a= 5.79 nmol min^{-1} L^{-1}. The model is therefore only appropriate for small Ra values. From the analytical solutions of the steady states (Equations 10, 12 and 13) and the bifurcation diagrams (see Appendix B.2.1, Figure 57) we can see that this is also the case for q_3, q_5 and q_6. In other words the molar mass of bound IGF-1/IGFBP-3 (150kDa), the molar mass of bound IGF-1/IGFBPs (50kDa), and the molar mass of free IGF-1 in the interstitial fluid all increase very rapidly in an unrealistic manner (moves towards infinity near Ra=5.79nmol min^{-1} L^{-1}).

Apart from this asymptote the structure of the model is relatively simple, it appears to be globally asymptotically stable.

3.6 Altered Boroujerdi et al. (1997) Model

The Boroujerdi et al. (1997) model did not take into consideration the breakdown of IGF-1 by the liver/protease in the body. As mentioned earlier free IGF-1 has a half life of approximately ten minutes, this means that the second differential equation (Equation 2) requires a decay term, say -$k_{02}q_2$, in it to represent this breakdown of IGF-1. The elimination rate constant would be found by using the half life of IGF-1: $k_{0,2} = \frac{log(2)}{10min}$.

3.6.1 Altered Boroujerdi et al. (1997) model equations

The new model equations can be seen below, where red indicates changes to the model (see Table 3 and 4 for definition of variables and parameters).

$$\frac{dq_1}{dt} = -k_{01}q_1 - k_{+1a}q_1q_2 + k_{-1a}q_3 + R_{a,1} \tag{15}$$

$$\frac{dq_2}{dt} = -k_{+1a}q_1q_2 + k_{-1a}q_3 - k_{+1b}q_4q_2 + k_{-1b}q_5 - k_{62}q_2 + k_{26}q_6 + R_a + Infu - k_{02}q_2 \tag{16}$$

$$\frac{dq_3}{dt} = k_{+1a}q_1q_2 - k_{-1a}q_3 \tag{17}$$

$$\frac{dq_4}{dt} = -k_{04}q_4 - k_{+1b}q_4q_2 + k_{-1b}q_5 + R_{a,2} \tag{18}$$

$$\frac{dq_5}{dt} = k_{+1b}q_4q_2 - k_{-1b}q_5 \tag{19}$$

$$\frac{dq_6}{dt} = k_{62}q_2 - k_{26}q_6 - k_{76}q_6(1 - \frac{q_7}{R}) \tag{20}$$

$$\frac{dq_7}{dt} = k_{76}q_6(1 - \frac{q_7}{R}) - k_{07}q_7 \tag{21}$$

After making this alteration we find the positive analytical steady state solutions of the $\boldsymbol{q}$'s (which now do not contain any singularities) in Equations 22-28.

$$q1 = \frac{R_{a,1}}{k_{01}} \tag{22}$$

$$q_2 = \frac{k_{76}^2(-k_{02} - k_{62} - 2k_{02}R_a - R_a k_{62}) + \sqrt{k_{76}(k_{02}^2 + 2k_{02}k_{62} + k_{62}^2 + 2kR_a k_{62} + 3R_a k_{62}^2)}}{k_{76}(-2k_{02}^2 - 2k_{62}k_{02})} \tag{23}$$

$$q_3 = (K_{+1a}R_{a1}k_{76}^2)\frac{(-k_{02} - k_{62} - 2k_{02}R_a - R_a k_{62}) + \sqrt{(k_{76})(k_{02}^2 + 2k_{02}k_{62} + k_{62}^2 + 2kR_a k_{62} + 3R_a k_{62}^2)}}{k_{01}k_{-1a}k_{76}(-2k_{02}^2 - 2k_{62}k_{02})} \tag{24}$$

$$q4 = \frac{R_{a,2}}{k_{04}} \tag{25}$$

$$q_5 = (k_{+1b}R_{a2}k_{76}^2)\frac{(-k_{02} - k_{62} - 2k_{02}R_a - R_a k_{62}) + \sqrt{(k_{76})(k_{02}^2 + 2k_{02}k_{62} + k_{62}^2 + 2kR_a k_{62} + 3R_a k_{62}^2)}}{k_{04}k_{-1b}k_{76}(-2k_{02}^2 - 2k_{62}k_{02})} \tag{26}$$

$$q_6 = \frac{(k_{02} + k_{62})(k_{76}^2)(-k_{02} - k_{62} - 2k_{02}R_a - R_a k_{62}) + \sqrt{(k_{76})(k_{02}^2 + 2k_{02}k_{62} + k_{62}^2 + 2kR_a k_{62} + 3R_a k_{62}^2)} - R_a}{k_{26}k_{76}(-2k_{02}^2 - 2k_{62}k_{02})} \tag{27}$$

$$q_7 = \frac{(k_{02} + k_{62})(Rk_{76}^3)(-k_{02} - k_{62} - 2k_{02}R_a - R_a k_{62}) + \sqrt{(k_{76})(k_{02}^2 + 2k_{02}k_{62} + k_{62}^2 + 2kR_a k_{62} + 3R_a k_{62}^2)} - R_a}{k_{26}k_{76}(-2k_{02}^2 - 2k_{62}k_{02})(k_{76} + Rk_{07})} \tag{28}$$

The q_2, q_3, q_5 and q_6 steady state equations no longer have an asymptote occurring in their graphs (the $k_{07}R - R_a$ term has disappeared from all of their denominators). The bifurcation diagrams with the $k_{02}q_2$ term included show that the asymptote has now gone from all the affected $\boldsymbol{q}$ steady state solutions (see Figure 9 and Appendix B.2.2, Figure 60 for other bifurcation graphs).

3.6.2 Bifurcation analysis of the altered Boroujerdi et al. (1997) model

The altered bifurcation diagram can be seen in Figure 9. It shows the asymptote has disappeared from the graph (see appendix B.2.2, Figure 60, for more bifurcation diagrams).

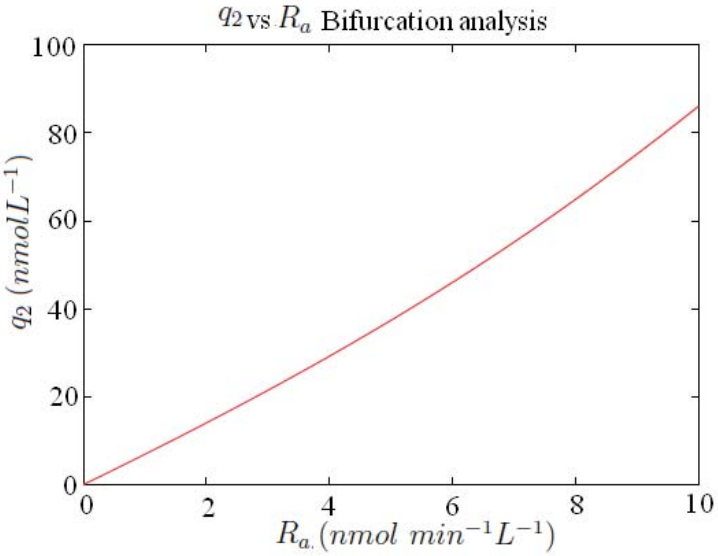

Figure 9: Bifurcation analysis showing the effect of IGF-1 production rate, R_a, on free plasma IGF-1, q_2. (Boroujerdi et al. (1997) model, -$k_{02}q_2$ term included). Red lines represent stable steady state solutions.

3.7 Mizuno et al. (2001) Model

Mizuno et al. (2001) created a simple two compartmental model to look at the interactions of free IGF-1 and IGF-1 bound to IGFBPs. The *in vivo* experiments they performed involved intravenous infusion of recombinant IGF-1. The treatments consisted of: 5 μg $h^{-1}kg^{-1}$ for 3 hours, 10 μg $h^{-1}kg^{-1}$ for 3 hours, 20 μg $h^{-1}kg^{-1}$ for 3 hours and 20 μg $h^{-1}kg^{-1}$ for 6 hours. Their model grouped all IGFBPs together and considered free IGF-1 as one concentration compartment and IGF-1 bound to IGFBPs as another compartment. For glossary of terms see Table 8 and 9 and for model diagram see Figure 10.

Variable	Description
C_b	Plasma concentration of bound IGF-1 (ng ml^{-1})
C_f	Plasma concentration of free IGF-1 (ng ml^{-1})

Table 8: Glossary of *in vivo* variables from Mizuno et al. (2001)

Parameter	Description
$C_{0,f}$	Endogenous free IGF-1 concentration (ng mL^{-1})
CL_{total}	Total body clearance calculated as dose/ $\triangle AUC$ (mL h^{-1} kg^{-1})
$CL_{total,b}$	Total clearance rate for bound IGF-1 (mL h^{-1} kg^{-1})
V_f	Distribution volume for free IGF-1 (mL kg^{-1})
V_b	Distribution volume for bound IGF-1 (mL kg^{-1})
V_{max}	Maximum velocity of saturable elimination (ng h^{-1} kg^{-1})
V_{syn}	Synthesis rate of endogenous IGF-1 (ng $mL^{-1}h^{-1}$), estimated as: $PS_{non} + V_{max}/(K_m + C_{O,f})C_{O,f}$
K_m	Michaelis constant for saturable elimination (ng mL^{-1})
k_{on}	Binding constant of IGF-1 with IGFBPs (ng mL^{-1} h^{-1})
k_{off}	Dissociation constant of IGF-1 with IGFBPs (h^{-1})
R_t	Equillibrium dissociation constant (ng mL^{-1})
PS_{non}	Non-saturable clearance for IGF-1(ml h^{-1} kg^{-1})
Inf	Infusion rate (ng $ml^{-1}h^{-1}$)

Table 9: Glossary of *in vivo* parameters from Mizuno et al. (2001)

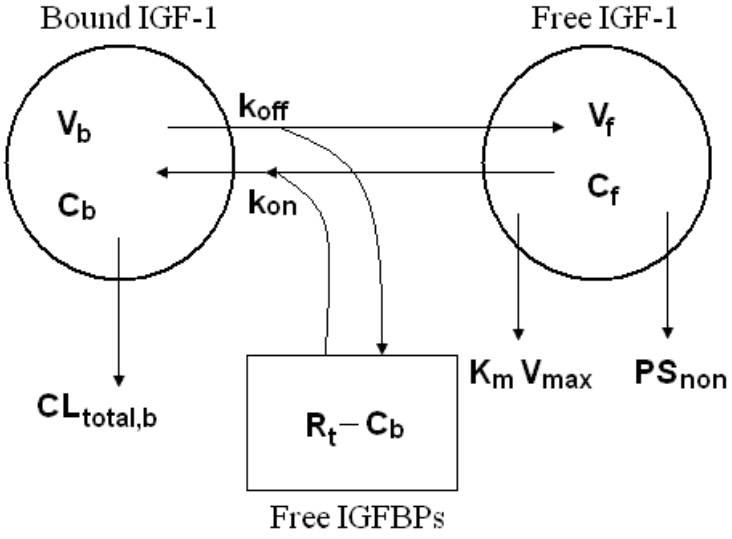

Figure 10: Schematic diagram of the two concentration compartments, reprinted from Mizuno et al. (2001). The circles represent the plasma concentration of IGF-1 in humans (in free form and bound form) and the rectangle represents free IGFBPs. The arrows represent the flow between these compartments and clearance from the model."Springer and Pharmaceutical Research, Mizuno, N., Kato, Y., Iwamoto, M., Urae, A., Amamoto, T., Niwa, T., & Sugiyama, Y, 18, 2001, pg 1204, Kinetic analysis of the disposition of insulin-like growth factor 1 in healthy volunteers, Figure 1, ®, with kind permission from Springer Science and Business Media"

3.8 Mizuno et al. (2001) Equations

The differential equations Mizuno et al. (2001) used were:

$$\begin{aligned} \frac{dC_f}{dt} &= (-k_{on}(R_t - C_b)C_f V_b + k_{off} C_b V_b \\ &- [PS_{non} + V_{max}/(K_m + C_f)]C_f + V_{syn} + Inf)/V_f \end{aligned} \tag{29}$$

$$\frac{dC_b}{dt} = (k_{on}(R_t - C_b)C_f V_b - k_{off} C_b V_b - CL_{total,b} C_b)/V_b \tag{30}$$

3.9 Results from the Mizuno et al. (2001) Model

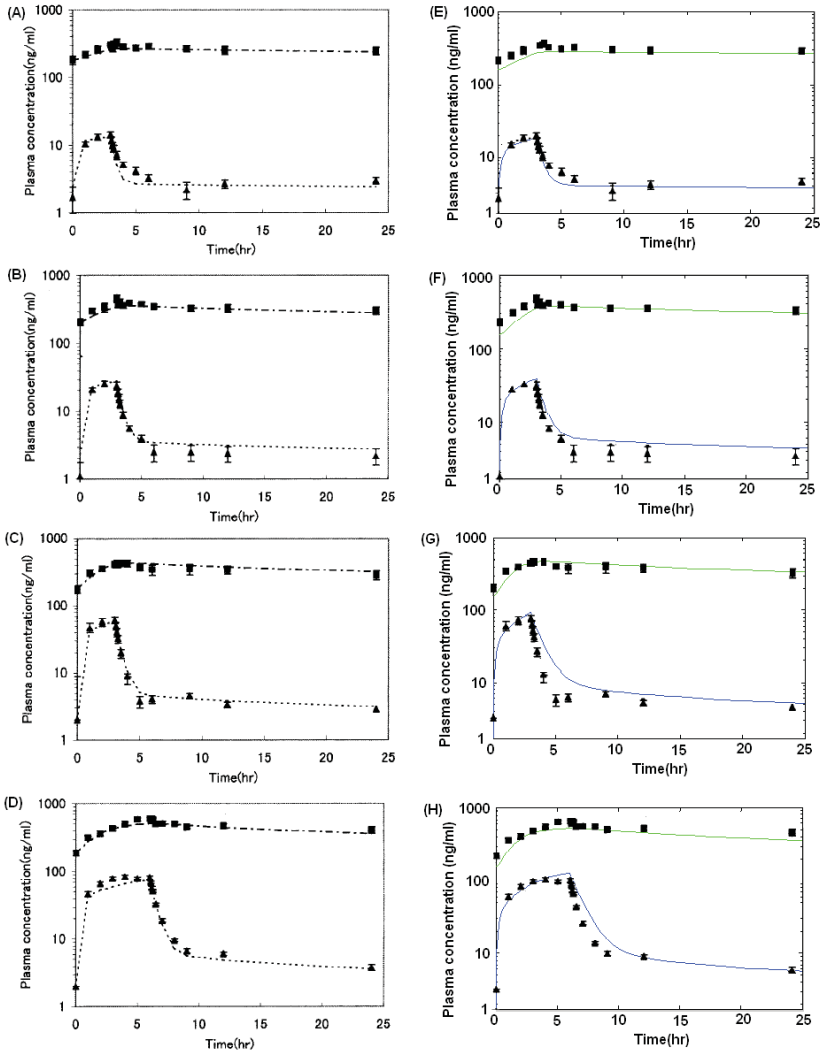

Figure 11: Reproduced Mizuno et al (2001) time series plots (left) alongside the replicated results (right). There were five treatments of IGF-1 infused intravenously these included: (A and E) 5 μg $h^{-1}kg^{-1}$ for 3 hours, (B and F) 10 μg $h^{-1}kg^{-1}$ for 3 hours, (C and G) 20 μg $h^{-1}kg^{-1}$ for 3 hours and (D and H) 20 μg $h^{-1}kg^{-1}$ for 6 hours. Green lines represent the fitted line of the plasma concentration of free IGF-1 data and blue lines represent the fitted line of the plasma concentration of bound IGF-1 data based on the mathematical model after intravenous infusion. The ▲ represent plasma concentration of free IGF-1 and ■ represent plasma concentration of bound IGF-1. "Springer and Pharmaceutical Research, Mizuno, N., Kato, Y., Iwamoto, M., Urae, A., Amamoto, T., Niwa, T., & Sugiyama, Y, 18, 2001, pg 1206, Kinetic analysis of the disposition of insulin-like growth factor 1 in healthy volunteers, Figure 2, ®, with kind permission from Springer Science and Business Media"

3.10 Discussion

The Mizuno et al. (2001) model was a very simple model, involving only two compartments (free IGF-1 and IGF-1 bound to IGFBPs). The model appeared to fit with the data they collected. Their research concluded that the IGFBPs were important to limit free IGF-1 distribution and elimination and thus keep free IGF-1 in circulation (Mizuno et al., 2001). No bifurcation analysis was performed on this model since the Boroujerdi et al. (1997) model subsumed the interactions into their larger and more detailed study.

The model by Boroujerdi et al. (1997) omitted an important physiological factor, the decay term for free IGF-1. Without this term the model was unable to accurately describe the breakdown of IGF-1 in the body. As a consequence of this missing term the analytical steady state solutions for q_2, q_3, q_5 and q_6 showed constraints on the IGF-1 production rate (see equations 9, 10, 12 and 13). A value of R_a= 5.79 nmol min^{-1} L^{-1}, resulted in a denominator of zero and therefore an asymptote in the graph of these equations. Boroujerdi et al. (1997) also did not analyse the long term solutions of the model or consider the potential for long term periodic orbit solutions (e.g. Hopf bifurcations). However, the analysis showed that there are no bifurcations occurring in the feasible region, only one stable equilibria throughout, indicating that it is globally asymptotically stable.

The overall finding was that the bifurcation diagrams have shown no onset of gross change in behaviour within the feasible region. The bifurcation diagrams from the Boroujerdi et al. (1997) model showed an increase in production rate of IGFBP-3 (150kDa) resulted in an increase in free IGFBPs (50kDa) and bound IGFBPs (50kDa) and no change in free IGF-1 levels, free receptor levels or bound receptor levels (see Appendix B.2.1, Figure 57). An increase in production rate of IGFBPs (50kDa) resulted in an increase in free IGFBP-3 (150kDa) and bound IGFBP-3 (150kDa) and no change in free IGF-1 levels, free receptor levels or bound receptor levels (see Appendix B.2.1, Figure 58).

Increasing the production rate of free IGF-1 resulted in an increase in bound IGFBPs (both 50kDa and 150kDa), free IGF-1 and receptor bound IGF-1 with no change in free IGFBPs (50kDa and 150kDa) for the original Boroujerdi et al. (1997) model with the $k_{02}q_2$ term added in Equation 16 (see Appendix B.2.1, Figure 59 and B.2.2, Figure 60).

4 *In Vivo* Model:

4.1 *In Vivo* Model Introduction

This model was produced to extend the current literature on IGF-1 interactions through *in vivo* (within the body) experiments investigating the role of CGP. There was no *in vivo* data involving CGP available to test this model. The equations were written to maintain a similar structure and notation to the previous models. By maintaining a similar structure, some of the parameters in this model could be calculated using the Boroujerdi et al. (1997) *in vivo* model parameters, see Table 12 for further explanation. Two feedback terms were introduced to the system; F and G and can be seen in Figure 12. These two terms follow from the hypothesis that changes in the feedback to the IGF-1 receptors and binding proteins are activated through CGP. These can be positive or negative feedbacks depending on whether the IGF-1 levels are below or above the physiological threshold. See Table 10 for glossary of terms.

Variable	Description
q_1	Concentration of free IGFBPs (nmol L^{-1})
q_2	Concentration of free IGF-1 (nmol L^{-1})
q_3	Concentration of bound IGF-1/IGFBPs (nmol L^{-1})
q_4	Concentration of receptor bound IGF-1 (nmol L^{-1})
q_5	Concentration of IGF-1 receptors (nmol L^{-1})
q_6	Concentration of CGP (nmol L^{-1})
Parameter	**Description**
k_{ij}	Rate constant, to compartment i from j (min^{-1}) where zero is outside the system (min^{-1})
k_{+1a}	Association rate constant (IGFBPs and IGF-1) ($nmol^{-1}$ min^{-1} L)
k_{+1b}	Association rate constant (receptor and IGF-1) ($nmol^{-1}$ min^{-1} L)
k_{-1a}	Dissociation rate constant (IGFBPs and IGF-1) (min^{-1})
$R_{a,1}$	IGFBPs production rate (nmol min^{-1} L^{-1})
$R_{a,2}$	IGF-1 production rate + infusion rate (nmol min^{-1} L^{-1})
$R_{a,5}$	Receptor production rate (nmol min^{-1} L^{-1})
$R_{a,6}$	CGP production rate + infusion rate (nmol min^{-1} L^{-1})
M_1	Rate constant in feedback term F (min^{-1})
M_2	Rate constant in feedback term G (min^{-1})
L_1	IGF-1 half effect (nmol L^{-1})
L_2	IGF-1 half effect (nmol L^{-1})
a_1	Proportionality constant/weighting factor (dimensionless)
a_2	Proportionality constant/weighting factor (dimensionless)

Table 10: Glossary of the new *in vivo* model variables and parameters

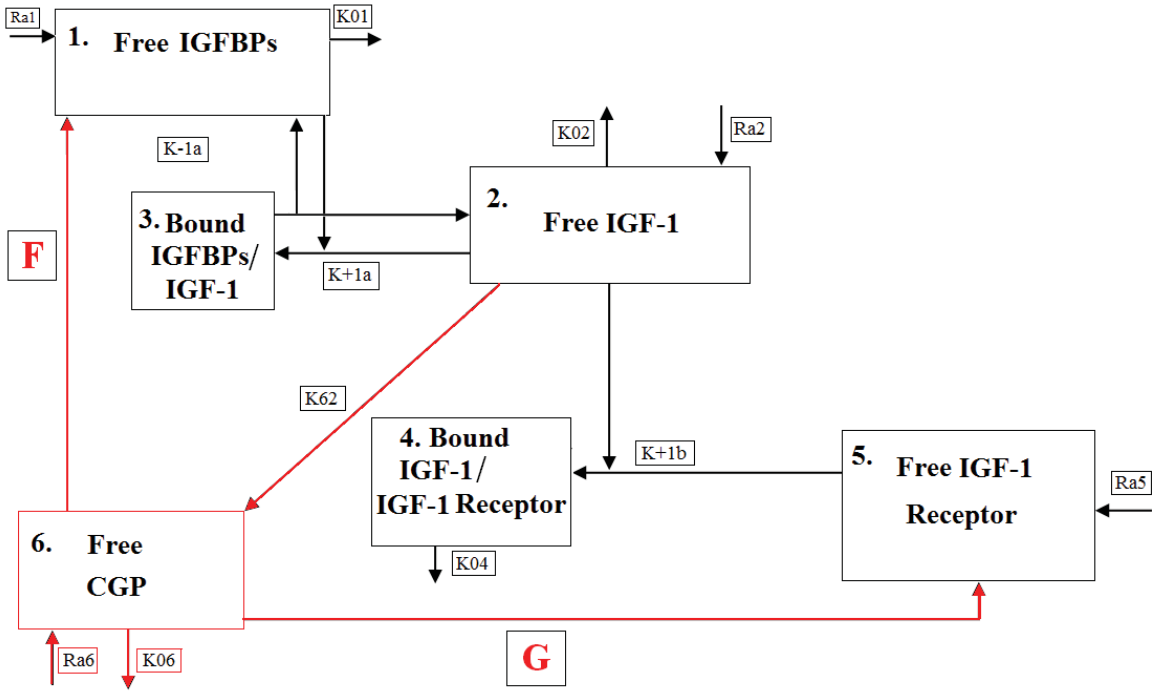

Figure 12: Schematic diagram of the six concentration compartments in the *in vivo* model. Each box represents a compartment, and the arrows represent transport between compartments. The red arrows are the main changes made to include the effects of CGP on the IGF-1 dynamics, implicitly through the two feedback terms; F and G.

4.2 *In Vivo* Model Equations

The *in vivo* model was developed to investigate the effect of CGP on IGF-1. Some of the model parameters were found by comparing similar Boroujerdi et al. (1997) parameters. Table 12 summarises how the Boroujerdi et al. (1997) parameter values can be used to find some of the *in vivo* model parameters. The model can be used to describe the interactions within the body of IGF-1 with binding proteins, receptors and CGP. The model also allows us to investigate the effect of IGFBP, IGF-1 and receptor production rates ($R_{a,1}$, $R_{a,2}$ and $R_{a,5}$ respectively) on IGF-1. The model consists of six compartments, see Figure 12.

In this model all free IGFBPs were grouped into one compartment, q_1, and all bound IGFBPs into another, q_3, to simplify the model. Often it is only possible to measure the total IGFBPs experimentally, rather than measuring IGFBP-3 separately. This new model has a separate compartment for IGF-1 receptors, q_5, since the receptors play a role in IGF-1 regulation. The plasma IGF-1 and interstitial IGF-1 were merged

into one compartment, q_2, for simplicity. Our newest addition was the CGP complex, q_6, which is derived from IGF-1 and is believed to regulate IGFBPs and IGF-1 receptors.

F and G allow the model to implicitly express CGP regulating IGF-1 actions through feedback to the IGFBPs and IGF-1 receptors. We define function F as: $\frac{M_1 q_4^2}{L_1^2+q_4^2}$ (in Equations 31 and 36) and function G as: $M_2 - \frac{M_2 q_4^2}{L_2^2+q_4^2}$ (in Equations 35 and 36).

The equations for this model are shown in Equations 31-36. In addition to the combining of IGFBPs, combining of the IGF-1 in plasma and IGF-1 in interstitial fluid and the adding of the receptor compartment, the main changes are shown in red.

$$\frac{dq_1}{dt} = -k_{01}q_1 - k_{+1a}q_1q_2 + k_{-1a}q_3 + R_{a,1} + \frac{M_1 q_4^2}{L_1^2 + q_4^2}q_6 \tag{31}$$

$$\frac{dq_2}{dt} = -k_{02}q_2 - k_{+1a}q_1q_2 + k_{-1a}q_3 - k_{+1b}q_5q_2 - k_{62}q_2 + R_{a,2} \tag{32}$$

$$\frac{dq_3}{dt} = k_{+1a}q_1q_2 - k_{-1a}q_3 \tag{33}$$

$$\frac{dq_4}{dt} = -k_{04}q_4 + k_{+1b}q_5q_2 \tag{34}$$

$$\frac{dq_5}{dt} = -k_{05}q_5 - k_{+1b}q_5q_2 + R_{a,5} + (M_2 - \frac{M_2 q_4^2}{L_2^2 + q_4^2})q_6 \tag{35}$$

$$\frac{dq_6}{dt} = -k_{06}q_6 + k_{62}q_2 + R_{a,6} - a_1\frac{M_1 q_4^2}{L_1^2 + q_4^2}q_6 - a_2(M_2 - \frac{M_2 q_4^2}{L_2^2 + q_4^2})q_6 \tag{36}$$

The F and G terms describe the feedback of IGF-1 on IGF-1 receptors and IGFBPs. The Hill equation was used to express the sigmoidal shape of this implicit process. When receptor bound IGF-1, q_4, is high, F is at it's maximum (see Figure 13). This causes an increase in free IGFBPs, q_1. This results in the free IGFBPs binding to the free IGF-1, q_2, to produce more bound IGFBPs, q_3. There will therefore be less free IGF-1 available to bind to receptors.

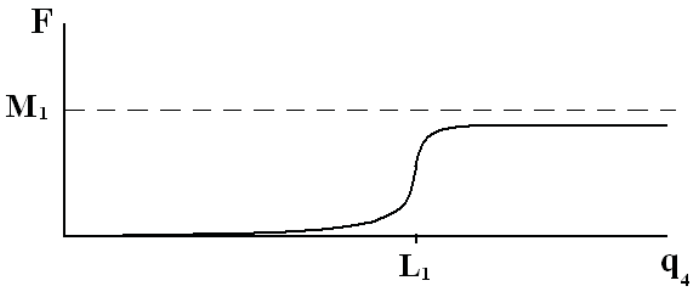

$$F = \frac{M_1 q_4^2}{q_4^2 + L_1^2}$$

Figure 13: Graph of Feedback term F vs receptor bound IGF-1 (q_4). This shows how M_1 and L_1 relate to the F curve in the implicit *in vivo* model.

As free IGF-1 becomes less available for binding to the receptors (resulting from a large F value), G is at a low value (high q_4, Figure 14). Therefore free receptors, q_5, are less readily available. Both these situations result in less IGF-1 binding to receptors. For high levels of receptor bound IGF-1, the F and G terms will provide negative feedback, reducing the size of the q_4 (receptor bound IGF-1) term.

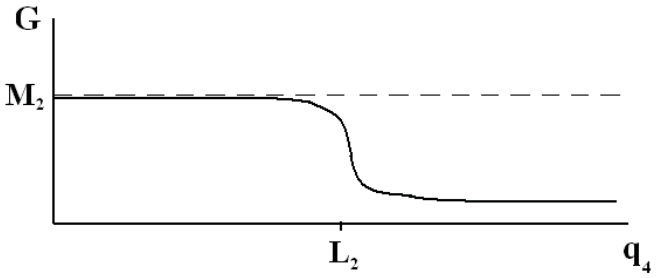

$$G = M_2 - \frac{M_2 q_4^2}{q_4^2 + L_2^2}$$

Figure 14: Graph of Feedback term G vs receptor bound IGF-1 (q_4). This shows how M_2 and L_2 relate to the G curve in the implicit *in vivo* model.

Small values of q_4, have the opposite effect. Low levels of receptor bound IGF-1 (q_4) result in a smaller F value and therefore lower amount of free IGFBP, q_1. In turn, fewer free IGFBPs result in less free IGF-1, q_2, binding to binding proteins and more IGF-1 becoming available in the free form. In unison with F being small, G is large (for our selected L_1 and L_2 values), increasing the availability of IGF-1 receptors, q_5. Low values of q_4 will result in the F and G terms increasing the levels of q_4 (positive feedback) by having more free IGF-1 and free receptors available.

The terms F and G were added to express the negative and positive feedbacks described by Dr Guan, which regulate IGF-1 levels. Changes in feedbacks to IGF-1 receptors and

binding proteins are influenced by IGF-1 levels. When IGF-1 levels are below the physiological threshold, F acts as a negative feedback on the free IGFBPs by reducing their numbers. At the same time G acts as a positive feedback on the free IGF-1 receptors to boost the number of free receptors. This results in more IGF-1 binding to the receptors to obtain more normal levels of activated IGF-1. Similarly, elevated levels of IGF-1 will result in F acting as a positive feedback on free IGFBPs by increasing their numbers. G acts as a negative feedback on free IGF-1 receptors by decreasing their numbers. This will mean there will be less free IGF-1 available to bind to the receptors and less free IGF-1 receptors so that activated IGF-1 levels (IGF-1 bound to their receptors) can be reduced.

4.3 *In Vivo* Model Results

To account for the grouping of IGFBPs we noted that at steady state, 30% of IGF-1 is bound to IGFBP-1 and 60% of IGF-1 is bound to IGFBP-3 (Boroujerdi et al., 1994), this gives us a ratio of 1:2. We set $w_1 = \frac{1}{3}$ and $w_2 = \frac{2}{3}$ to approximate our new parameters using a weighted average of Boroujerdi's values. Taking into account these ratios, we get from the Boroujerdi et al. (1997) parameters:

Parameter	How it was found	Value
$k_{0,1}$	$w_1\ old\ k_{01} + w_2\ old\ k_{04}$	0.0029 (min^{-1})
$k_{0,4}$	$old\ k_{07}$	0.082 (min^{-1})
k_{-1a}	$w_1\ old\ k_{-1a} + w_2\ old\ k_{-1b}$	0.0255 (min^{-1})
k_{+1a}	$w_1\ old\ k_{+1a} + w_2\ old\ k_{+1b}$	0.00428 ($\text{nmol}^{-1}\text{min}^{-1}$ L)
k_{+1b}	$\frac{oldk_{76}}{oldR}$	0.00116 (nmol^{-1} min^{-1} L)
$R_{a,1}$	$oldR_{a,1} + oldR_{a,2}$	0.25 (nmol min^{-1} L^{-1})
$R_{a,2}$	$oldR_a$	0.15 (nmol min^{-1} L^{-1})
Variable	How it was found	Initial value
q_1	$w_1 oldq_1 + w_2 oldq_4$	71.057 (nmol L^{-1})
q_2	$oldq_2$	1.910 (nmol L^{-1})
q_3	$w_1 oldq_3 + w_2 oldq_5$	15.251 (nmol L^{-1})
q_4	$oldq_7$	1.797 (nmol L^{-1})
q_5	$oldR - oldq_7$	68.819 (nmol L^{-1})

Table 11: How the *in vivo* parameter and initial variable values were estimated from using the Borojerdi et al. (1997) parameters.

Since we know the half lives of IGF-1 and CGP we can estimate k_{02} and k_{06}:

$k_{02} = \frac{log(2)}{10} = 0.0693$ (IGF-1 has a half life of approximately 10 min).

$k_{06} = \frac{log(2)}{360} = 0.00192$ (CGP has a half life of approximately 6 hr).

Notice that in the differential equations (Equations 31-36) there are no k_{-1b} terms. This is because IGF-1 binding to the receptors is non reversible. Also note that these parameters are just estimates and will not be completely accurate. The first two assumptions made, were that $R_{a,5}$ and $R_{a,6}$ are both equal to zero for simplicity. k_{62} can be found by setting the second differential equation (Equation 32) to zero and rearranging in terms of k_{62}. Similarly, a_1 can be found by setting the sixth differential equation (Equation 36) to zero and rearranging in terms of a_1 (when a_2 has been estimated). To find our missing parameters, since we have no *in vivo* data involving CGP, we resorted to a guess and check method using the Boroujerdi et al. (1997) parameters. This involved guessing estimates for L_1, L_2, M_1, M_2 and a_1, calculating the other parameters based on our estimated parameter and initial variable values (see Tables 12 and 13) and running XPPaut to produce the steady state values: q_1, q_2, q_3, q_4, q_5 and q_6. These values are then used to recalculate k_{62} and a_2, then the procedure is rerun and the steps repeated until we get no change in the steady state values. To get steady state values close to the required values in Table 11, this process needs to be repeated as L_1, L_2, M_1, M_2 and a_1 are altered. The resulting final parameter values are shown in Table 12.

Parameter	How it was found	Value
k_{01}	w_1 *old* k_{01} + w_2 *old* k_{04}	0.0029 (min^{-1})
k_{02}	half life of 10 min	0.069 (min^{-1})
k_{04}	*old* k_{07}	0.082 (min^{-1})
k_{05}	guess and check	0.001 (min^{-1})
k_{06}	half life of 6 hours	0.0019 (min^{-1})
k_{-1a}	w_1 *old* k_{-1a} + w_2 *old* k_{-1b}	0.0255 (min^{-1})
k_{+1a}	w_1 *old* k_{+1a} + w_2 *old* k_{+1b}	0.00428 (nmol^{-1} min^{-1} L)
k_{+1b}	$\frac{oldk_{76}}{oldR}$	0.00116 (nmol^{-1} min^{-1} L)
$R_{a,1}$	*old* $R_{a,1}$ + *old* $R_{a,2}$ altered	0.358 (nmol min^{-1} L^{-1})
$R_{a,2}$	*old* R_a altered	0.368 (nmol min^{-1} L^{-1})
$R_{a,5}$	*assumed*	0 (nmol min^{-1} L^{-1})
$R_{a,6}$	*assumed*	0 (nmol min^{-1} L^{-1})
k_{62}	rearranging Equation 2	0.227 (min^{-1})
M_1	guess and check	10 (min^{-1})
M_2	guess and check	115 (min^{-1})
L_1	guess and check	1 (nmol L^{-1})
L_2	guess and check	2 (nmol L^{-1})
a_1	rearranging Equation 6	0.01 (units)
a_2	guess and check	1.61 (units)

Table 12: Final parameter values estimated from Boroujerdi et al. (1997) model and a guess and check method which produced steady state values as close as possible to the estimates.

The resulting and initial $\boldsymbol{q}$ values are shown in Table 13.

Variable	How it was found	Initial value
q_1	comparison to Boroujerdi et al. (1997)	126.17 (nmol L^{-1})
q_2	comparison to Boroujerdi et al. (1997)	0.99 (nmol L^{-1})
q_3	comparison to Boroujerdi et al. (1997)	20.97 (nmol L^{-1})
q_4	comparison to Boroujerdi et al. (1997)	0.91 (nmol L^{-1})
q_5	comparison to Boroujerdi et al. (1997)	64.97 (nmol L^{-1})
q_6	XPPaut ran to find steady state	0.0015 (nmol L^{-1})

Table 13: Steady state values found using estimated parameters from Boroujerdi et al. (1997) model and then a guess and check method involving XPPaut.

4.3.1 Bifurcation analysis of a_1 and a_2

Since we did not know the range of a_1 or a_2, we needed to justify the values used. To make sure that the values used were not important we looked at the effect of choosing a_1 to be a low, medium and high value then calculated the corresponding a_2 value. From here the three different states of a_1 were fixed and we looked at the effect of a_2 on q_4 steady states (bifurcation analysis of a_2 see Figures 15-17). In all three cases the results were stable steady states and no bifurcation occurred in the system. This was repeated for a low, medium and high value of a_2, the a_2 value was fixed and a bifurcation analysis of a_1 alongside q_4 was produced (see Figures 18-20). This resulted in stable steady state solutions, i.e. no bifurcations. We can conclude based on this that no matter what a_1 or a_2 are, there is no bifurcation occurring and the results are qualitatively the same.

We also looked at a_1 or a_2 having negative values, in this case we did find Hopf bifurcations occurring. This is biologically not feasible but it is mathematically interesting that the negative values introduce this new behaviour into the system.

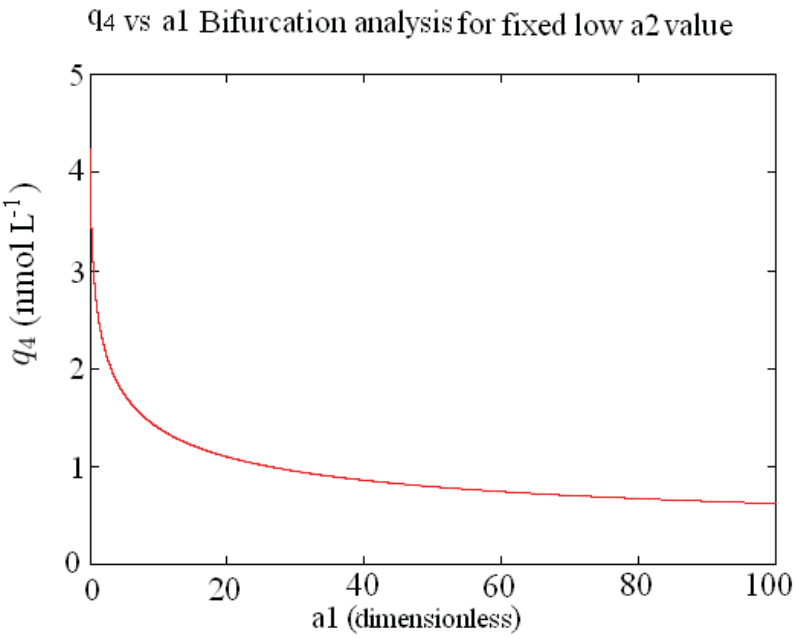

Figure 15: Bifurcation analysis showing receptor bound IGF-1 (q_4) vs a_1 (fixed low a_2 value). Red indicates stable steady state solutions.

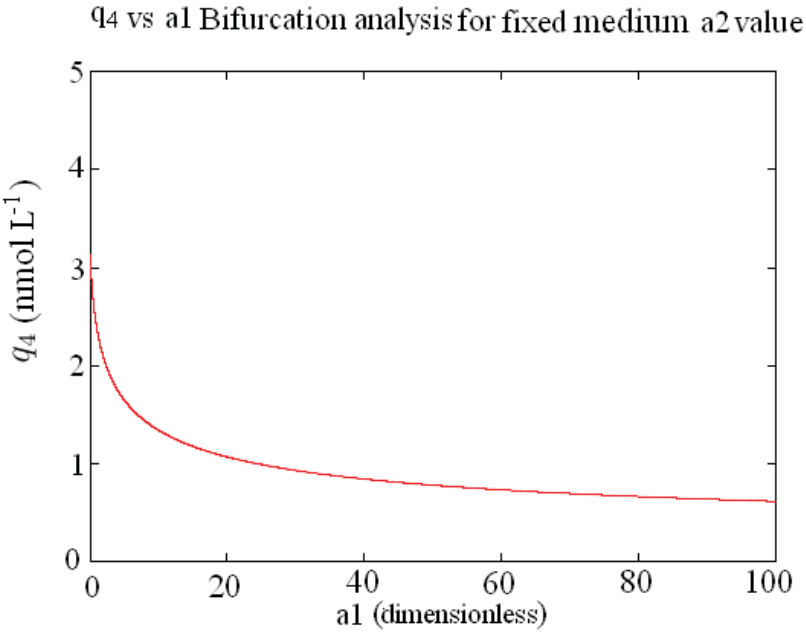

Figure 16: Bifurcation analysis showing receptor bound IGF-1 (q_4) vs a_1 (fixed medium a_2 value). Red indicates stable steady state solutions.

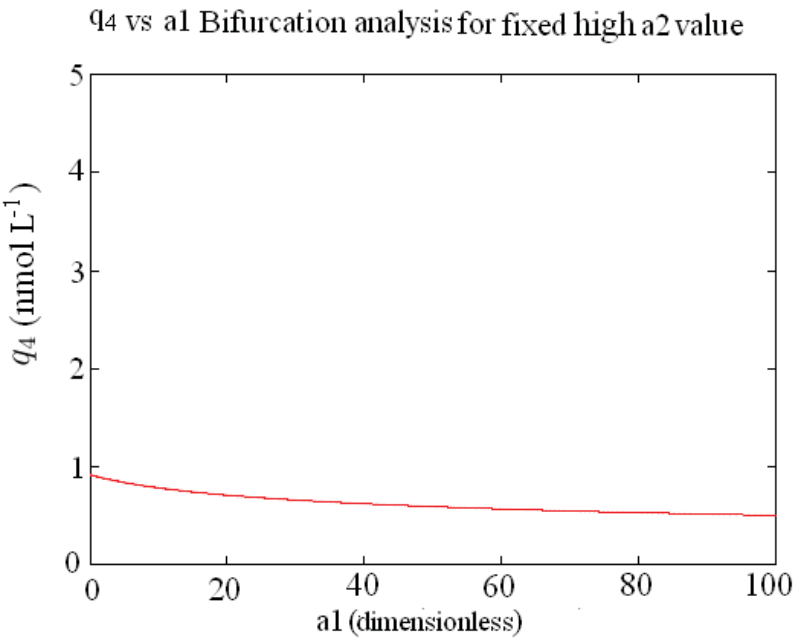

Figure 17: Bifurcation analysis showing receptor bound IGF-1 (q_4) vs a_1 (fixed high a_2 value). Red indicates stable steady state solutions.

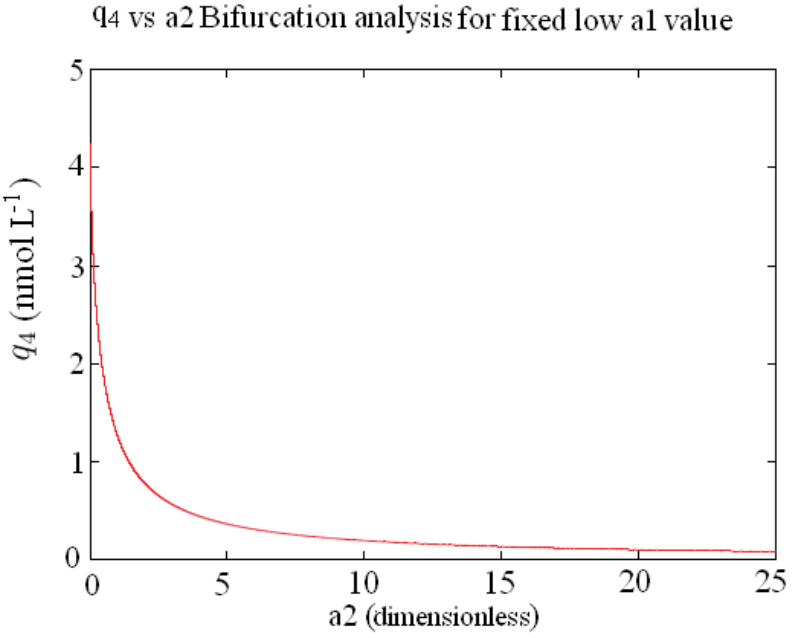

Figure 18: Bifurcation analysis showing receptor bound IGF-1 (q_4) vs a_2 (fixed low a_1 value). Red indicates stable steady state solutions.

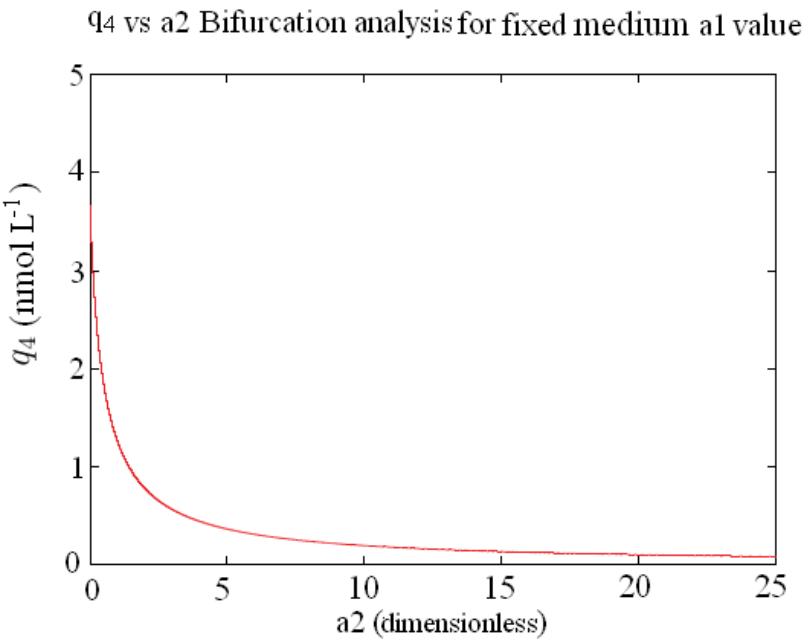

Figure 19: Bifurcation analysis showing receptor bound IGF-1 (q_4) vs a_2 (fixed medium a_1 value). Red indicates stable steady state solutions.

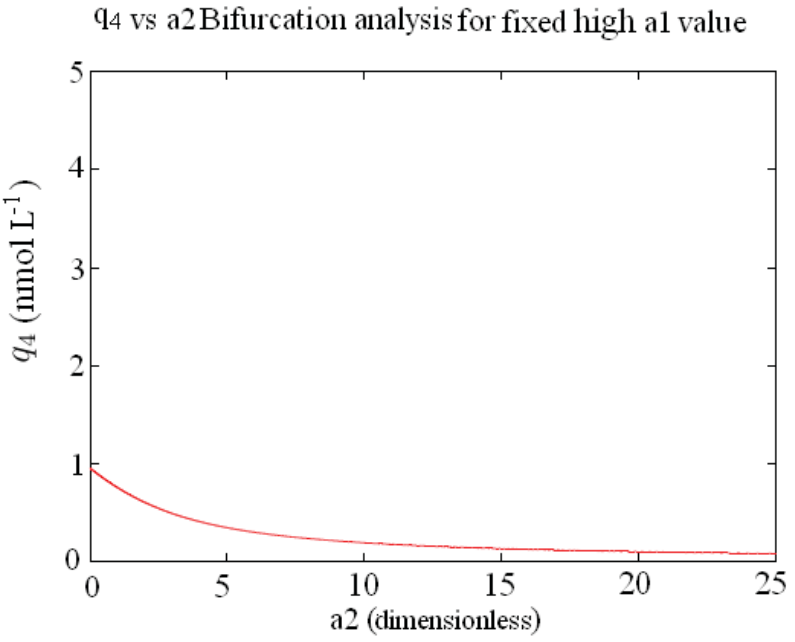

Figure 20: Bifurcation analysis showing receptor bound IGF-1 (q_4) vs a_2 (fixed high a_1 value). Red indicates stable steady state solutions.

Looking at the negative region of a_1 (looking at only positive **q** behaviour) resulted in the bifurcation diagrams in Figure 21-22.

In Figure 21, we can see q_4 (receptor bound IGF-1) against a_1 in the negative a_1 region (positive **q**'s only). This plot has two bifurcations occurring, a Saddle-Node bifurcation and a Hopf bifurcation. The Saddle-Node occurs as the stability changes from stable to unstable (bottom right stable red line, towards the left direction turning into an unstable black line). Looking at this along the x-axis from left to right, the system goes from having no equilibria, to having one equilibrium (at the bifurcation point), to having two equilibria after the bifurcation point (a stable and an unstable one). The Hopf bifurcation occurs when there is a change in the number of positive complex eigenvalues in the system. The stability is unstable before and after the Hopf in this case but there is a change in sign of the eigenvalues with complex terms. This most likely means that the dimension of the unstable manifold changes.

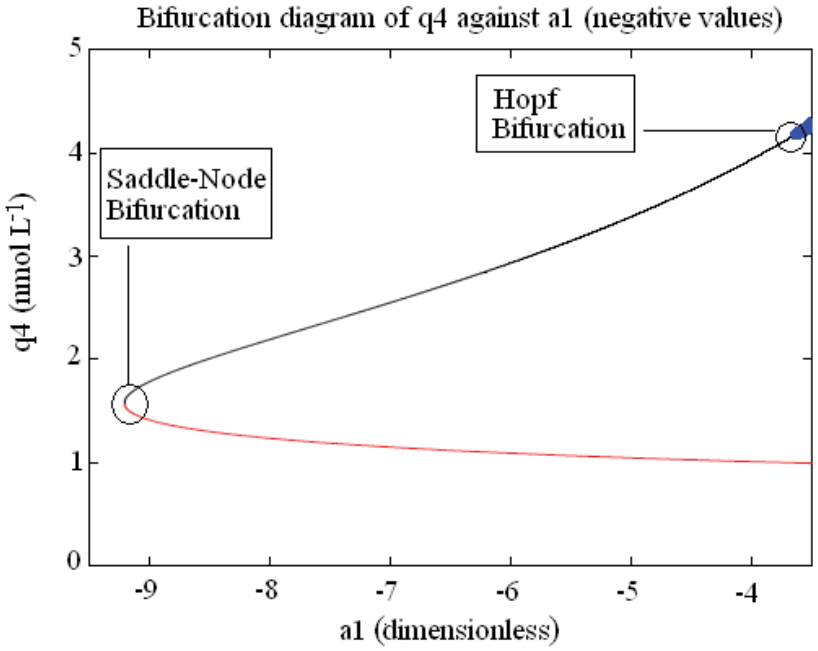

Figure 21: Bifurcation analysis showing receptor bound IGF-1 (q_4) vs negative a_1 showing a Hopf bifurcation and a Saddle-Node bifurcation. Black lines indicate unstable steady states, red lines indicate stable steady states. Blue circles represent stable periodic orbits.

In Figure 22, we can see an enlarged picture of the stable periodic orbits (blue open circles) coming from the Hopf bifurcation.

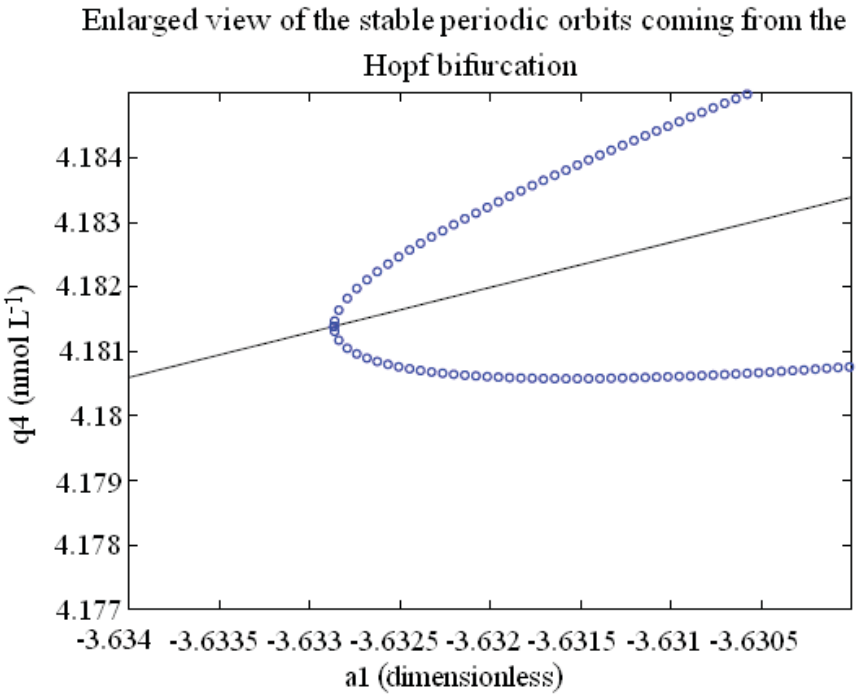

Figure 22: Enlarged view of the Hopf bifurcation when looking at receptor bound IGF-1 (q_4) vs negative a_1. Black lines indicate unstable steady states, blue open circles represent stable periodic orbits.

The behaviour seen here is not relevant biologically as the input variables (a_1 and a_2) must be positive. Mathematically it is interesting that such large changes in behaviour occur. The only equilibria considered were those that existed for all positive $\boldsymbol{q}$ values. The Hopf bifurcation behaviour in Figure 21 and Figure 22, where the stability is unstable before and after the Hopf, can only be seen in large systems (such as this six dimensional system).

Looking at the negative region of a_2 (only looking at positive $\mathbf{q}$ behaviour) resulted in the bifurcation diagrams in Figures 23-24. In Figure 23 we can see q_4 (receptor bound IGF-1) against a_2 in the negative a_2 region. In this plot we can see a Hopf occurring as the stability of the system changes from stable (red line) to unstable (black line) and unstable periodic orbits emerging from the bifurcation point (green closed circles). In Figure 24 we enlarge the region surrounding the bifurcation. From here we see the unstable periodic orbits begin with stable periodic orbits (open blue circles). The scale makes it difficult to see how this happens, but the stable periodic orbits come out along the unstable equlibria (black line) and turn back towards to stable equilibria

(red line). When they pass the bifurcation point they become unstable periodic orbits this is called a subcritical Hopf bifurcation.

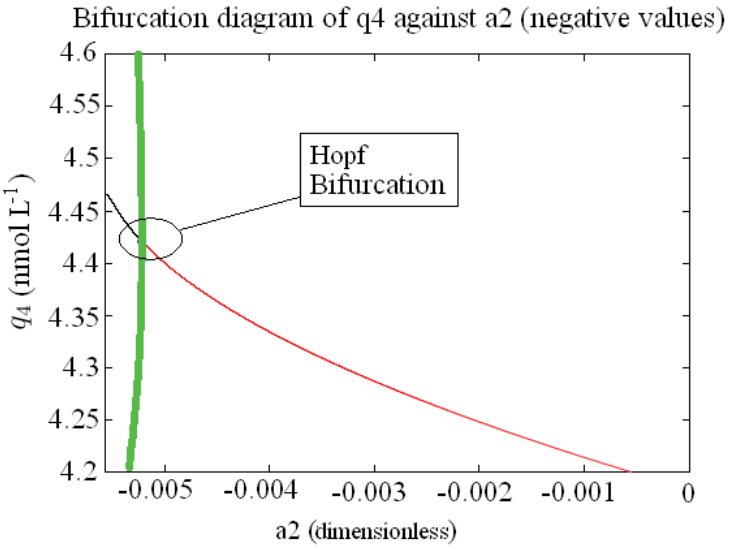

Figure 23: Bifurcation analysis of receptor bound IGF-1 (q_4) vs negative a_2 showing a Hopf bifurcation. Black lines indicate unstable steady states, red lines indicate stable steady states. Blue circles represent stable periodic orbits and green circles represent unstable periodic orbits.

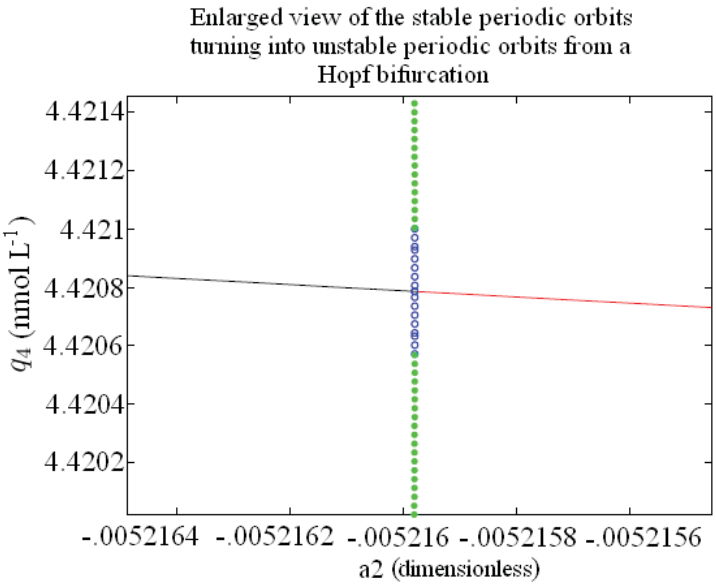

Figure 24: Enlarged view of the Hopf bifurcation when looking at receptor bound IGF-1 (q_4) vs negative a_2. Black lines indicate unstable steady states, red lines indicate stable steady states. Blue circles represent stable periodic orbits and green circles represent unstable periodic orbits.

4.3.2 Bifurcation analysis of q variables

The steady state solutions of the equations cannot be found analytically therefore a bifurcation analysis was performed. Once all our parameters are estimated the model can be investigated using XPPaut to characterise the qualitative behaviour of the model. We look at the effect of varying the production rates; R_{a1}, R_{a2}, R_{a5} and R_{a6} on the steady state solutions of the model. These are shown in Figure's 25-28 (see Appendix B.2.3, Figures 61-64 for the other $\boldsymbol{q}$ variable bifurcation diagrams):

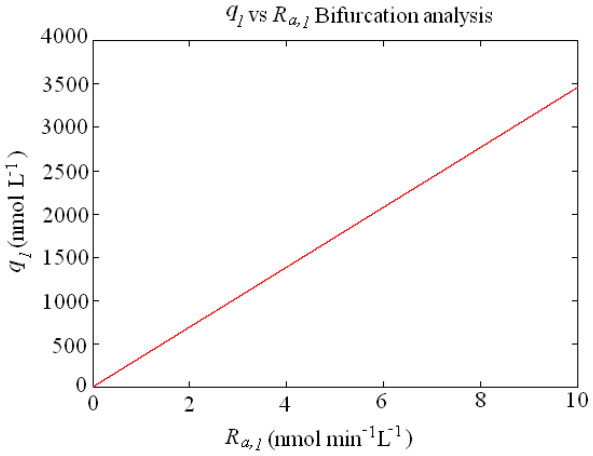

Figure 25: Bifurcation analysis showing free IGFBPs, q_1, against IGFBP production rate, $R_{a,1}$, (*In Vivo* Model). Red lines indicate stable steady state solutions.

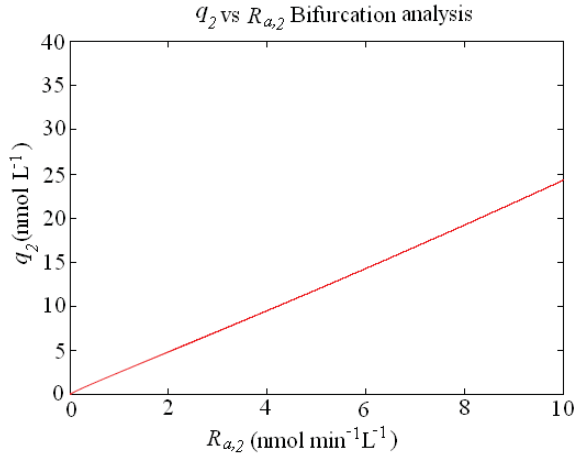

Figure 26: Bifurcation analysis showing free IGF-1, q_2, against IGF-1 production rate, $R_{a,2}$, (*In Vivo* Model). Red indicates stable steady state solutions.

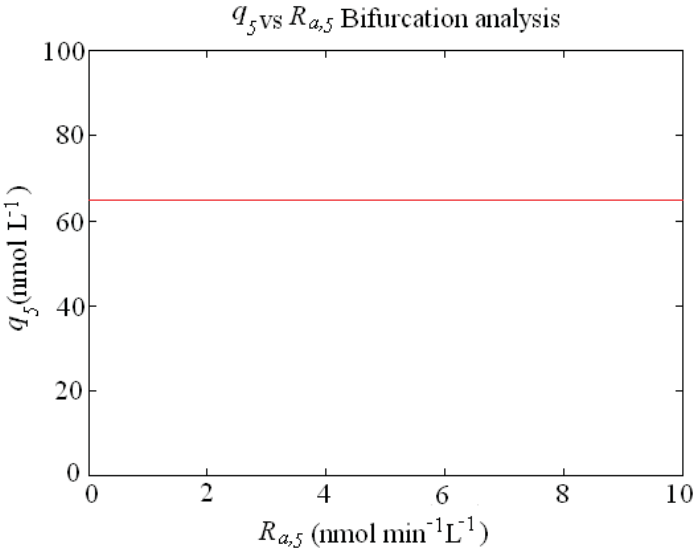

Figure 27: Bifurcation analysis showing free IGF-1 receptors, q_5, against IGF-1 receptor production rate, $R_{a,5}$, (*In Vivo* Model). Red indicates stable steady state solutions.

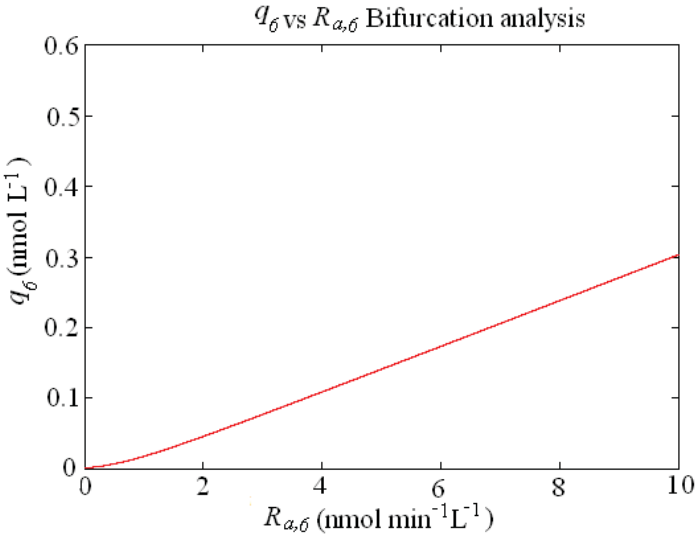

Figure 28: Bifurcation analysis showing free CGP, q_6, against CGP production rate, $R_{a,6}$, (*In Vivo* Model). Red indicates stable steady state solutions.

Once again the result is globally asymptotically stable steady states occurring for all bifurcation plots.

4.4 *In Vivo* Model Discussion

The previous IGF-1 models did not show the role of CGP on IGF-1 actions. This *in vivo* model uses similar notation and equations to the Boroujerdi et al. (1997) model to incorporate CGP effects. The model extends the work by Boroujerdi et al. (1997) by using simplifications and added feedback terms to implicitly show CGP's role in the system. Thus, this model allows an estimate of CGP's effects on IGF-1 within the body. Since no CGP data was used for this, it is not an accurate account of activity, however it gives a good idea of the long term effects of all the involved components interacting within the body. The overall finding was that the plots have shown no onset of gross change in behaviour within the feasible region as was the case in the Boroujerdi et al. (1997) model.

The bifurcation diagrams from both the Boroujerdi et al. (1997) model and the *in vivo* model showed that an increase in production rate of IGFBPs resulted in an increase in bound IGFBP levels and no change in free IGF-1 levels, free receptor levels or bound receptor levels (no change in free CGP in the new model, see Appendix B.2.3, Figure 61).

Increasing the production rate of free IGF-1 resulted in an increase in bound IGFBPs, free IGF-1 and receptor bound IGF-1 with no change in free IGFBPs for the original Bourojerdi et al. (1997) model with the $k_{02}q_2$ term added. The extended model showed similar effects with an increase in CGP levels and an increase in free IGFBP levels (see B.2.3, Figure 62).

Increasing the production rate of CGP in the extended model resulted in an increase in IGFBP, free receptor, free CGP and receptor bound IGF-1 levels. It also showed a decrease in bound IGFBP and free IGF-1 levels.

From the bifurcation diagrams (see Figure 64 in Appendix B.2.3) it appears that an increased production rate of CGP causes more IGF-1 to bind to the receptors. This is what causes the reduction in free IGF-1 levels. IGFBP levels remain the same while the bound (to IGF-1) IGFBP levels decrease. This can be explained by CGP binding to these binding proteins that have unbound from IGF-1.

5 *In Vitro* Model One and Two (Implicit):

5.1 *In Vitro* Model One Introduction

This is an implicit model showing the feedbacks between CGP and IGF-1 in a cell culture situation (outside of the body). The F and G terms (also used in the *in vivo* model) allow us to implicitly show CGP regulating IGF-1 through feedbacks to the IGFBPs and IGF-1 receptors.

This model involves using the *in vivo* parameters and altering these to fit the cell culture data by using nonlinear least squares. One extra compartment is added to this model to represent cell number (see Figure 29). Before fitting to the data, it is useful to see if the model can qualitatively reproduce the *in vitro* experiments. Next MATLAB is used (Fminsearch) until the SSE values converge for our best parameter estimations. For a glossary of the parameter values see Table 14 and for a glossary of the $\boldsymbol{q}$ variables see Table 15.

Parameter	Description
k_{ij}	Rate constant, to compartment i from j (min^{-1}) where zero is outside the system (min^{-1})
K	Rate of IGF-1 induced cell growth (cell min^{-1})
K_2	IGF-1 half maximal cell growth (nmol L^{-1})
M_1	Rate constant in feedback term F (min^{-1})
M_2	Rate constant in feedback term G (min^{-1})
L_1	IGF-1 half effect (nmol L^{-1})
L_2	IGF-1 half effect (nmol L^{-1})
a_1	Proportionality constant/weighting factor (dimensionless)
a_2	Proportionality constant/weighting factor (dimensionless)
a_3	Reciprical of the concentration of CGP when the sign of the switching term changes (nmol^{-1} L)
k_{+1a}	Association rate constant (IGFBPs and IGF-1) (nmol^{-1} min^{-1} L)
k_{+1b}	Association rate constant (receptor and IGF-1) (nmol^{-1} min^{-1} L)
k_{-1a}	Dissociation rate constant (IGFBPs and IGF-1) (min^{-1})
$R_{a,1}$	IGFBPs production rate (nmol min^{-1} L^{-1})
$R_{a,2}$	IGF-1 production rate + infusion rate (nmol min^{-1} L^{-1})
$R_{a,5}$	Receptor production rate (nmol min^{-1} L^{-1})
$R_{a,6}$	CGP production rate + infusion rate (nmol min^{-1} L^{-1})

Table 14: Glossary of the implicit *in vitro* model one and two parameters

Variable	Description
q_1	Concentration of free IGFBPs (nmol L^{-1})
q_2	Concentration of free IGF-1 (nmol L^{-1})
q_3	Concentration of bound IGF-1/IGFBPs (nmol L^{-1})
q_4	Concentration of receptor bound IGF-1 (nmol L^{-1})
q_5	Concentration of IGF-1 receptors (nmol L^{-1})
q_6	Concentration of CGP (nmol L^{-1})
q_7(data1)	Cell number/absorbance for IGF-1 only treatment (cell)
q_7(data2)	Cell number/absorbance for CGP only treatment (cell)
q_7(data3)	Cell number/absorbance for combination one treatment (cell)
q_7(data4)	Cell number/absorbance for combination two treatment (cell)

Table 15: Glossary of the implicit *in vitro* model one and two variables

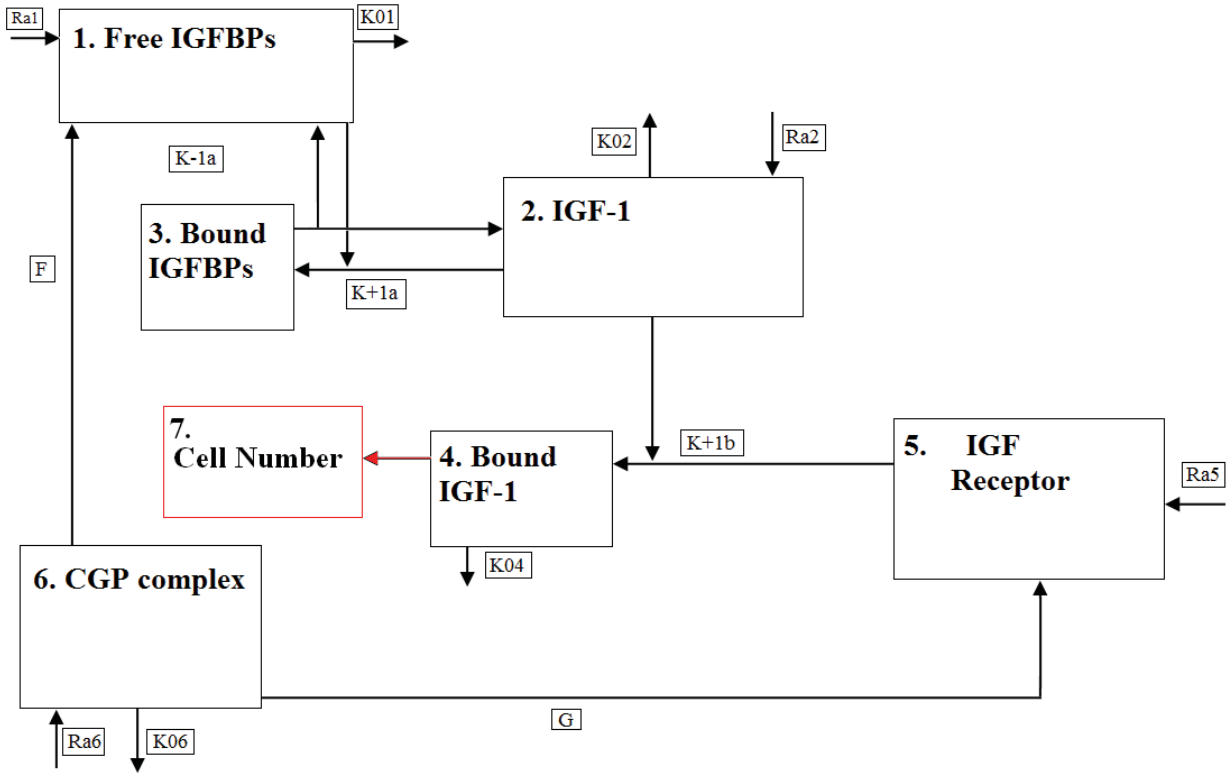

Figure 29: Schematic diagram of the seven concentration compartments in the first *in vitro* model (implicit). Each box represents a compartment, and the arrows represent transport between compartments. Red indicates the latest changes to the model. The new q_7 term represents the cell number levels in the cell culture (*in vitro*) experiments.

5.2 *In Vitro* Model One Equations

The same equations were used as those in the *in vivo* model, with the exceptions that k_{62} was set to zero and an extra differential equation was added to represent the cell growth. Cell number was assumed to be proportional to the cell absorbance measured in the experiments. Three equations were compared to find which described the effect of IGF-1 treatment on cell number the best.

The equations which were compared were: $q = At + b$, $q = \frac{At}{B+t}$, and $q = \frac{At}{B+t} + C$, where q represents cell number after 6 days incubation, and t represents the IGF-1 treatment (which is converted into nM).

To find the best suited equations from these options, we first looked at finding parameter values for each case using nonlinear optimisation (finding the lowest SSE value). To do this we used Fminsearch and plotted the fit for each (see Figure 30-32).

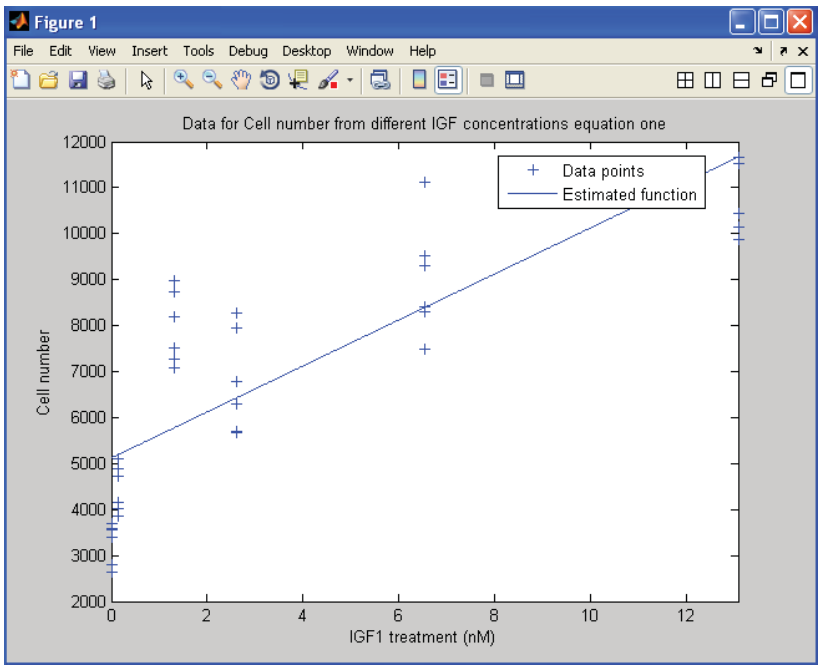

Figure 30: Equation one: $q = At + b$, q=cell number and t=IGF-1 treatment. Where parameter calibration using IGF-1 only data is done to produce parameter estimation. The resulting graph is plotted against the data points (+) and then the R^2 (0.70) is calculated. The serum free control experiments (0 nM IGF-1 treatment) contain unknown amounts of basal IGF-1.

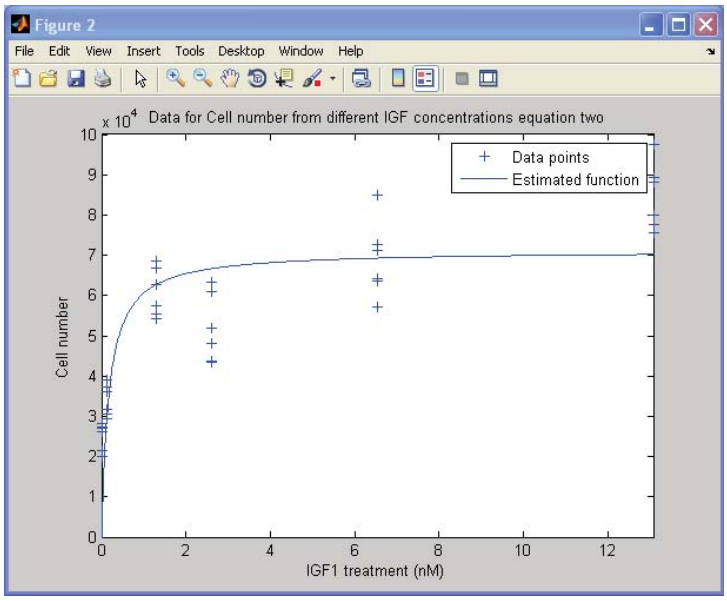

Figure 31: Equation two: $q = \frac{At}{B+t}$, q=cell number and t=IGF-1 treatment. Where parameter calibration using IGF-1 only data is done to produce parameter estimation. The resulting graph is plotted against the data points (+) and then the R^2 (0.71) is calculated. The serum free control experiments (0 nM IGF-1 treatment) contain unknown amounts of basal IGF-1.

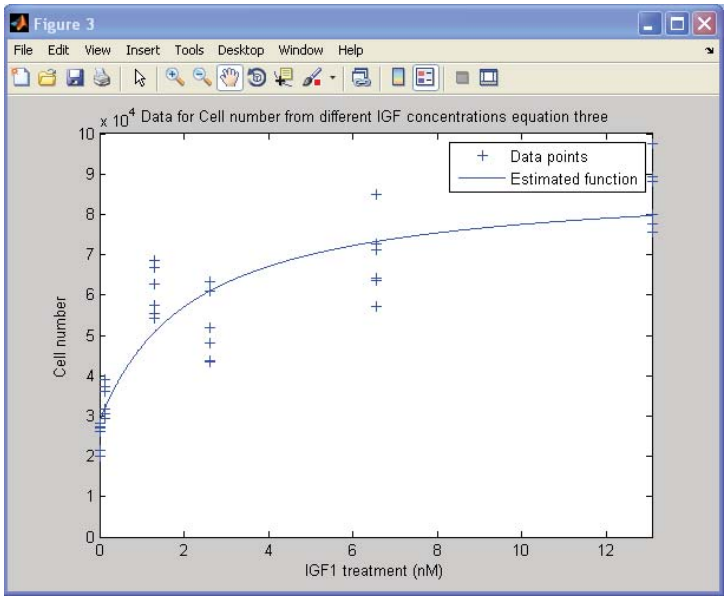

Figure 32: Equation three: $q = \frac{At}{B+t} + C$, q=cell number and t=IGF-1 treatment. Where parameter calibration using IGF-1 only data is done to produce parameter estimation. The resulting graph is plotted against the data points (+) and then the R^2 (0.82) is calculated. The serum free control experiments (0 nM IGF-1 treatment) contain unknown amounts of basal IGF-1.

Looking at these graphs we can see that equation two (two parameter model in Figure 31) and equation three (three parameter model in Figure 32) fit better than equation one (two parameter model in Figure 30). Equation two is a special case of equation three (C=0). Equation one is also a limiting case of equation three (when B is large). Therefore, of the three candidate models, equation three provides the most general description of growth. The variance-covariance matrix, calculated for each model, allows us to obtain standard errors for the estimated model parameters and see how the parameters depend on each other. This process (including running Fminsearch to find approximate parameter values) was done for each of the three options. The resulting parameter values and variance-covariance matrix for each equation are shown in Tables 16-18.

$q = At + b$	beta one (A)	beta two (B)
beta one (A)	185254.71	-730620.64
beta two (B)	-730620.64	6860968.98

Table 16: Equation one variance covariance matrix (A=3830.48 and B=39152.89)

$q = \frac{At}{B+t}$	beta one (A)	beta two (B)
beta one (A)	14741164.09	139.61
beta two (B)	139.61	0.0045

Table 17: Equation two variance covariance matrix (A=71142.26 and B=0.17)

$q = \frac{At}{B+t} + C$	beta one (A)	beta two (B)	beta three (C)
beta one (A)	38663879.94	3097.85	-4806723.50
beta two (B)	3097.85	0.663	1185.38
beta three (C)	-4806723.50	1185.38	9054668.97

Table 18: Equation three variance covariance matrix(A=59596.03 and B=2.22 and C=28751.95)

From Table 18, C = 28752 $\pm$ $\sqrt{9054669}$ = 28752 $\pm$ 3009. This means that C is significantly greater than zero (i.e. cells grow if you do not add any IGF-1). Because IGF-1 is a prerequisite for cell growth (i.e. if the concentration of IGF-1 is zero in the growth media then the cells do not grow), this implies that there is a basal level of IGF-1 in the growth media. However, the serum free control experiments contained an unknown amount of basal IGF-1 (inherent IGF-1 present in the cells). Model three, which provides the most general description of growth, was used to describe the relationship between t (IGF-1 treatment) and cell number. From making use of the transformation

q_4=t+d (i.e. the concentration in the media is the sum of the applied IGF-1 (t) and the basal IGF-1 (d)), the biological constraint that $\frac{dq_7}{dt}$=0 when q_4=0, that B is suitably large, and the assumption that the concentration of receptor bound IGF-1 is proportional to the concentration of IGF-1, allows us to select model two for describing the relationship between q_4 and $\frac{dq_7}{dt}$.

The equations for the *in vitro* model one (implicit), where q_7 is shown in red can be seen in Equations 37-43.

$$\frac{dq_1}{dt} = -k_{01}q_1 - k_{+1a}q_1q_2 + k_{-1a}q_3 + R_{a,1} + \frac{M_1q_4^2}{L_1^2+q_4^2}q_6 \tag{37}$$

$$\frac{dq_2}{dt} = -k_{02}q_2 - k_{+1a}q_1q_2 + k_{-1a}q_3 - k_{+1b}q_5q_2 + R_{a,2} \tag{38}$$

$$\frac{dq_3}{dt} = k_{+1a}q_1q_2 - k_{-1a}q_3 \tag{39}$$

$$\frac{dq_4}{dt} = -k_{04}q_4 + k_{+1b}q_5q_2 \tag{40}$$

$$\frac{dq_5}{dt} = -k_{04}q_5 - k_{+1b}q_5q_2 + R_{a,5} + (M_2 - \frac{M_2q_4^2}{L_2^2+q_4^2})q_6 \tag{41}$$

$$\frac{dq_6}{dt} = -k_{06}q_6 + R_{a,6} - a_1\frac{M_1q_4^2}{L_1^2+q_4^2}q_6 - a_2(M_2 - \frac{M_2q_4^2}{L_2^2+q_4^2})q_6 \tag{42}$$

$$\frac{dq_7}{dt} = \frac{Kq_4}{q_4+K_2} \tag{43}$$

5.3 *In Vitro* Model One Parameter Estimates

Most of the parameter estimates were the same parameter estimates used in the *in vivo* model (see Table 12). Some parameter estimates were left assumed and others were then fit to data using nonlinear least squares. The MATLAB function 'Fminsearch' was used to obtain a vector of parameters which minimised the SSE of the model compared to the data (MATLAB, 2009).

The assumed parameter and initial value estimates are based on a combination of Table 12 and manually changing the parameters while looking at the graphs against the data. Parameter and initial values which are assumed are in Table 19. Parameter and initial values which will be fit to data are listed in Table 20.

Parameter	Assumed Parameter Value
k_{01}	0.00289 (min^{-1})
k_{02}	0.0693 (min^{-1})
k_{04}	0.0820 (min^{-1})
k_{06}	0.0092 (min^{-1})
k_{-1a}	0.0255 (min^{-1})
k_{+1a}	0.00428 (nmol^{-1} min^{-1} L)
k_{+1b}	0.00116 (nmol^{-1} min^{-1} L)
$R_{a,1}$	0.245 (nmol min^{-1} L^{-1})
$R_{a,2}$	0.149 (nmol min^{-1} L^{-1})+IGF-1 treatment
Variable	Assumed Initial Value
q_1	71.1 (nmol L^{-1})
q_2	1.9 (nmol L^{-1})
q_3	15.3 (nmol L^{-1})
q_4	1.8 (nmol L^{-1})
q_5	68.8 (nmol L^{-1})

Table 19: Parameter and initial values which are assumed for the *in vitro* model one (Implicit) based on Tables 11-13.

Parameter	Initial Parameter Estimate
K	1000 (cell min^{-1})
K_2	100 (nmol L^{-1})
$R_{a,5}$	0 (nmol min^{-1} L^{-1})
$R_{a,6}$	0 (nmol min^{-1} L^{-1})+CGP treatment
M_1	10 (min^{-1})
M_2	115 (min^{-1})
L_1	1 (nmol L^{-1})
L_2	2 (nmol L^{-1})
a_1	0.01 (dimensionless)
a_2	1.61 (dimensionless)
Variable	Estimate of Initial Value
q_6	0.002 (nmol L^{-1})
q_7 data 1	1000 (cell)
q_7 data 2	10000 (cell)
q_7 data 3	10000 (cell)
q_7 data 4	10000 (cell)

Table 20: Estimated parameter and Initial values before being fit to data for the *in vitro* model one (Implicit).

5.4 *In Vitro* Model one Results

Four initial cell number values were used, one for each data set, as the initial cell number was not calculated and varied in the four experiments. The parameter and initial value estimates were substituted into the equations then K, K2 and the initial q_7 values (for each set of data) were all altered manually to get a closer resembling graph to the plot of the data. To obtain the best possible fit, some of the other fixed parameters had to be altered individually by checking the graphs until the data fit visually and then the nonlinear optimisation procedure was run.

Four sets of data were used, each with a different treatment type and each were run for six days with six replicates. The first is IGF-1 only, the second CGP only and the last two were different combinations of IGF-1 and CGP (see Table 21).

Type of Treatment	Level							
IGF-1 only (ng/ml):	0	1	10	20	50	100		
CGP only (nM):	0	1	5	10	20	50	100	
Combination one:								
IGF (ng/ml, note 10ng/ml=1.31nM):	10	10	10	10	10	10	10	10
CGP (nM):	0	0	1	5	10	20	50	100
Combination two:								
IGF (ng/ml, note 50ng/ml=6.54nM):	50	50	50	50	50	50	50	50
CGP (nM):	0	0	1	5	10	20	50	100

Table 21: Type of data used for fitting parameters (molar mass of IGF is approx 7649g/mol). Each treatment had six replications and was ran for six days (data not shown).

To fit the equations to the data, an estimate of q_7 after six days is calculated using numerical integration. Fminsearch adjusts the parameters being fitted in each iteration and produces a SSE value by using the error of each treatment estimate compared to the corresponding data. The raw data was used, no average values of replications were taken to produce SSE values. This stops the individual random factors having any influence over our results. Since the variance does not change with each treatment and each treatment was of the same scale, a weighted least squares method was not needed. An R^2 value (for each of the four groups) was calculated, as well as an overall calibration R^2 value. This gives a better indication of how well the model fits, compared to looking at the large, scale dependent SSE values. Since the R^2 value is independent of scale it is an objective measure for goodness of fit.

The final parameter and initial values which were assumed and the parameter and initial values which were fit to the data are shown in Tables 22-23:

Parameter	Final Parameter Value
k_{01}	0.00289 (min^{-1})
k_{02}	1 (min^{-1})
k_{04}	0.0685 (min^{-1})
k_{06}	0.0116 (min^{-1})
k_{-1a}	0.153 (min^{-1})
k_{+1a}	0.00481 (nmol^{-1} min^{-1} L)
k_{+1b}	0.00351 (nmol^{-1} min^{-1} L)
$R_{a,1}$	0.220 (nmol min^{-1} L^{-1})
$R_{a,2}$	0.131 (nmol min^{-1} L^{-1})+IGF-1 treatment
K	12.82 (cell min^{-1})
K_2	0.058 (nmol L^{-1})
$R_{a,5}$	0.0438 (nmol min^{-1} L^{-1})
$R_{a,6}$	0.000211 (nmol min^{-1} L^{-1})+CGP treatment
M_1	435557731.421 (min^{-1})
M_2	46245.295 (min^{-1})
L_1	1.421 (nmol L^{-1})
L_2	0.00106 (nmol L^{-1})
a_1	0.00000511 (dimensionless)
a_2	0.00749 (dimensionless)

Table 22: Final parameter values for *in vitro* model one which are assumed (top) and parameter values after the equations were fit to data (bottom).

Variable	Initial Value
q_1	61.48 (nmol L^{-1})
q_2	2.26 (nmol L^{-1})
q_3	15.27 (nmol L^{-1})
q_4	1.91 (nmol L^{-1})
q_5	17.59 (nmol L^{-1})
q_6	0.000000044 (nmol L^{-1})
q_7 data 1	1618.54 (cell)
q_7 data 2	132012.50 (cell)
q_7 data 3	134564.25 (cell)
q_7 data 4	151518.57 (cell)

Table 23: Initial values of *in vitro* model one (implicit) which were assumed (top) and initial values after being fit to data (bottom).

Using the parameter and initial values shown in Tables 22-23, the equations were numerically integrated to produce day six cell numbers. Then the resulting cell number values for each treatment were plotted in bar graphs and compared to the data bar graphs. These can be seen in Figures 33-36.

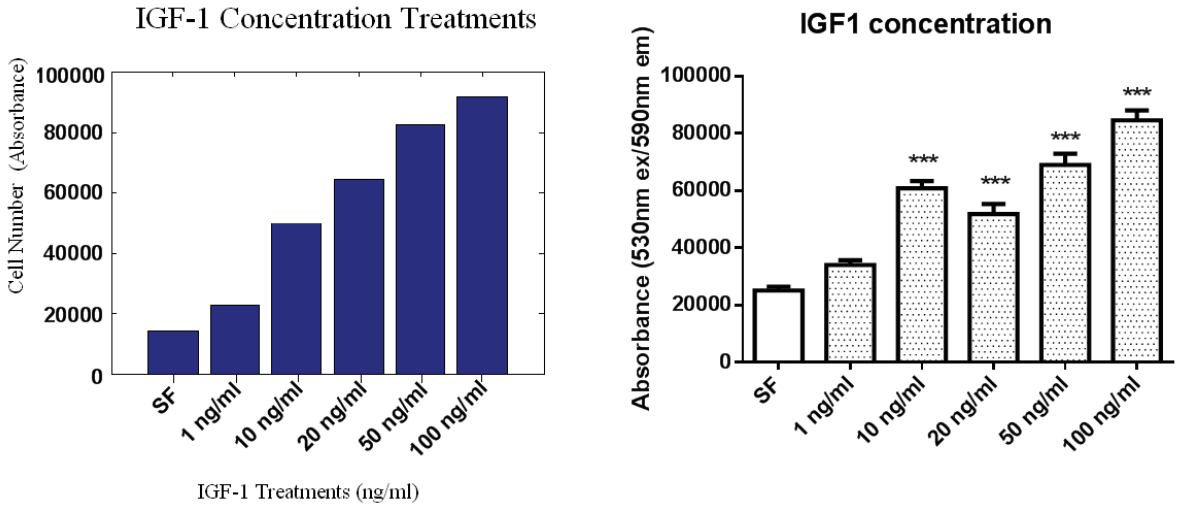

Figure 33: *In vitro* model one predictions for IGF-1 only treatments (left) and IGF-1 only treatment data, where error bars denote standard errors (right), R^2=0.8218. White indicates the control condition, grey indicates IGF-1 treatment and *** indicates p<0.001.

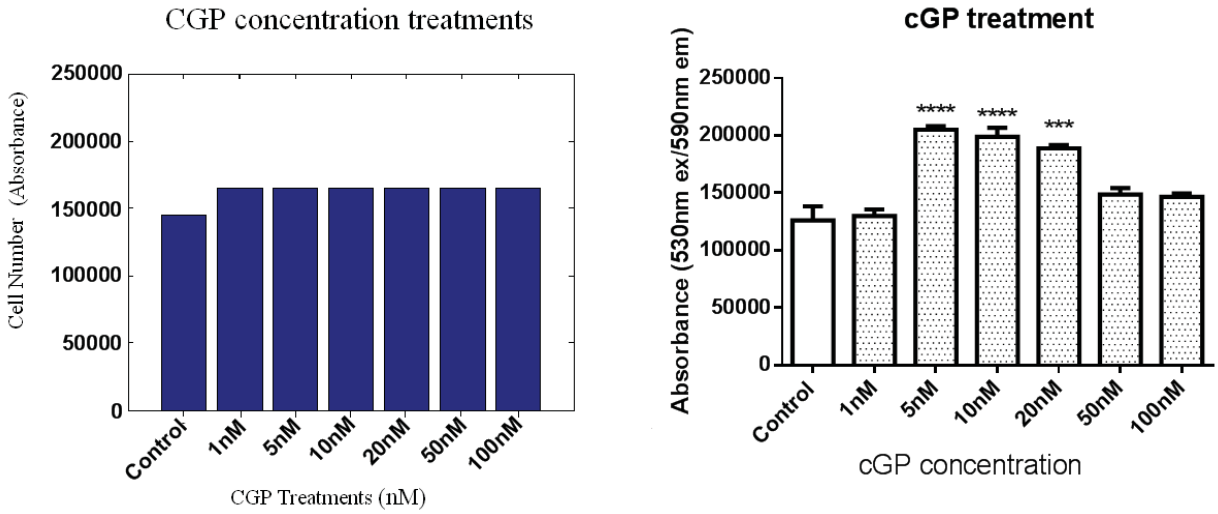

Figure 34: *In vitro* model one predictions for CGP only treatments (left) and CGP only treatment data, where error bars denote standard errors (right), R^2=0.1842. White indicates the control condition, grey indicates CGP only treatment, *** indicates p<0.001 and **** indicates p<0.0001.

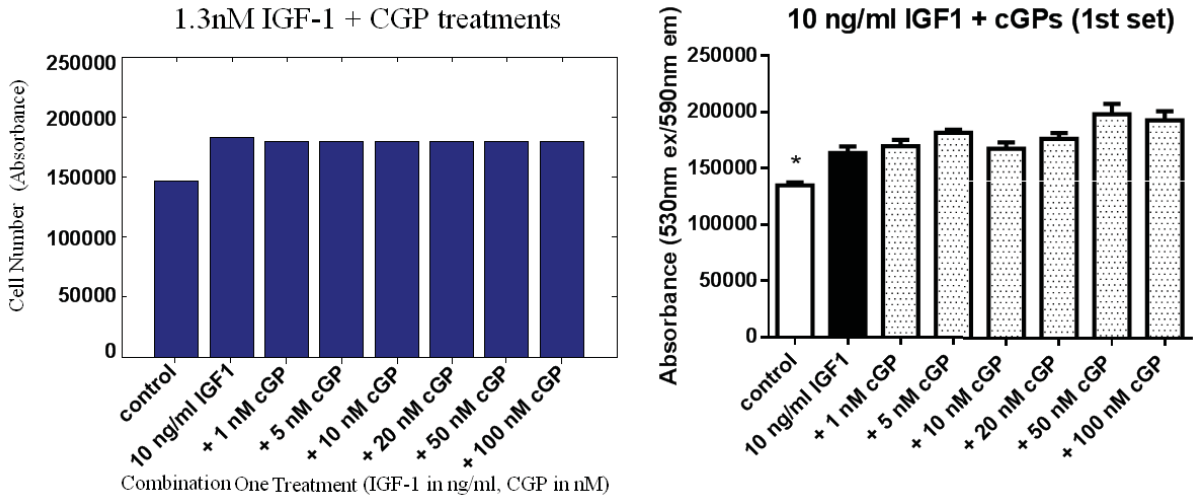

Figure 35: *In vitro* model one predictions for combination one treatments (left) and combination one treatment data, where error bars denote standard errors (right), R^2=0.3025. White indicates the control condition, black indicates IGF-1 only treatment, grey indicates IGF-1 treatment and * indicates p<0.05.

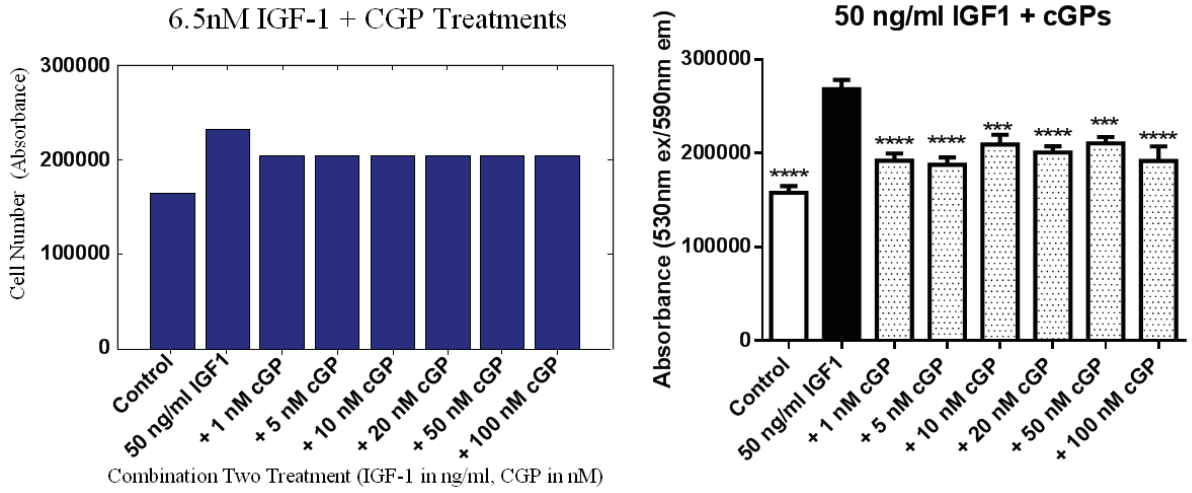

Figure 36: *In vitro* model one predictions for combination two treatments (left) and combination two treatment data, where error bars denote standard errors (right), R^2=0.5318. White indicates the control condition, black indicates IGF-1 only treatment, grey indicates combination of IGF-1 and CGP treatments, *** indicates p<0.001 and **** indicates p<0.0001.

The overall calibration R^2 value was 0.8352. Although the IGF-1 only treatment produced very similar results to the data, the model did not represent CGP treatments very well. The model did not show a reduction in cell number levels for higher concentrations of CGP being added (see Figure 34).

5.5 *In Vitro* Model Two Introduction

Model one failed to show the reduction in cell number levels for higher concentrations of added CGP (see Figure 34). It was revised slightly to show this effect by introducing a quadratic term (see Equations 41 and 42), q_6 became q_6-$a_3q_6^2$ at the end of the G term. By introducing the quadratic term into Equation 42, it allows the value of q_6-$a_3q_6^2$ to be negative when q_6 is large and positive when q_6 is small (the opposite for Equation 41). Therefore a large treatment of CGP (e.g. 100nM) would result in the quadratic term reducing the amount of CGP, q_6, and increasing the amount of free receptors, q_5. This would mean that more free IGF-1, q_2, can bind to the free receptors, q_5, causing more receptor bound IGF-1, q_4. This increase in receptor bound IGF-1 would increase the cell number level. See Figure 29 for model diagram and Tables 14-15 for a glossary of parameters and variables.

5.6 *In Vitro* Model Two Equations

The *in vitro* model two equations can be seen in Equations 44-50, where the most recent changes are shown in red.

$$\frac{dq_1}{dt} = -k_{01}q_1 - k_{+1a}q_1q_2 + k_{-1a}q_3 + R_{a,1} + \frac{M_1q_4^2}{L_1^2+q_4^2}q_6 \tag{44}$$

$$\frac{dq_2}{dt} = -k_{02}q_2 - k_{+1a}q_1q_2 + k_{-1a}q_3 - k_{+1b}q_5q_2 + R_{a,2} \tag{45}$$

$$\frac{dq_3}{dt} = k_{+1a}q_1q_2 - k_{-1a}q_3 \tag{46}$$

$$\frac{dq_4}{dt} = -k_{04}q_4 + k_{+1b}q_5q_2 \tag{47}$$

$$\frac{dq_5}{dt} = -k_{04}q_5 - k_{+1b}q_5q_2 + R_{a,5} + (M_2 - \frac{M_2q_4^2}{L_2^2+q_4^2})(q_6 - a_3q_6^2) \tag{48}$$

$$\frac{dq_6}{dt} = -k_{06}q_6 + R_{a,6} - a_1\frac{M_1q_4^2}{L_1^2+q_4^2}q_6 - a_2(M_2 - \frac{M_2q_4^2}{L_2^2+q_4^2})(q_6 - a_3q_6^2) \tag{49}$$

$$\frac{dq_7}{dt} = \frac{Kq_4}{q_4+K_2} \tag{50}$$

5.7 *In Vitro* Model Two Results

The parameter values and initial conditions which came from fitting the new equations can be seen in Table 24 and Table 25, respectively:

Parameter	Final Parameter Value
k_{01}	0.00289 (min^{-1})
k_{02}	1 (min^{-1})
k_{04}	0.0685 (min^{-1})
k_{06}	0.0116 (min^{-1})
k_{-1a}	0.153 (min^{-1})
k_{+1a}	0.00481 (nmol^{-1} min^{-1} L)
k_{+1b}	0.00351 (nmol^{-1} min^{-1} L)
$R_{a,1}$	0.220 (nmol min^{-1} L^{-1})
$R_{a,2}$	0.131 (nmol min^{-1} L^{-1})+IGF-1 treatment
K	10.67 (cell min^{-1})
K_2	0.0449 (nmol L^{-1})
$R_{a,5}$	0.067 (nmol min^{-1} L^{-1})
$R_{a,6}$	4.57e-14 (nmol min^{-1} L^{-1})+CGP treatment
M_1	858701056.15 (min^{-1})
M_2	623521.56 (min^{-1})
L_1	3.19 (nmol L^{-1})
L_2	0.00010 (nmol L^{-1})
a_1	0.00000032 (dimensionless)
a_2	0.000010 (dimensionless)
a_3	0.00013 (nmol^{-1} L)

Table 24: Final parameter values for *in vitro* model two (implicit) with quadratic q_6 term added, which were assumed (top) and parameter values which were fit to data (bottom).

Variable	Initial Value
q_1	61.48 (nmol L^{-1})
q_2	2.26 (nmol L^{-1})
q_3	15.27 (nmol L^{-1})
q_4	1.91 (nmol L^{-1})
q_5	17.59 (nmol L^{-1})
q_6	0.00000026 (nmol L^{-1})
q_7 data 1	1401.49 (cell)
q_7 data 2	137773.42 (cell)
q_7 data 3	137310.85 (cell)
q_7 data 4	159260.14 (cell)

Table 25: Initial values for *in vitro* model two (implicit) with quadratic q_6 term added, which were assumed (top) and initial values which were fit to data (bottom).

Once again the final parameter and initial values were plugged into the equations. The equations were numerically integrated to produced day six cell number values. The cell number values from each treatment type were then plotted in bar graphs and the resulting treatment plots can be seen in Figures 37-40 alongside the data plots.

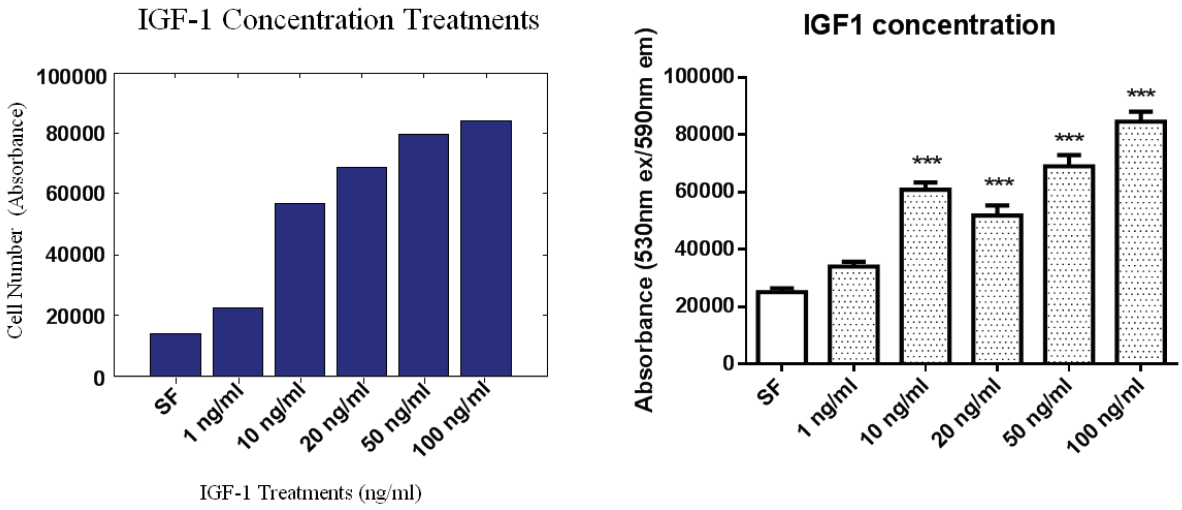

Figure 37: *In vitro* model two predictions IGF-1 only treatments (left) and IGF-1 only treatment data, where error bars denote standard errors (right), R^2=0.8023. White indicates the control condition, grey indicates IGF-1 treatment and *** indicates p<0.001.

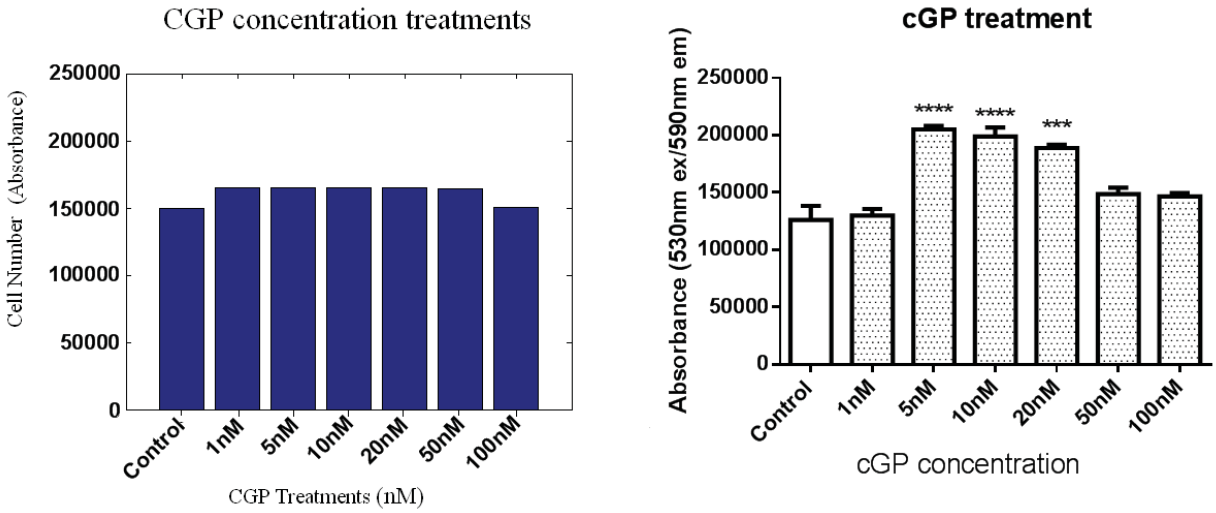

Figure 38: *In vitro* model two predictions CGP only treatments (left) and CGP only treatment data, where error bars denote standard errors (right), R^2=0.2220. White indicates the control condition, grey indicates CGP only treatment, *** indicates p<0.001 and **** indicates p<0.0001.

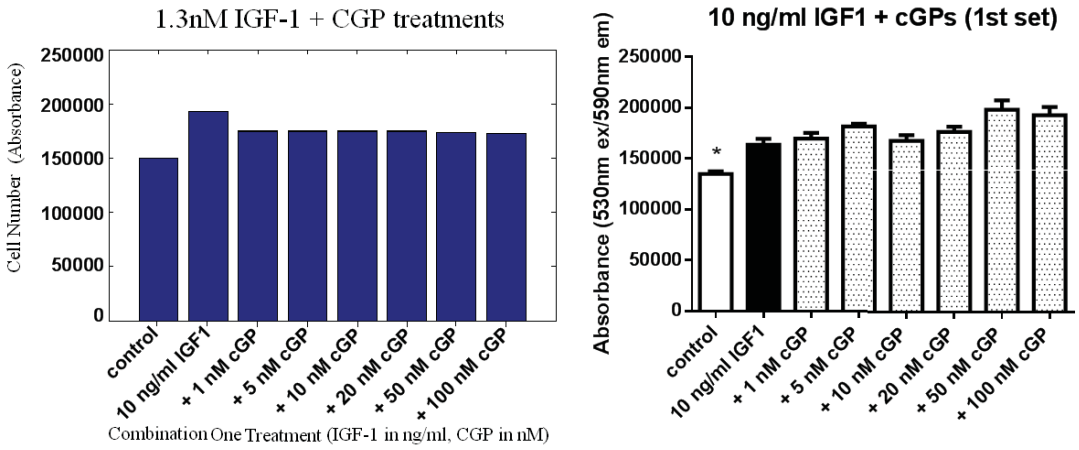

Figure 39: *In vitro* model two predictions for combination one treatments (left) and combination one treatment data, where error bars denote standard errors (right), R^2=0.1365. White indicates the control condition, black indicates IGF-1 only treatment, grey indicates IGF-1 treatment and * indicates p<0.05.

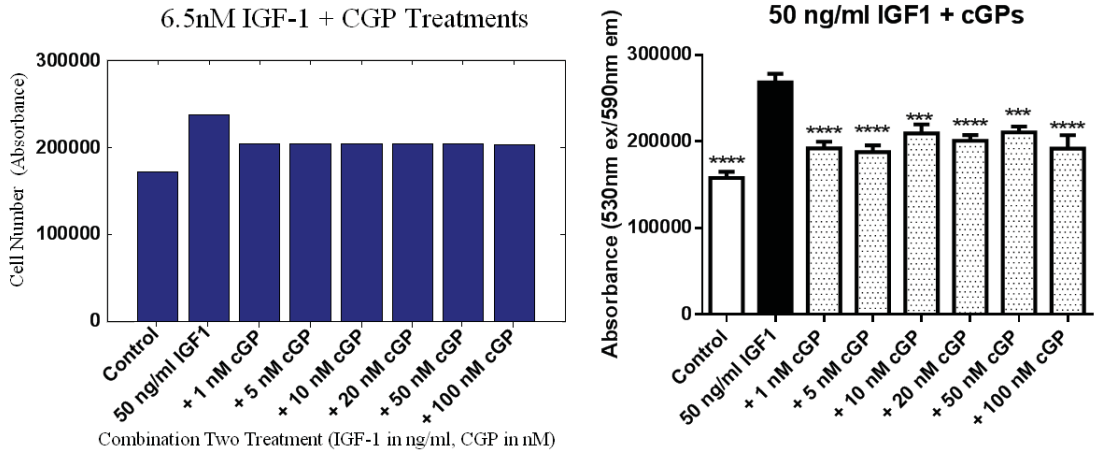

Figure 40: *In vitro* model two predictions combination two treatments (left) and combination two treatment data, where error bars denote standard errors (right), R^2=5901. White indicates the control condition, black indicates IGF-1 only treatment, grey indicates combination of IGF-1 and CGP treatments, *** indicates p<0.001 and **** indicates p<0.0001.

This model has a calibration R^2 squared value of 0.8319, compared to the calibration R^2 of 0.8352 earlier. Although the R^2 is slightly lower, the plots now match the data plots more closely for all of the different treatments (instead of IGF-1 only treatments alone). There is now a reduction in cell number for large CGP treatments (see Figure 38).

5.8 Discussion of *In Vitro* Model One and Two (Implicit)

An unknown amount of basal IGF-1 (cell growth over time with no added treatments) was present in the serum free control experiments. The suitability of three equations to represent cell growth in response to IGF-1 treatments was examined. The compared equations were: q=At+B, $q = \frac{At}{B+t}$ and $q = \frac{At}{B+t}$+C, where t is added IGF-1 treatments (does not include basal IGF-1). The equation chosen to represent cell number in our model was $q = \frac{At}{B+t} + C$, which includes the first two models as special (limiting) cases. After applying the constraints and transformation of variables to this model, the relationship between q_4 and $\frac{dq_7}{dt}$ is described by model two.

The two implicit models we looked at produced similar results with calibration R^2 values of 0.8352 and 0.8319 respectively. Both models represented the IGF-1 only treatments and combination two treatments reasonably well. The first model did not portray the CGP only treatment very accurately for high doses of CGP. There was a decrease in cell number for high CGP treatment levels in this set of data. The improved model was introduced for this purpose, to represent the 'bell shaped' curve seen in the data by replacing the q_6 term (in the fifth and sixth ODEs, see Equations 41 and 42) with $q_6 - a_3 q_6^2$. This term means that for large CGP levels the $-a_3 q_6^2$ term dominates, introducing a negative term to the fifth ODE (Equation 41). This has the effect of decreasing q_5 (free receptor) levels, which has the effect of reducing q_4 (receptor bound IGF-1) levels shown in the comparative graph (see Figure 38) as this means q_7 (cell number) levels are reduced. For this set of data the second improved model seemed to fit better, however there is variability between other experiments of the same kind. Some data sets do not show this 'bell shaped' effect occurring until the CGP dosage levels are much higher (approx 1000nM, Guan et al., 2012).

6 *In Vitro* Model Three and Four (Explicit):

6.1 *In Vitro* Model Three Introduction

This explicit model directly shows the competitive binding between CGP and IGF-1 for free IGFBPs in a cell culture situation. CGP has a similar binding site to IGF-1 as it was derived from IGF-1, we can therefore include a pool of CGP bound to IGFBPs (pool 8, see Figure 41). CGP does not bind to the IGF-1 receptors. This model involved using approximated parameters and altering them by fitting to the cell culture data through nonlinear regression to obtain the best values for the model. The previous implicit model does not include mechanisms of interaction between CGP, IGFBPs and IGF-1 receptors. During the course of this thesis some new mechanisms of interaction were discovered. The first of which is the competitive binding between CGP and IGF-1 for IGFBPs. The goal of this model is to investigate the role of this mechanism in the effect of CGP on IGF-1 induced cell growth. For a glossary of parameters and variables see Tables 26-27.

Variable	Description
q_1	Concentration of free IGFBPs (nmol L^{-1})
q_2	Concentration of free IGF-1 (nmol L^{-1})
q_3	Concentration of bound IGF-1/IGFBPs (nmol L^{-1})
q_4	Concentration of receptor bound IGF-1 (nmol L^{-1})
q_5	Concentration of free IGF-1 receptors (nmol L^{-1})
q_6	Concentration of free CGP (nmol L^{-1})
q_7(data1)	Cell number/absorbance for IGF-1 only treatment (cell)
q_7(data2)	Cell number/absorbance for CGP only treatment (cell)
q_7(data3)	Cell number/absorbance for combination one treatment (cell)
q_7(data4)	Cell number/absorbance for combination two treatment (cell)
q_8	Concentration of bound IGFBPs/CGP (nmol L^{-1})
q_9	Concentration of free antibodies (nmol L^{-1})
q_{10}	Concentration of bound IGFBPs/antibodies (nmol L^{-1})

Table 26: Glossary of the explicit *in vitro* model three and four variables

Parameter	Description
k_{ij}	Rate constant, to compartment i from j, where zero is outside the system (min^{-1})
K	Rate of IGF-1 induced cell growth (cell min^{-1})
K_2	IGF-1 half maximal cell growth (nmol L^{-1})
k_{+1a}	Association rate constant (IGFBPs and IGF-1) ($nmol^{-1}$ min^{-1} L)
k_{+1b}	Association rate constant (receptor and IGF-1) ($nmol^{-1}$ min^{-1} L)
k_{+1c}	Association rate constant (CGP and IGFBPs) ($nmol^{-1}$ min^{-1} L)
k_{+1d}	Association rate constant (antibody and IGFBPs) ($nmol^{-1}$ min^{-1} L)
k_{-1a}	Dissociation rate constant (IGFBPs and IGF-1) (min^{-1})
k_{m1b}	Dissociation rate constant (receptors and IGF-1) (min^{-1})
k_{-1c}	Dissociation rate constant (CGP and IGFBPs) (min^{-1})
k_{-1d}	Dissociation rate constant (antibody and IGFBPs) (min^{-1})
$R_{a,1}$	IGFBPs production rate (nmol min^{-1} L^{-1})
$R_{a,2}$	IGF-1 production rate + infusion rate (nmol min^{-1} L^{-1})
$R_{a,5}$	Receptor production rate (nmol min^{-1} L^{-1})
$R_{a,6}$	CGP production rate + infusion rate (nmol min^{-1} L^{-1})

Table 27: Glossary of the explicit *in vitro* model three and four parameters

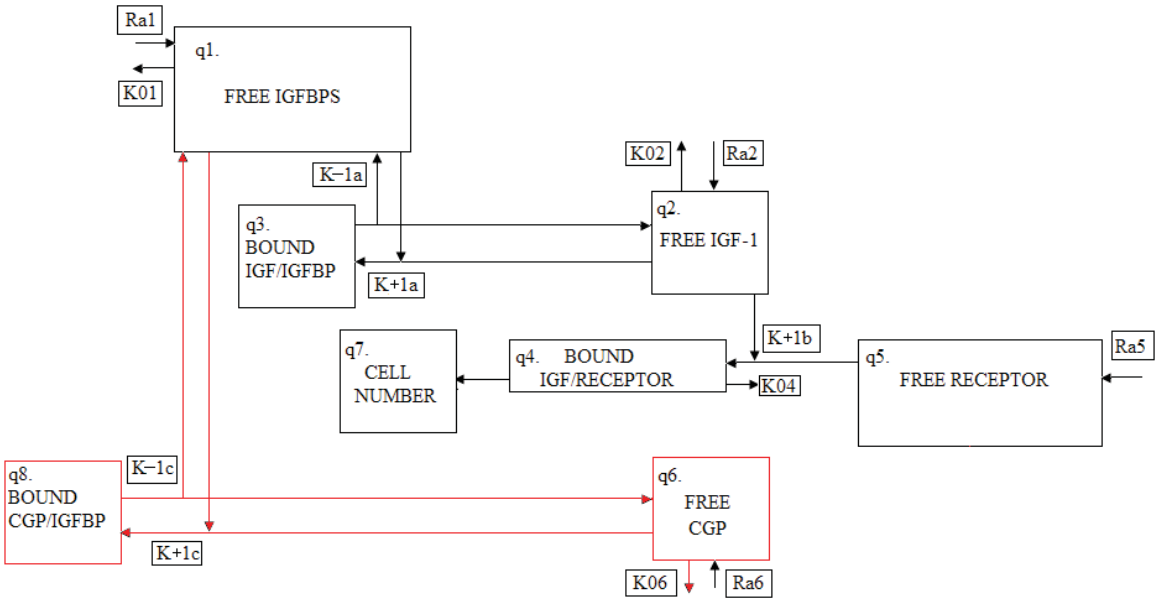

Figure 41: Schematic diagram of the eight concentration compartments in the third *in vitro* model (explicit). Each box represents a compartment, and the arrows represent transport between compartments. Where the red boxes and arrows represent the most recent changes. The eighth compartment was introduced to represent the competitive binding between IGF-1 and CGP for the binding proteins.

To demonstrate the biological aspect of competitive binding, used in this model, the affinities of IGF-1 and CGP for bovine serum albumin (BSA) were measured (data provided by Dr Jian Guan, Liggins Institute). BSA binds to IGF-1 and CGP and is likely to be similar to IGFBP-3 (used as a substitute in experiments). Figure 42, shows that the affinities of the BSA for IGF-1 and CGP are similar (equal concentrations of CGP/IGF-1 roughly halve the amount of bound IGF-1 compared to IGF-1 only). This demonstrates the biological aspect of competitive binding used in this model.

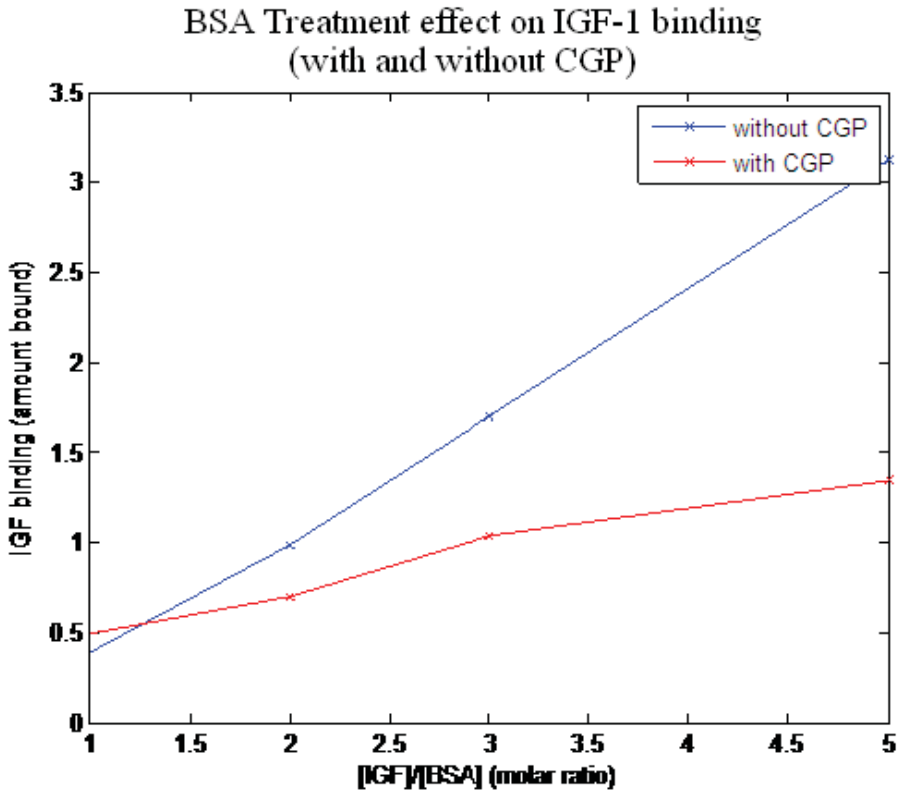

Figure 42: Graph of BSA influence over IGF-1 binding with and without CGP. Data provided by Dr Jian Guan (Liggins Institute). The red line is BSA treatment with CGP (equimolar with IGF-1) and the blue line is BSA treatment without CGP.

Similarly the trend has been shown to go in the opposite direction for binding of CGP to BSA in the absence and presence of IGF-1.

In this model we have eight compartments. The model directly incorporates the competitive binding between IGF-1 and CGP with the binding proteins (instead of through the previous F and G terms in the implicit models). The extra q_8 compartment shows how CGP takes up some of the available free IGFBPs (q_1) by binding to them so that the free IGF-1 (q_2) is not able to bind to the IGFBPs and is therefore more available to bind to the receptors. Model testing is done on a simplified version of this model using an independent data set.

6.2 *In Vitro* Model Three Equations

Our resulting equations can be seen in equations 51-58, where the terms coloured red represent the most recent changes. The feedback terms have been removed, instead CGPs influence on IGF-1 is shown directly through competitive binding (red terms).

$$\frac{dq_1}{dt} = -k_{01}q_1 + k_{-1a}q_3 - k_{+1a}q_2q_1 + R_{a,1} + k_{-1c}q_8 - k_{+1c}q_6q_1 \tag{51}$$

$$\frac{dq_2}{dt} = -k_{02}q_2 + k_{-1a}q_3 - k_{+1a}q_2q_1 - k_{+1b}q_2q_5 + R_{a,2} \tag{52}$$

$$\frac{dq_3}{dt} = -k_{-1a}q_3 + k_{+1a}q_2q_1 \tag{53}$$

$$\frac{dq_4}{dt} = -k_{04}q_4 + k_{+1b}q_2q_5 \tag{54}$$

$$\frac{dq_5}{dt} = -k_{04}q_5 - k_{+1b}q_2q_5 + R_{a,5} \tag{55}$$

$$\frac{dq_6}{dt} = -k_{06}q_6 + R_{a,6} + k_{-1c}q_8 - k_{+1c}q_6q_1 \tag{56}$$

$$\frac{dq_7}{dt} = \frac{Kq_4}{K_2 + q_4} \tag{57}$$

$$\frac{dq_8}{dt} = -k_{-1c}q_8 + k_{+1c}q_6q_1 \tag{58}$$

6.3 *In Vitro* Model Three Parameter Estimates

The assumed *in vitro* model three (explicit) parameters and initial values are in Table 28. These are estimated based on the final values from the first *in vitro* model parameters in Table 22-23 or modified versions of these by plotting the graph for a visual fit.

Parameter	Assumed Parameter Value
k_{01}	0.00289 (min^{-1})
k_{02}	0.1 (min^{-1})
k_{04}	0.0685 (min^{-1})
k_{06}	0.0116 (min^{-1})
k_{-1a}	0.1531 (min^{-1})
k_{+1a}	0.00481 (nmol^{-1} min^{-1} L)
k_{+1b}	0.00351 (nmol^{-1} min^{-1} L)
$R_{a,1}$	0.220 (nmol min^{-1} L^{-1})
$R_{a,2}$	0.131 (nmol min^{-1} L^{-1})+IGF-1 treatment
Variable	**Assumed Initial Value**
q_1	61.48 (nmol L^{-1})
q_2	2.263 (nmol L^{-1})
q_3	15.27 (nmol L^{-1})
q_4	1.91 (nmol L^{-1})
q_5	17.60 (nmol L^{-1})

Table 28: Assumed parameter and initial values for the *in vitro* model three (Explicit)

The initial value and initial parameter estimates for the third *in vitro* model (explicit) before being fit to data are in Table 29:

Parameter	Initial Parameter Estimate
K	1000 (cell min^{-1})
K_2	100 (nmol L^{-1})
k_{-1c}	0.0012 (min^{-1})
k_{+1c}	0.0035 (nmol^{-1} min^{-1} L)
$R_{a,5}$	0 (nmol min^{-1} L^{-1})
$R_{a,6}$	0 (nmol min^{-1} L^{-1})+CGP treatment
Variable	**Estimate of Initial Value**
q_6	0.002 (nmol L^{-1})
$q_7 data1$	1000 (cell)
$q_7 data2$	1000 (cell)
$q_7 data3$	1000 (cell)
$q_7 data4$	1000 (cell)
q_8	1 (nmol L^{-1})

Table 29: Parameter and initial value estimates for the third *in vitro* model (explicit)

6.4 *In Vitro* Model Three Results

The final parameter values from the third *in vitro* model (explicit) which were assumed and the parameter values which were fit to data, are shown in Table 30:

Parameter	Final Parameter Value
k_{02}	0.1 (min^{-1})
k_{04}	0.0685 (min^{-1})
k_{06}	0.0116 (min^{-1})
k_{-1a}	0.1531 (min^{-1})
k_{+1a}	0.00481 (nmol^{-1} min^{-1} L)
k_{+1b}	0.00351 (nmol^{-1} min^{-1} L)
$R_{a,1}$	0.220 (nmol min^{-1} L^{-1})
$R_{a,2}$	0.131 (nmol min^{-1} L^{-1})+IGF-1 treatment
K	898.06 (cell min^{-1})
K_2	3821.91 (nmol L^{-1})
k_{+1c}	0.00014 (nmol^{-1} min^{-1} L)
k_{-1c}	0.00086 (min^{-1})
$R_{a,5}$	3.37 (nmol min^{-1} L^{-1})
$R_{a,6}$	0.0016 (nmol min^{-1} L^{-1})+CGP treatment

Table 30: Parameter values for the third *in vitro* model (explicit) which were assumed (top) and parameter values which have been fit to data (bottom).

The initial values used in the third *in vitro* model (explicit) which were assumed and the initial values which have been fit to data, are shown in Table 31:

Variable	Initial Value
q_1	61.48 (nmol L^{-1})
q_2	2.263 (nmol L^{-1})
q_3	15.27 (nmol L^{-1})
q_4	1.91 (nmol L^{-1})
q_5	17.60 (nmol L^{-1})
q_6	621419.06 (nmol L^{-1})
$q_7 data1$	189.3 (cell)
$q_7 data2$	157916.2 (cell)
$q_7 data3$	136220.2 (cell)
$q_7 data4$	115754.5 (cell)
q_8	7116.0 (nmol L^{-1})

Table 31: Initial values for the third *in vitro* model (explicit) which were assumed (top) and initial values which have been fit to data (bottom).

Using these parameters the equations were numerically integrated to find day six cell number levels for each of the treatments. The following comparative graphs were produced (Figures 43-46):

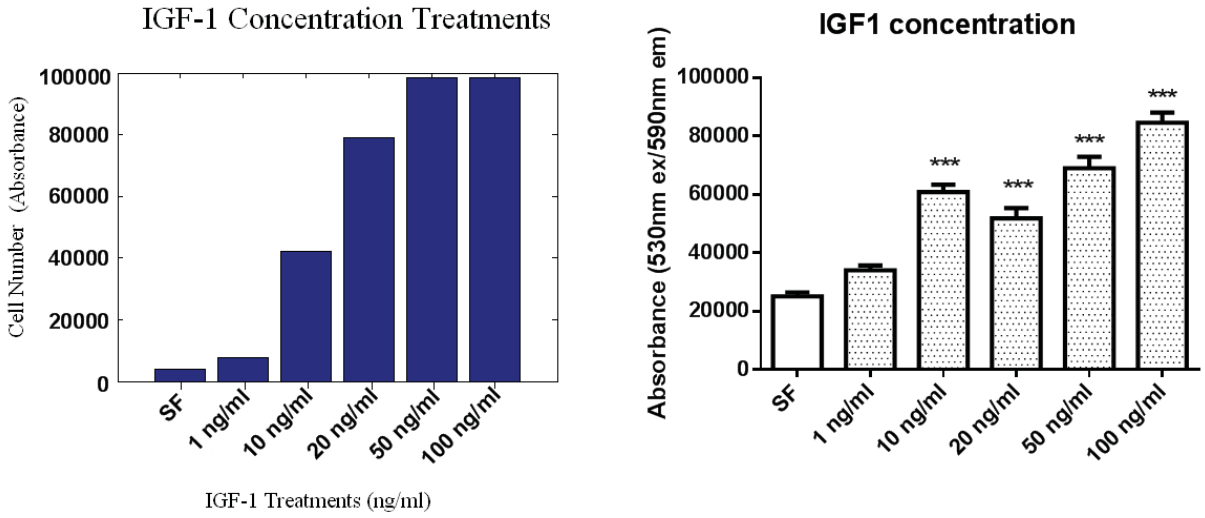

Figure 43: *In vitro* model three predictions for IGF-1 only treatments (left) and IGF-1 only treatment data, where error bars denote standard errors (right), R^2=0.7184. White indicates the control condition, grey indicates IGF-1 treatment and *** indicates p<0.001.

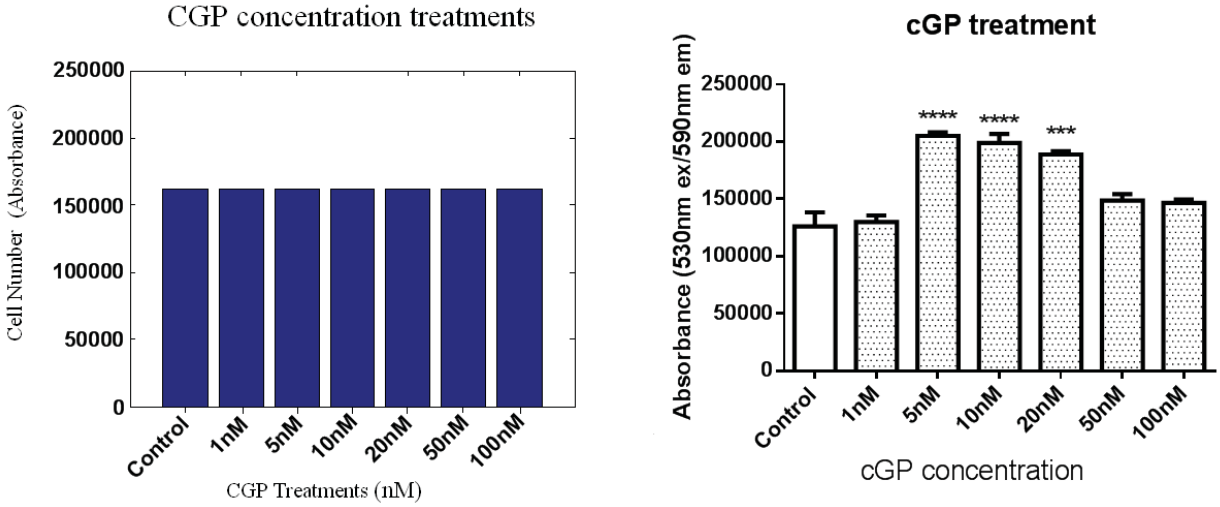

Figure 44: *In vitro* model three predictions for CGP only treatments (left) and CGP only treatment data, where error bars denote standard errors (right), R^2=0.1292. White indicates the control condition, grey indicates CGP only treatment, *** indicates p<0.001 and **** indicates p<0.0001.

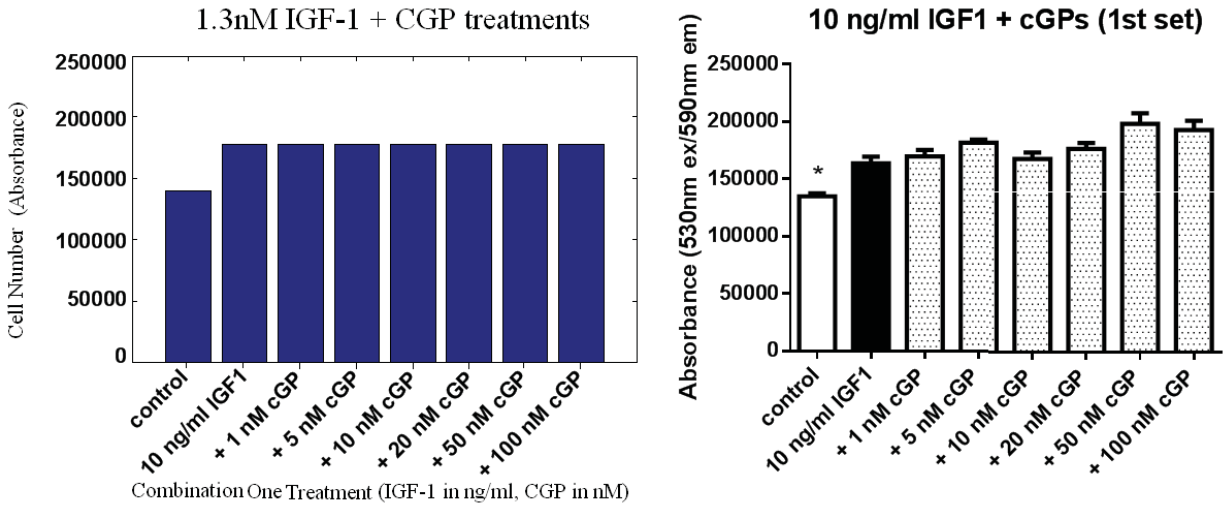

Figure 45: *In vitro* model three predictions for combination one treatments (left) and combination one treatment data, where error bars denote standard errors (right), R^2=0.3269. White indicates the control condition, black indicates IGF-1 only treatment, grey indicates IGF-1 treatment and * indicates p<0.05.

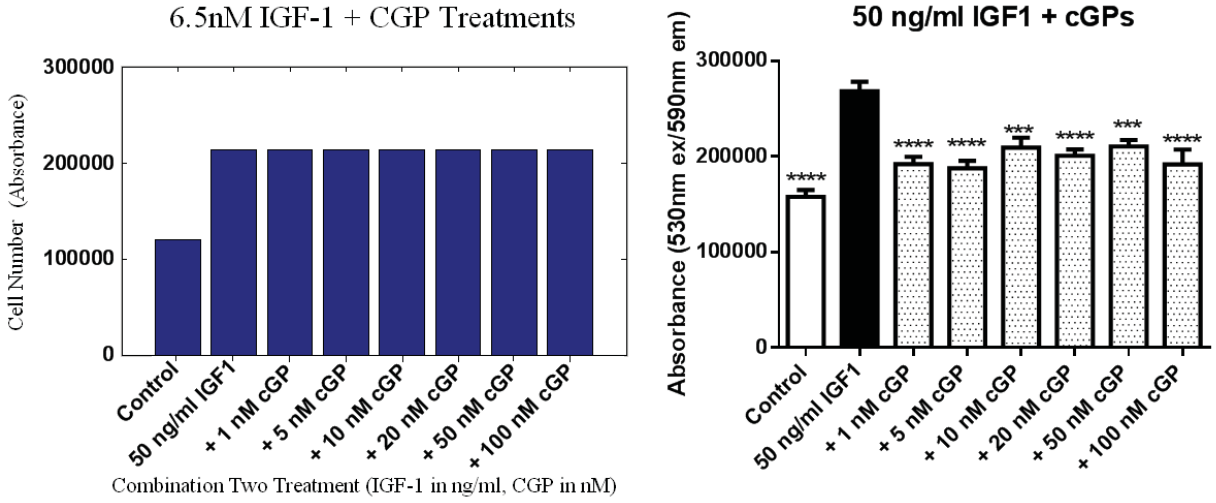

Figure 46: *In vitro* model three predictions for combination two treatments (left) and combination two treatment data, where error bars denote standard errors (right), R^2=0.2165. White indicates the control condition, black indicates IGF-1 only treatment, grey indicates combination of IGF-1 and CGP treatments, *** indicates p<0.001 and **** indicates p<0.0001.

The overall calibration R^2 value for this model was 0.7700. The IGF-1 treatment resembled the data to a degree (see Figure 43) but the graphs did not show any response to CGP treatments (see Figures 44-46).

Analytical steady state solutions to these equations were found (see Equations 59-63).

$$q_1 = \frac{R_{a,1}}{k_{01}} \tag{59}$$

$$q_2 = \frac{(R_{a,2} - R_{a,5})}{k_{02}} \tag{60}$$

$$q_3 = \frac{k_{+1a} R_{a,1} (R_{a,2} - R_{a,5})}{k_{02} k_{01} k_{-1a}} \tag{61}$$

$$q_4 = \frac{R_{a,5}}{k_{04}} \tag{62}$$

$$q_5 = \frac{R_{a,5} k_{02}}{k_{+1b} (R_{a,2} - R_{a,5})} \tag{63}$$

$$q_6 = \frac{R_{a,6}}{k_{06}} \tag{64}$$

$$q_8 = \frac{k_{+1c} R_{a,1} R_{a,6}}{k_{06} k_{01} k_{-1c}} \tag{65}$$

Since q_7 was just used to estimate the cell number measured in the data no steady state solution can be calculated for this. Of note, the ($R_{a,2}$-$R_{a,5}$) term in the denominator of the q_5 steady state equation (Equation 63) means that if $R_{a,5}$ is too large then q_5 goes to infinity (in other words the free receptors build up). This is not a problem in our situation because physiologically, $R_{a,5}$ has to be small. The main problem with our analytical steady state solutions was that the steady state of q_4 turned out to be independent of $R_{a,2}$ and $R_{a,6}$ (see Equation 62) and this explains the flat response observed in the model graphs.

6.5 *In Vitro* Model Four Introduction

The steady state solutions showed that q4 was independent of IGF-1 and CGP production rates. This is why no cell number response occurred in any of the CGP treatments in the third model. To get around this problem we introduced a simplified model (which may represent cell culture data better). In the cell culture there are constant amounts of receptors, IGFBPs and CGP, so by taking out all the R_a and k_{0n} terms we can fix these values to resemble the *in vitro* experiments. We added the k_{m1b} term to ensure q_4 does not accumulate, since the removal of the k_{04} causes q_4 to increase. See Figure 47 for the new model diagram.

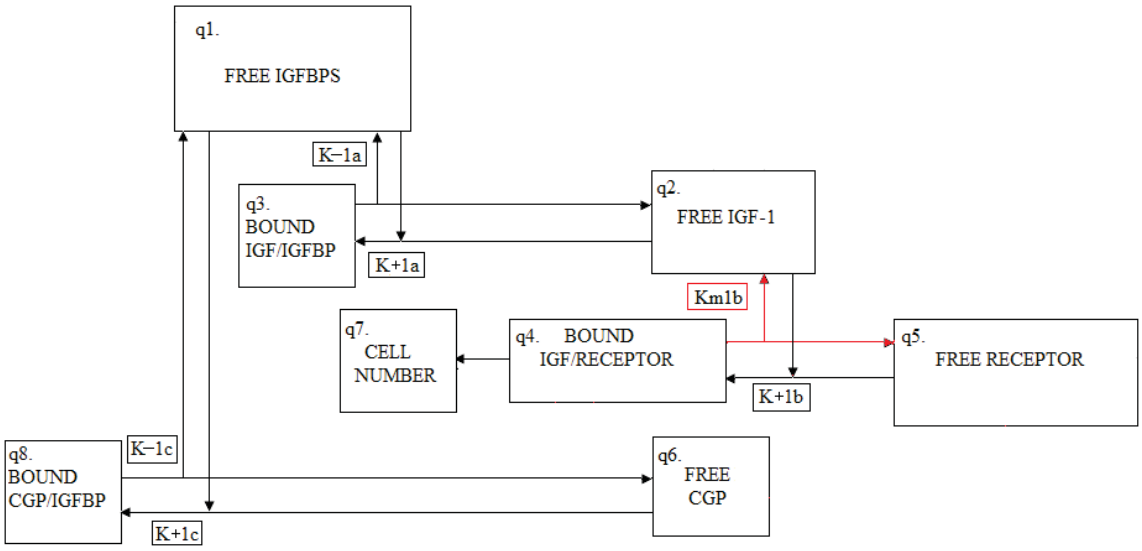

Figure 47: Schematic diagram of the eight concentration compartments in the fourth *in vitro* model (explicit). Each box represents a compartment, and the arrows represent transport between compartments. The red box and arrows represent the most recent change along with the removal of all the arrows which left the system.

6.6 *In Vitro* Model Four Equations

The changes made lead to the Equations 66-73. $R_{a,1}$ and $R_{a,5}$ have been removed. $R_{a,2}$ and $R_{a,6}$ are now zero if there is no IGF-1 or CGP treatment. All k_{0n} terms have been removed, and k_{m1b} (shown in red) has been added to stop the constant build up of receptor bound IGF-1 (q4).

$$\frac{dq_1}{dt} = k_{-1a}q_3 - k_{+1a}q_2q_1 + k_{-1c}q_8 - k_{+1c}q_6q_1 \tag{66}$$

$$\frac{dq_2}{dt} = k_{-1a}q_3 - k_{+1a}q_2q_1 - k_{+1b}q_2q_5 + k_{m1b}q_4 + R_{a,2} \tag{67}$$

$$\frac{dq_3}{dt} = -k_{-1a}q_3 + k_{+1a}q_2q_1 \tag{68}$$

$$\frac{dq_4}{dt} = k_{+1b}q_2q_5 - k_{m1b}q_4 \tag{69}$$

$$\frac{dq_5}{dt} = -k_{+1b}q_2q_5 + k_{m1b}q_4 \tag{70}$$

$$\frac{dq_6}{dt} = k_{-1c}q_8 - k_{+1c}q_1q_6 + R_{a,6} \tag{71}$$

$$\frac{dq_7}{dt} = \frac{Kq_4}{(K_2 + q_4)} \tag{72}$$

$$\frac{dq_8}{dt} = -k_{-1c}q_8 + k_{+1c}q_1q_6 \tag{73}$$

Next we set $q_1(0)$, $q_2(0)$, $q_5(0)$ and $q_6(0)$ to be fitting parameters and fixed previously fitted values. This resulted in fewer parameters which simplified the system. Before being fit to data, the initial value of $q_1(0)$ is set to be the total amount of binding proteins estimated to be in the system. The initial value of $q_2(0)$ is estimated to be all the IGF-1 that is in the system. Finally the initial value of $q_5(0)$ is set to be the total amount of receptors in the system.

6.7 *In Vitro* Model Four Results

Parameter estimates were made based on model three final parameters (Table 30). $q_3(0)$, $q_4(0)$ and $q_8(0)$ where set to zero. $q_1(0)$ was estimated as the total amount of IGFBPs, $q_2(0)$ was estimated as the total amount of IGF-1, $q_5(0)$ was estimated as the total amount of receptors and $q_6(0)$ was estimated as the total amount of CGP. The final parameter and initial values from the *in vitro* model four (explicit) are shown in Table 32 and 33, respectively.

Parameter	Final Parameter Value
K	1154.4 (cell min^{-1})
K_2	4530.4 (nmol L^{-1})
k_{-1a}	0.1531 (min^{-1})
k_{-1c}	0.15 (min^{-1})
$R_{a,2}$	0 (nmol min^{-1} L^{-1}) + IGF-1 treatment
$R_{a,6}$	0 (nmol min^{-1} L^{-1}) + CGP treatment
k_{+1a}	0.0031 (nmol^{-1} min^{-1} L)
k_{+1b}	0.00090 (nmol^{-1} min^{-1} L)
k_{+1c}	0.091 (nmol^{-1} min^{-1} L)
k_{m1b}	0.021 (nmol^{-1} min^{-1} L)

Table 32: Parameter values for the fourth *in vitro* model (explicit) which were assumed (top) and parameter values after being fit to data (bottom).

Variable	Initial Value
q_3	0 (nmol L^{-1})
q_4	0 (nmol L^{-1})
q_8	0 (nmol L^{-1})
q_1	9498.3 (nmol L^{-1})
q_2	1071.3 (nmol L^{-1})
q_5	29.4 (nmol L^{-1})
q_6	0.038 (nmol L^{-1})
$q_7 data1$	10708.5 (cell)
$q_7 data2$	113191.7 (cell)
$q_7 data3$	120009.4 (cell)
$q_7 data4$	146000.2 (cell)

Table 33: Initial values for the fourth *in vitro* model (explicit) which were assumed (top) and initial values after being fit to data (bottom).

The parameter estimates were substituted into the equations, these were then numerically integrated (using the initial values in Table 33) to produce day six results. The resulting cell number levels for each treatment were then plotted in bar graphs to compare to the data plots (see Figures 48-51).

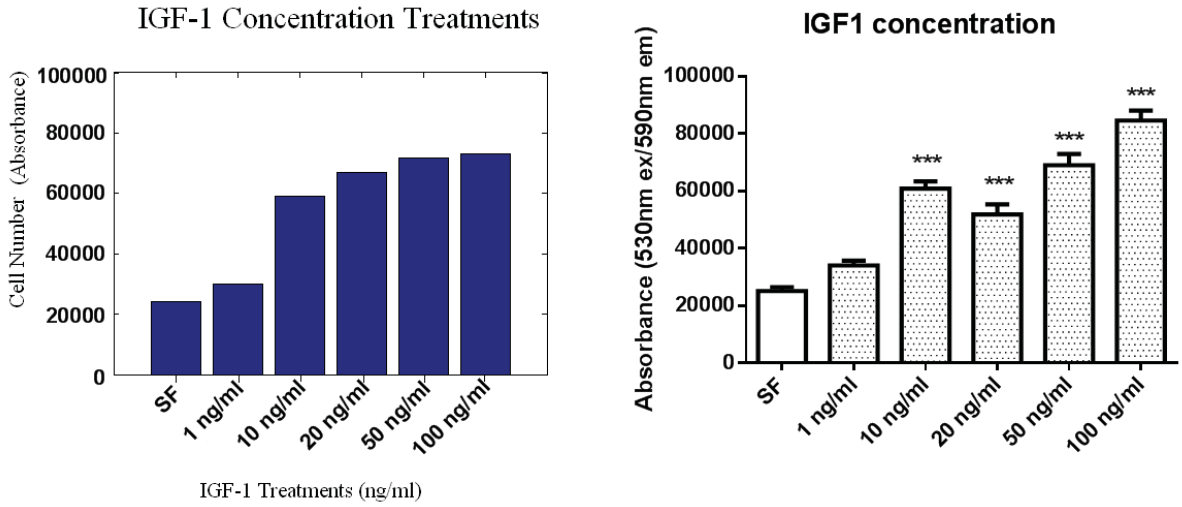

Figure 48: *In vitro* model four predictions for IGF-1 only treatments (left) and IGF-1 only treatment data, where error bars denote standard errors (right), R^2=0.7676. White indicates the control condition, grey indicates IGF-1 treatment and *** indicates p<0.001.

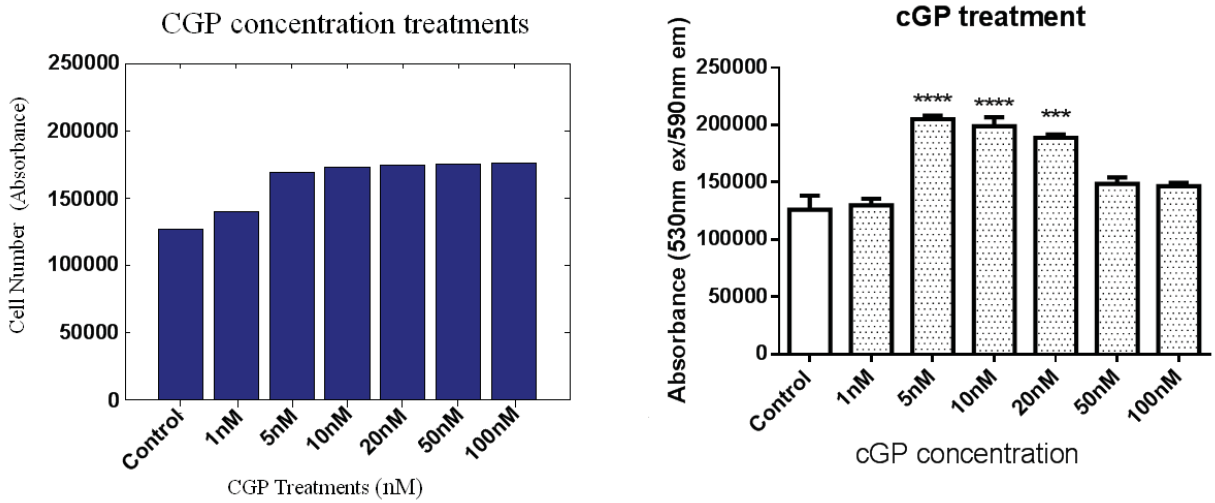

Figure 49: *In vitro* model four predictions for CGP only treatments (left) and CGP only treatment data, where error bars denote standard errors (right), R^2=0.2868 . White indicates the control condition, grey indicates CGP only treatment, *** indicates p<0.001 and **** indicates p<0.0001.

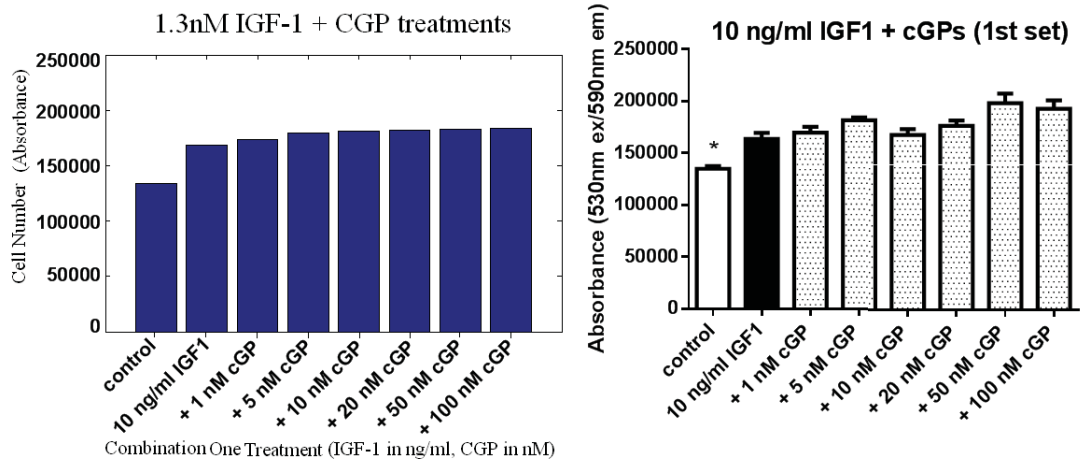

Figure 50: *In vitro* model four predictions for combination one treatments (left) and combination one treatment data, where error bars denote standard errors (right), R^2=0.4016. White indicates the control condition, black indicates IGF-1 only treatment, grey indicates IGF-1 treatment and * indicates p<0.05.

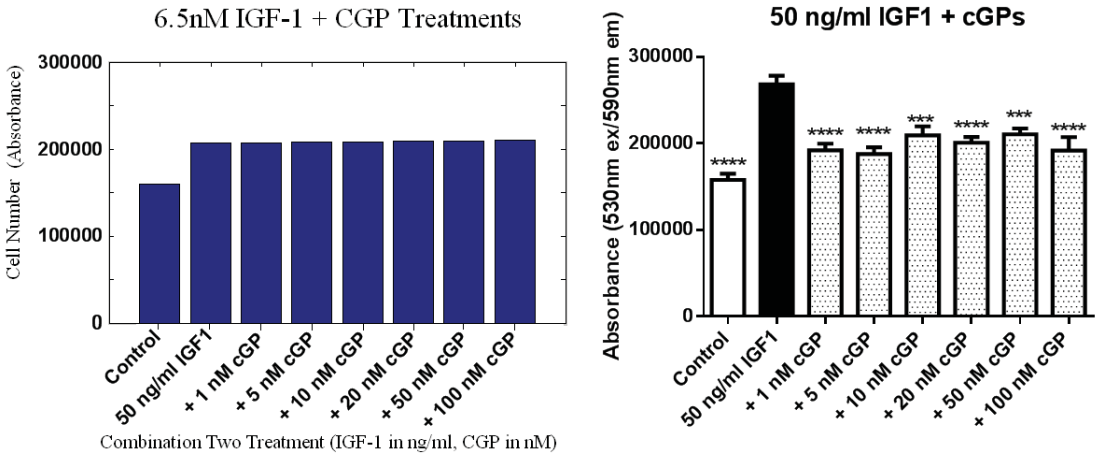

Figure 51: *In vitro* model four predictions for combination two treatments (left) and combination two treatment data, where error bars denote standard errors (right), R^2=0.1996. White indicates the control condition, black indicates IGF-1 only treatment, grey indicates combination of IGF-1 and CGP treatments, *** indicates p<0.001 and **** indicates p<0.0001.

Resulting from this change, CGP appeared to make the cells grow (see Figure 49), showing that there is now a CGP response. The IGF-1 only treatment also resembled the data more closely in this model compared to model three (see Figure 48). The overall calibration R^2 value was 0.8311 for this model. This result indicates the role of competitive binding between CGP and IGF-1 for binding proteins, in regulating cell growth.

6.8 Testing of *In Vitro* Model Four Against Independent Data Set

The independent data for model testing was data involving treatment with and without antibodies. These antibodies reduce the number of binding proteins in the system by binding to them themselves. To test the model an extra two compartments were added; one for free antibodies, and one for antibodies bound to IGFBPs (see Figure 52).

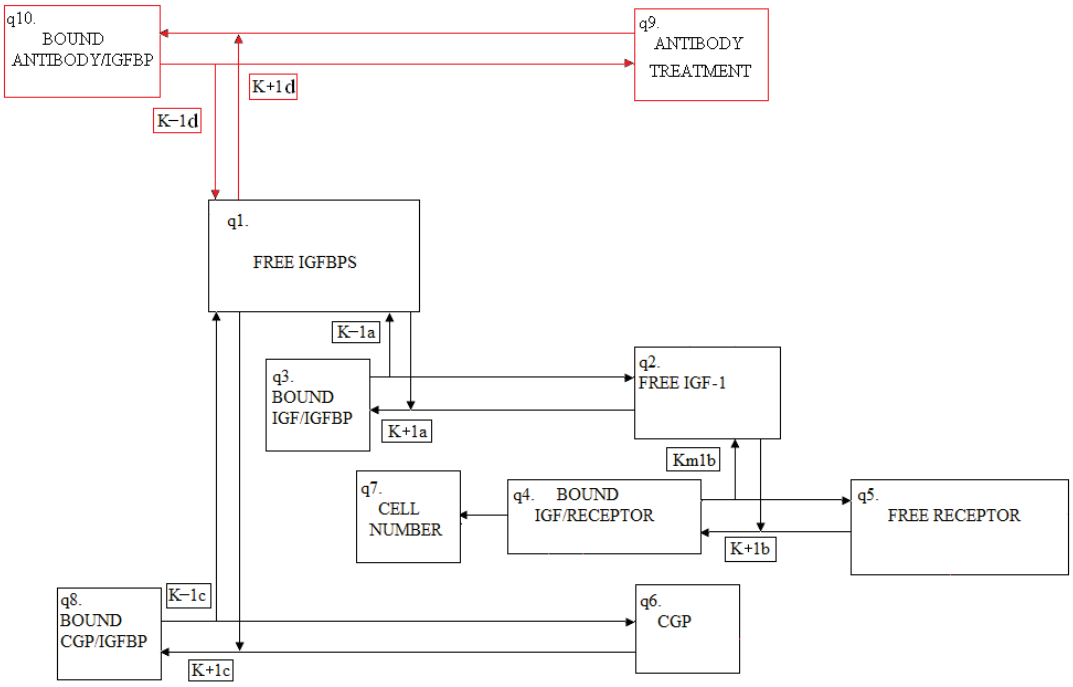

Figure 52: Schematic diagram of the ten concentration compartments in the fourth *in vitro* model (explicit) used to test the model. Each box represents a compartment, and the arrows represent transport between compartments. The red compartments are the most recent additions used to test the model.

The equations for this model can be seen in Equations 74-83, where the most recent changes are in red.

$$\frac{dq_1}{dt} = k_{-1a}q_3 - k_{+1a}q_2q_1 + k_{-1c}q_8 - k_{+1c}q_6q_1 - k_{+1d}q_1q_9 + k_{-1d}q_{10} \tag{74}$$

$$\frac{dq_2}{dt} = k_{-1a}q_3 - k_{+1a}q_2q_1 - k_{+1b}q_2q_5 + k_{m1b}q_4 + R_{a,2} \tag{75}$$

$$\frac{dq_3}{dt} = -k_{-1a}q_3 + k_{+1a}q_2q_1 \tag{76}$$

$$\frac{dq_4}{dt} = k_{+1b}q_2q_5 - k_{m1b}q_4 \tag{77}$$

$$\frac{dq_5}{dt} = -k_{+1b}q_2q_5 + k_{m1b}q_4 \tag{78}$$

$$\frac{dq_6}{dt} = k_{-1c}q_8 - k_{+1c}q_1q_6 + R_{a,6} \tag{79}$$

$$\frac{dq_7}{dt} = \frac{Kq_4}{(K_2 + q_4)} \tag{80}$$

$$\frac{dq_8}{dt} = -k_{-1c}q_8 + k_{+1c}q_1q_6 \tag{81}$$

$$\frac{dq_9}{dt} = k_{-1d}q_{10} - k_{+1d}q_1q_9 \tag{82}$$

$$\frac{dq_{10}}{dt} = -k_{-1d}q_{10} + k_{+1d}q_1q_9 \tag{83}$$

Each experiment was run for six days and consisted of two data types. The first involved different treatment levels of IGF-1 and CGP without antibodies. This consisted of six replicates for the first two levels, and three replicates for the last three levels. The second data set included antibody with different IGF-1 and CGP treatments, which consisted of six replicates for the first level and three replicates for the last four levels (see Table 34).

Type of Treatment	Level				
No IGFBP treatment:					
IGF (nM):	0	1	1	1	1
CGP (nM):	0	0	1	10	100
IGFBP treatment:					
IGF (nM):	0	1	1	1	1
CGP (nM):	0	0	1	10	100

Table 34: Type of data used for testing *in vitro* model four. Each treatment was run for six days. The IGF-1 and CGP treatments with no antibodies involved six replicates for the first two treatment levels, and three replicates for the last three levels. The IGF-1 and CGP treatments with antibodies involved six replicates for the first treatment level, and three replicates for the last four levels (data not shown).

The initial cell number level, $q_7(0)$, was found by setting the initial antibody treatment value to zero and altering the initial cell number level until the SSE error reduced to approximately zero. This was done using the first bar in the no treatment data plot i.e., no IGF-1 ($R_{a,2}$=0 nmol min^{-1} L^{-1}) and no CGP ($R_{a,6}$=0 nmol min^{-1} L^{-1}) with no antibody treatment ($q_9(0)$=0 nM.

The initial antibody value was found by then comparing the model to the antibody treatment control data i.e. no IGF-1 ($R_{a,2}$=0 nmol min^{-1} L^{-1}) and no CGP ($R_{a,6}$=0 nmol min^{-1} L^{-1}) with antibody treatment, and altering the initial antibody level until the SSE value was reduced. From here the estimated initial cell number and initial antibody values were substituted in to the model to produce a plot of estimated cell number levels for each of the IGF and CGP treatments. See Figures 53-54 for the model testing where Figure 53 is the untreated data and Figure 54 is the antibody treated data.

The testing of the model resulted in an estimate for antibody treatment of 8004 nM. The initial antibody level, $q_{10}(0)$=8004 nM, is much greater than the initial amount of CGP, $q_6(0)$=0.00382 nM, in the system. The antibody treatment therefore inundates the CGP effect since there is so much more of it. As expected, this result is reduced for the increased CGP/IGF-1 treatments as the ratio of antibody to CGP is reduced (CGP levels go up for 1-100 nM treatments of CGP).

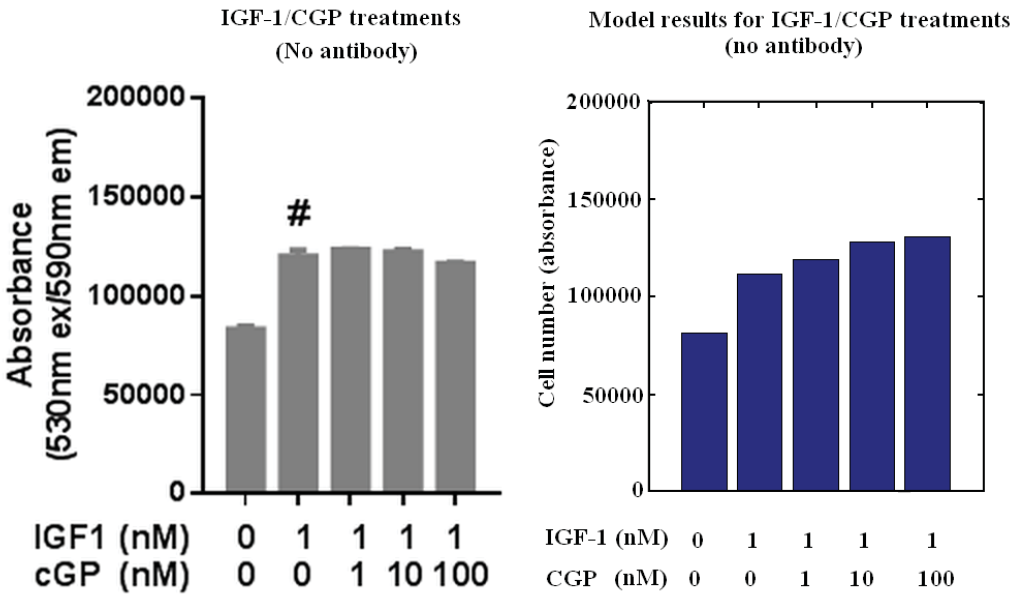

Figure 53: Model testing results for IGF-1 and CGP treatments with no antibodies data plot (left) next to model predicted values (right), R^2=0.6890. Each treatment was run for six days. The first two levels had six replicates, and the last three levels had three replicates.

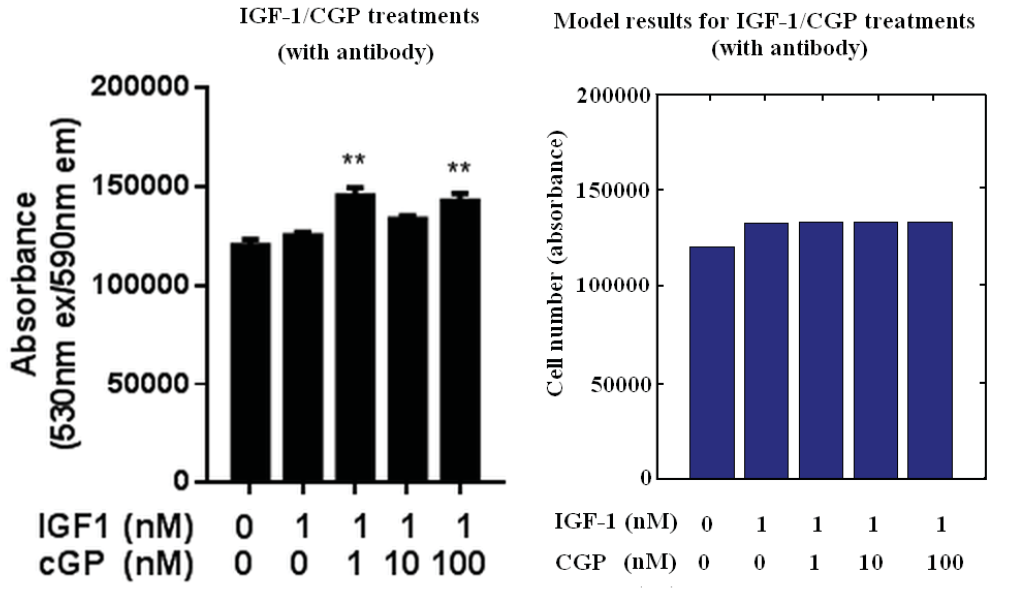

Figure 54: Model testing results for IGF-1 and CGP treatments with antibodies data plots (left) next to model predicted values (right), R^2=0.7815. Each treatment was run for six days. The first level had six replicates, and the last four levels had three replicates.

6.9 Discussion of *In Vitro* Model Three and Four (Explicit)

During the course of this study, discoveries were made about IGF-1 and CGP interactions with binding proteins. *In vitro* models three and four were designed to incorporate this new understanding with the implicit *in vitro* models used earlier. The third model shows the competitive binding between CGP and IGF-1 for the binding proteins in cell cultures. Following from this, the third model included a pool which had CGP bound to binding proteins (see Figure 41). This model failed to show any CGP effect (see Figures 44-46). A reason for this could be that although the equations account for competition between binding sites, influencing the dynamics, there are other mechanisms which may be affecting the system.

The steady state solutions for this model (see Equations 59-65) indicated no CGP response being observed due to the q_4, receptor bound IGF-1, having no dependence on CGP or treatments, $R_{a,6}$ (see Equation 62). It also showed that q_4 did not depend on IGF-1 treatments, $R_{a,2}$. The q_5 (free IGF-1 receptors) steady state solution had $R_{a,2}$-$R_{a,5}$ in the denominator (see Equation 63). This implies that if the IGF-1 receptor production rate ($R_{a,5}$) gets too large then free IGF-1 receptors (q_5) will build up. This is not a problem as physiologically, $R_{a,5}$ is restricted to be small.

A new, simplified model was created (model four), which ensured receptor bound IGF-1's (q_4) dependence on IGF-1 and CGP treatments ($R_{a,2}$ and $R_{a,6}$), see Figure 47. The parameter K_{m1b} was introduced to prevent q_4's continuous build up. The model was also adjusted to resemble cell culture situations more closely. In the third *in vitro* model the R_a and k_{0n} terms dominated the steady state. These terms were removed as there is a constant amount of receptors, binding proteins and CGP in the *in vitro* experiments. The initial values of q_3, q_4, and q_8 were set to zero so that all IGFBPs, CGP and IGF-1 would be free and the initial values of q_1, q_2, q_5 and q_6 were estimated as the total amount of IGFBP, IGF-1, receptors and CGP respectively to be in the system and were then fit to the data. The simplified model produced cell growth in response to an increase in IGF-1 and CGP levels (see Figures 48-51).

The third *in vitro* model had a calibration R^2 value of 0.7700, while the calibration R^2 value for the fourth model was 0.8311. Model three did not express some important

physiology (no CGP effect), while model four had the specific dynamics which were required and had a higher R^2 value. The fourth model is therefore more useful for representing the *in vitro* data, compared to the third *in vitro* model.

The predicted R^2 for the no antibody treatment simulation was 0.6890 and the predicted R^2 for the antibody treatment simulation was 0.7815. Fitting with the independent data (data with and without antibodies), model testing showed that the antibody treatment inundated the CGP in the control condition by the large size difference (CGP=0.00382nM and antibody=8004nM). As more CGP was introduced, this effect was reduced as expected, see Figure 54. The initial antibody prediction which came from the model testing was 8004nM (not measured in the experiments). The model demonstrates that the competitive binding played a key role in driving the antibody treatment model dynamics.

7 Conclusion

The main goal of this study was to create a dynamical model which described the effect of Insulin-like Growth Factor-1 on human cell growth. The research was aimed at better representing trends in current data being collected on IGF-1 and CGP effects on cell growth.

Treatment using IGF-1 has many side effects and it has a restricted central uptake since IGF-1 is so large. CGP is a metabolite of IGF-1 and is sufficiently small that it can be directed to specific sites within the body. It has been shown to regulate IGF-1 activity when levels of IGF-1 are raised above or below the physiological threshold. The data collected for the current *in vitro* models showed the efficacy of CGP on IGF-1 induced cell growth depended on the ratio of CGP/IGF-1 concentrations (doses). A treatment with higher CGP/IGF-1 ratio stimulated IGF-1 mediated cell growth, whereas a lower ratio inhibited IGF-1 associated cell growth. CGP did not alter cell growth when the CGP/IGF-1 concentrations were more or less the same.

An *in vivo* mathematical model describing IGF-1 and CGP interactions extended previous *in vivo* research by Boroujerdi et al. (1997). Analytical steady state solutions were calculated and bifurcation diagrams were performed for the Boroujerdi et al. (1997) research, then the model was extended to include CGP interactions. Bifurcation diagrams were then produced for the new *in vivo* model. No bifurcations were found in the feasible region of any of these models. There was no onset of gross change observed in the behaviour of the model, all systems resulted in globally asymptotically stable steady states in the feasible region.

Four *in vitro* models were developed by extending the *in vivo* model. To extend the *in vivo* model an extra differential equation was added which represents cell growth. Three candidate equations were compared to find the model that best described the relationship between the levels of added IGF-1 and cell growth. To provide estimates of parameter uncertainty, the variance covariance matrix was calculated for each model option (see Tables 16-18). The best equation for describing this relationship was $q = \frac{At}{B+t} + C$, which allowed for cell growth over time with no added IGF-1 (after transformation of variables). This model was consistent with cell growth on day six in the control experiments with no IGF-1 or CGP (first bar in Figures 33-40, 43-46 and 48-51).

The first two *in vitro* models were implicit models which used feedback terms to de-

scribe CGP's influence on IGF-1 function (concentration). The first implicit model had an overall calibration R^2 value of 0.8352 but did not represent data for CGP treatments very accurately for high doses of CGP. The data showed decreasing cell number levels for high concentrations of CGP, which was not observed in the first implicit model. To account for this trend in the data, the first model was altered to include the term $q_6 - a_3 q_6^2$ (see Equations 48-49). This addition to the model meant that high dose treatments of CGP would result in the -$a_3 q_6^2$ dominating the equation, introducing a negative term to the fifth ODE (Equation 41) and a positive term in the sixth ODE (Equation 42) and therefore reducing cell number levels. The calibration R^2 value of this model was 0.8319.

In vitro models three and four were designed to explicitly show the competitive binding of IGF-1 and CGP with the IGFBPs. The first of these resulted in a calibration R^2 value of 0.7700. This model was designed to incorporate the biological physiology, but failed to show all of the properties required, no CGP response was observed. This was evident through the analytical steady state solutions. The receptor bound IGF-1, q_4, was independent of the IGF-1 treatments, $R_{a,2}$, and CGP treatments, $R_{a,6}$, (see Equation 62). Because of this, a new simplified, explicit *in vitro* model was produced. This simplified model, which ensured the steady state solution of receptor bound IGF-1 (q_4) depended on IGF-1 treatments ($R_{a,2}$) and CGP treatments ($R_{a,6}$), was designed to resemble cell culture conditions more closely. The calibration R^2 value of this simplified model was 0.8311, and the result was CGP response being observed (see Figure 49).

The fourth *In vitro* model was tested against an independent data set. This data involved antibody treatments, see Figure 52 for their interactions in the model. The antibody treatments reduce the concentration of bound IGF-1 with IGFBPs, q_3, by binding to the IGFBPs to form q_{10}. The predicted R^2 value for the no antibody treatment (not used to determine parameter values) simulation was 0.6890 and the predicted R^2 value of the antibody treatment data was 0.7815. The model testing produced an increase in cell number to the same extent shown in the data. The resulting prediction was an initial antibody value of 8004nM, which was not measured by experiments. This demonstrates that the competition mechanisms described by the model characterise the features of the antibody experiments.

The fourth *in vitro* model fitted with the hypothesis that CGP regulates IGF-1 through competitive binding to the IGFBPs. The third *in vitro* model could not accurately ac-

count for variations in the data because of other influencing mechanisms. The model only accounted for one factor, although there are many other factors influencing the system. The fourth model introduced the required dynamics and produced predictions which fitted with the data showing that competitive binding was a key component of the system. However, model one and two (which used the feedback terms to implicitly show CGP regulating IGF-1) represented the change in cell number from the data more accurately. There are other underlying biological processes which cannot be described by the explicit models. Therefore the implicit model, which does not have to rely on mapping biological processes directly into mathematical terms, provides a better description of the data than the explicit models.

Model four successfully allowed us to see that competitive binding is an important mechanism in IGF-1 dynamics. However, there are other biological mechanisms in place that affect cell growth. Once these mechanisms have been defined the model can be extended to include these extra mechanisms. The models developed in this research provide a better understanding of IGF-1 dynamics and can be used to predict cellular responses in human cells.

References

Blanchard, P., Devaney, R. L., & Hall, G. R. (2006). *Differential equations (third edition).* New York, USA: Thomson Brooks/Cole.

Boroujerdi, M. A., Jones, R. H., Sonksen, P. H., & Russell-Jones, D. L. (1997). Simulation of IGF-I pharmacokinetics after infusion of recombinant IGF-I in human subjects. *Am J Physiol Endocrinol Metab*, *273*, 438–447.

Boroujerdi, M. A., Sonksen, P. H., & Jones, R. H. (1994). A Compartmental Model for Simulation of IGF-I kinetics and metabolism. *Methods of Information in Medicine*, *33*, 514–521.

Briggs, G. E., & Haldane, J. B. S. (1925). A note on the kinetics of enzyme actions. *Growth Hormone and IGF Research*, *19*, 338–339.

Clemmons, D. R. (1991). Insulin-like Growth Factor Binding Proteins: Roles in regulating IGF physiology. *Journal of Developmental Physiology*, *15*, 105-110.

Edelstein-Keshet, L. (2005). *Mathematical Models in Biology.* New York, USA: Society for industrial and applied mathematics.

Fox, J., & Weisberg, S. (2011). *An R companion to applied regression (second edition).* USA: Sage Publications.

Guan, J., & Gluckman, P. D. (2009). IGF-1 derived small neuropeptides and analogues: a novel strategy for the development of pharmaceuticals for neurological conditions. *British Journal of Pharmacology*, *157*, 881-891.

Guan, J., Svedin, P., Mathai, S., Zhang, R., Wang, X., Gustavsson, M., ... Mallard, C. (2007). Delayed peripheral administration of a GPE analogue induces astrogliosis and angiogenesis and reduces inflammation and brain injury following hyposia-ischemia in the neonatal rat. *Developmental Neuroscience*, *29*, 393–402.

Humbel, R. E. (1991). Review Insulin-like Growth Factors I and II. In P. Christen & E. Hofmann (Eds.), *Ejb reviews 1990* (Vol. 190, p. 109-126). Springer Berlin Heidelberg.

Keener, J., & Sneyd, J. (2009). *Mathematical Physiology 1: Cellular Physiology (second edition).* New York, USA: Springer.

Klipp, E., Herwig, R., Kowald, A., Wierling, C., & Lehrac, H. (2005). *Systems biology in practice: Concepts, implementation and application.* Berlin, Germany: Wiley-VCH.

MATLAB. (2009). *Version 7.8.0.347 (R2009a).* Natick, USA: The MathWorks Inc.

Michaelis, M., & Menten, L. (1913). Die kinetik der invertinwirkung. *Biochemische Zeitschrift*, *49*, 333–369.

Mizuno, N., Kato, Y., Iwamoto, M., Urae, A., Amamoto, T., Niwa, T., & Sugiyama, Y. (2001). Kinetic Analysis of the Disposition of Insulin-Like Growth Factor-I in Healthy Volunteers. *Pharmaceutical Research*, *18*, 1203–1209.

Moon, S. (2011). *The regulatory role of Insulin-like Growth Factor-I N-terminal tripeptide and diketopiperazine derivative in Insulin-like Growth Factor-I mediated angiogenesis*. Unpublished master's thesis, The University of Auckland.

Motulsky, H., & Christopoulos, A. (2009). *Fitting models to biological data using linear and nonlinear regression: A practical guide to curve fitting*. New York, USA: Springer.

Pollard, J. H. (1977). *A handbook of numerical and statistical techniques*. Cambridge, Great Britain: Cambride university press.

Strogratz, S. H. (1994). *Nonlinear dynamics and chaos*. USA: Perseus Books Publishing.

Werner, H. (2000). The Insulin-like Growth Factor I Receptor: Molecular biology, heterogeneity, and regulation. , 251–263.

XPPaut. (2002). *Version 7.0 for Windows*. Pittsburgh, USA: B. Ermentrout.

A Subject 2-4 Parameter Values Boroujerdi et al. (1997):

A.1 Subject 2

Parameter Name	Value	Converted To Correct Units
Infu (First 3hrs)	43.7 (pmol min^{-1} kg^{-1})	3.39986 (nmol min^{-1})
Weight	94.6 (kg)	94.6 (kg)
V_2	45.5 (ml kg^{-1})	4.304 (L)
V_6	150 (ml kg^{-1})	14.190 (L)
R	0.88 (nmol kg^{-1})	83.25 (nmol)
k_{01}	0.0058 (min^{-1})	0.0058 (min^{-1})
k_{04}	0.00144 (min^{-1})	0.00144 (min^{-1})
k_{07}	0.037 (min^{-1})	0.037 (min^{-1})
k_{76}	0.037 (min^{-1})	0.037 (min^{-1})
k_{52}	0.0374 (min^{-1})	0.0374 (min^{-1})
k_{32}	0.094 (min^{-1})	0.094 (min^{-1})
k_{62}	0.05 (min^{-1})	0.05 (min^{-1})
k_{26}	0.015 (min^{-1})	0.015 (min^{-1})
k_{+1a}	0.00457 ($nmol^{-1}$ min^{-1} L)	0.00106 ($nmol^{-1}$ min^{-1})
k_{+1b}	0.00491 ($nmol^{-1}$ min^{-1} L)	0.00114 ($nmol^{-1}$ min^{-1})
k_{-1a}	0.0945 (min^{-1})	0.0945 (min^{-1})
k_{-1b}	0.0995 (min^{-1})	0.0995 (min^{-1})
$R_{a,1}$	0.119 (nmol min^{-1} L^{-1})	0.513 (nmol min^{-1})
$R_{a,2}$	0.110 (nmol min^{-1} L^{-1})	0.472 (nmol min^{-1})
R_a	0.156 (nmol min^{-1} L^{-1})	0.636 (nmol min^{-1})
Variable	Initial value	Converted To Correct Units
q_1	20.6 (nmol L^{-1})	88.5 (nmol)
q_2	4.5 (nmol L^{-1})	19.2 (nmol)
q_3	4.4 (nmol L^{-1})	19.1 (nmol)
q_4	76.2 (nmol L^{-1})	328.1 (nmol)
q_5	16.8 (nmol L^{-1})	72.2 (nmol)
q_6	4.5 (nmol L^{-1})	21.7 (nmol)
q_7	4.2 (nmol L^{-1})	17.2 (nmol)

Table 35: Subject two parameter and initial values reproduced from Boroujerdi et al. (1997).

A.2 Subject 3

Parameter Name	Value	Converted To Correct Units
Infu (First 3hrs)	43.7 (pmol min^{-1} kg^{-1})	3.39986 (nmol min^{-1})
Weight	73.9 (kg)	73.9 (kg)
V_2	45.5 (ml kg^{-1})	3.362 (L)
V_6	150 (ml kg^{-1})	11.08 (L)
R	0.88 (nmol kg^{-1})	83.25 (nmol)
k_{01}	0.0058 (min^{-1})	0.0058 (min^{-1})
k_{04}	0.00144 (min^{-1})	0.00144 (min^{-1})
k_{07}	0.072 (min^{-1})	0.072 (min^{-1})
k_{76}	0.072 (min^{-1})	0.072 (min^{-1})
k_{52}	0.0374 (min^{-1})	0.0374 (min^{-1})
k_{32}	0.094 (min^{-1})	0.094 (min^{-1})
k_{62}	0.062 (min^{-1})	0.062 (min^{-1})
k_{26}	0.019 (min^{-1})	0.019 (min^{-1})
k_{+1a}	0.00571 ($nmol^{-1}$ min^{-1} L)	0.00170 ($nmol^{-1}$ min^{-1})
k_{+1b}	0.00628 ($nmol^{-1}$ min^{-1} L)	0.00187 ($nmol^{-1}$ min^{-1})
k_{-1a}	0.0439 (min^{-1})	0.0439 (min^{-1})
k_{-1b}	0.0336 (min^{-1})	0.0336 (min^{-1})
$R_{a,1}$	0.0955 (nmol min^{-1} L^{-1})	0.321 (nmol min^{-1})
$R_{a,2}$	0.0858 (nmol min^{-1} L^{-1})	0.289 (nmol min^{-1})
R_a	0.0807 (nmol min^{-1} L^{-1})	0.269 (nmol min^{-1})
Variable	Initial value	Converted To Correct Units
q_1	16.5 (nmol L^{-1})	55.5 (nmol)
q_2	1.7 (nmol L^{-1})	5.6 (nmol)
q_3	3.5 (nmol L^{-1})	11.9 (nmol)
q_4	59.6 (nmol L^{-1})	200.4 (nmol)
q_5	18.4 (nmol L^{-1})	61.9 (nmol)
q_6	1.1 (nmol L^{-1})	4.0 (nmol)
q_7	1.1 (nmol L^{-1})	3.7 (nmol)

Table 36: Subject three parameter and initial values reproduced from Boroujerdi et al. (1997).

A.3 Subject 4

Parameter Name	Value	Converted To Correct Units
Infu (First 3hrs)	43.7 (pmol min^{-1} kg^{-1})	3.39986 (nmol min^{-1})
Weight	90.5 (kg)	90.5 (kg)
V_2	45.5 (ml kg^{-1})	4.118 (L)
V_6	150 (ml kg^{-1})	13.575 (L)
R	0.88 (nmol kg^{-1})	79.64 (nmol)
k_{01}	0.0058 (min^{-1})	0.0058 (min^{-1})
k_{04}	0.00144 (min^{-1})	0.00144 (min^{-1})
k_{07}	0.083 (min^{-1})	0.083 (min^{-1})
k_{76}	0.083 (min^{-1})	0.083 (min^{-1})
k_{52}	0.0374 (min^{-1})	0.0374 (min^{-1})
k_{32}	0.094 (min^{-1})	0.094 (min^{-1})
k_{62}	0.103 (min^{-1})	0.103 (min^{-1})
k_{26}	0.031 (min^{-1})	0.031 (min^{-1})
k_{+1a}	0.0717 (nmol^{-1} min^{-1} L)	0.00174 (nmol^{-1} min^{-1})
k_{+1b}	0.00369 (nmol^{-1} min^{-1} L)	0.000896 (nmol^{-1} min^{-1})
k_{-1a}	0.0333 (min^{-1})	0.0333 (min^{-1})
k_{-1b}	0.0177 (min^{-1})	0.0177 (min^{-1})
$R_{a,1}$	0.0761 (nmol min^{-1} L^{-1})	0.313 (nmol min^{-1})
$R_{a,2}$	0.146 (nmol min^{-1} L^{-1})	0.601 (nmol min^{-1})
R_a	0.0762 (nmol min^{-1} L^{-1})	0.311 (nmol min^{-1})
Variable	Initial value	Converted To Correct Units
q_1	13.1 (nmol L^{-1})	54.0 (nmol)
q_2	1.1 (nmol L^{-1})	4.2 (nmol)
q_3	2.9 (nmol L^{-1})	11.9 (nmol)
q_4	1.0 (nmol L^{-1})	417.5 (nmol)
q_5	21.6 (nmol L^{-1})	88.9 (nmol)
q_6	0.9 (nmol L^{-1})	3.9 (nmol)
q_7	0.9 (nmol L^{-1})	3.7 (nmol)

Table 37: Subject four parameter and initial values reproduced from Boroujerdi et al. (1997).

B Graphs:

B.1 Comparison of Boroujerdi et al. (1997) Simulations

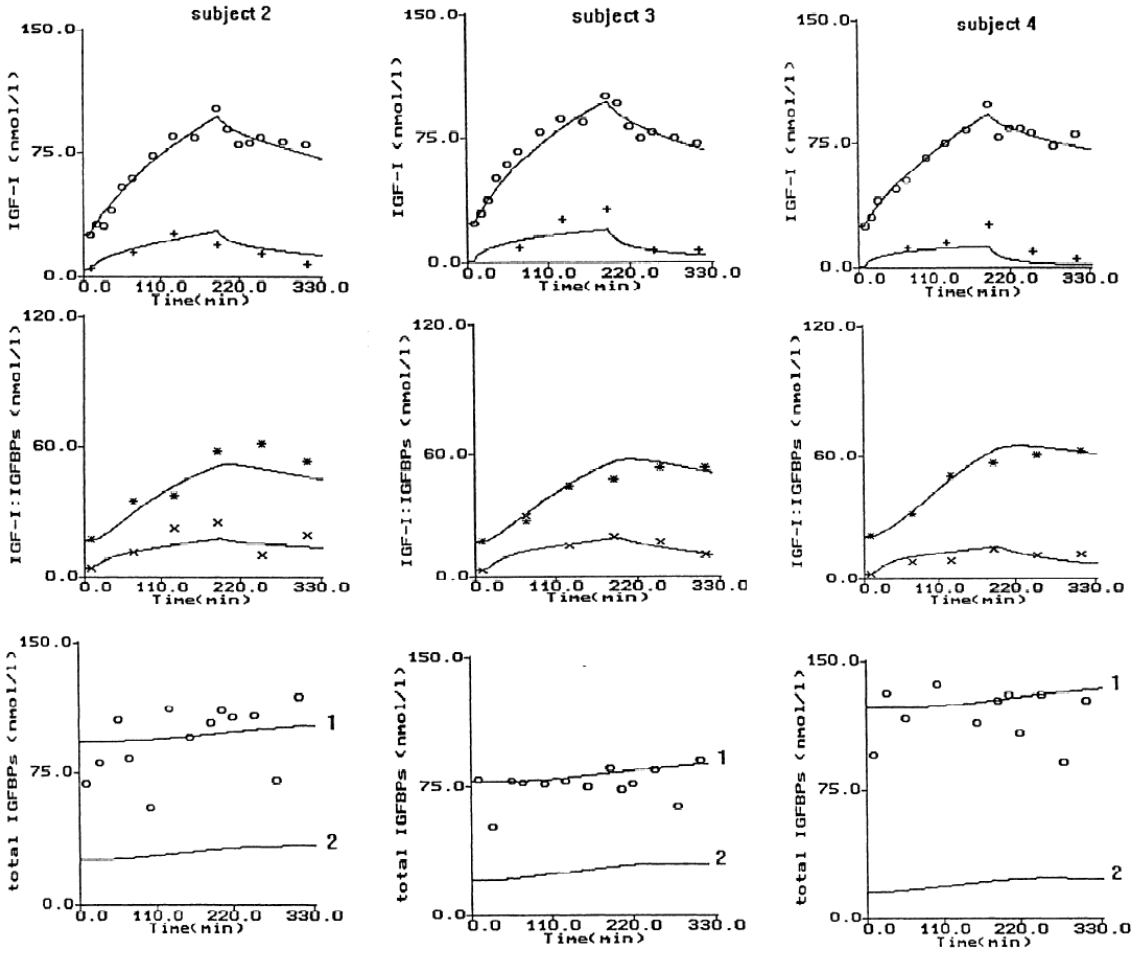

Figure 55: Model simulations reproduced from Boroujerdi et al. (1997) for subjects 2-4. In the first row of graphs; o, represents total IGF-1 (nM) and +, represents free IGF-1 (nM). In the second row of graphs; *, represents IGF-1 in 150kDa plasma fraction (nM) and x, represents IGF-1 in 50kDa plasma fraction (nM). In the last row of graphs (1) represents total IGFBPs in 150kDa plasma fraction (q_4+q_5), (2) represents total IGFBPs in 50kDa plasma fraction (q_1+q_3), nM and o, represents measured IGFBP-3 (nM). The infusion starts at time=10min and is stopped at time=190min.

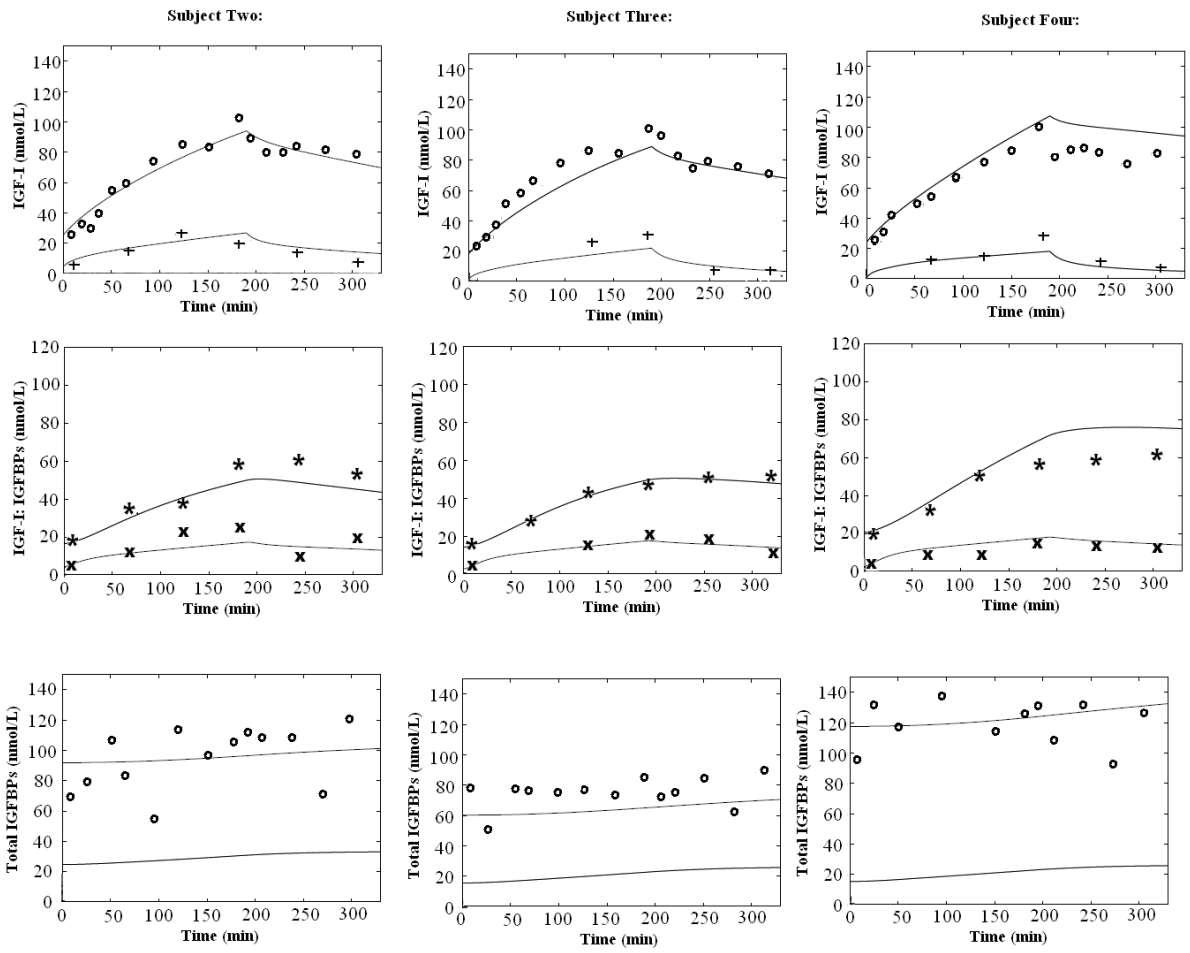

Figure 56: Replicated model simulations for subjects 2-4 with Boroujerdi et al. (1997) data points. In the first row; o, represents total IGF-1 (nM) and +, represents free IGF-1 (nM). In the second row of graphs; *, represents IGF-1 in 150kDa plasma fraction (nM) and x, represents IGF-1 in 50kDa plasma fraction (nM). In the last row of graphs (1) represents total IGFBPs in 150kDa plasma fraction (q_4+q_5), (2) represents total IGFBPs in 50kDa plasma fraction (q_1+q_3), nM and o, represents measured IGFBP-3 (nM). The infusion starts at time=10min and is stopped at time=190min.

B.2 Bifurcation Diagrams

B.2.1 Boroujerdi et al. (1997) Original Model Bifurcation Diagrams

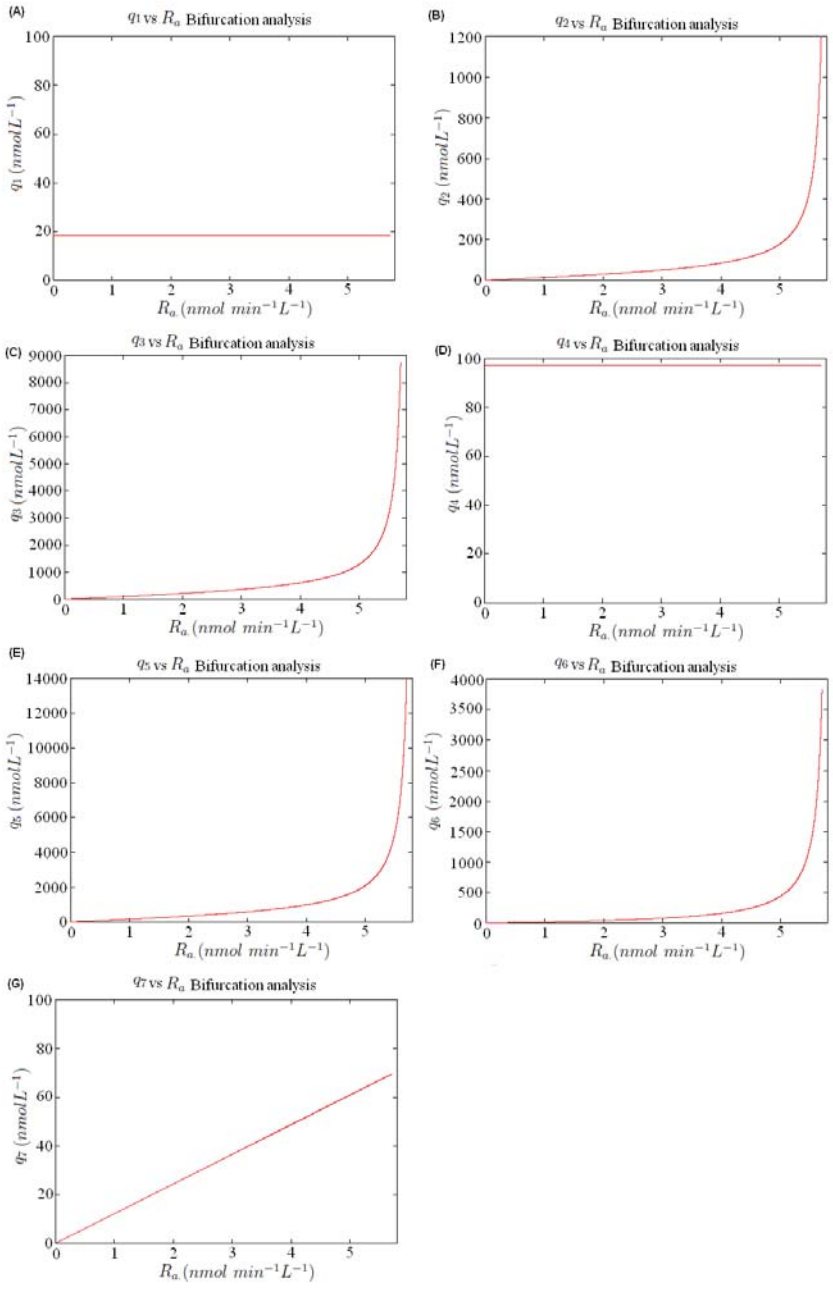

Figure 57: Bifurcation analysis for $\mathbf{q}$ variables against IGF-1 production rate, R_a in nmol min^{-1} L^{-1} (Boroujerdi et al. (1997) model). Bifurcation diagrams of (A) Free IGFBPs (50kDa) vs. R_a, (B) free IGF-1 in the plasma vs. R_a, (C) bound IGF-1/IGFBP (50kDa) vs. R_a, (D) free IGFBP-3 (150kDa) vs. R_a, (E) bound IGF-1/IGFBPs (50kDa) vs. R_a, (F) free IGF-1 in interstitial fluid vs. R_a and (G) Receptor bound IGF-1 vs. R_a.

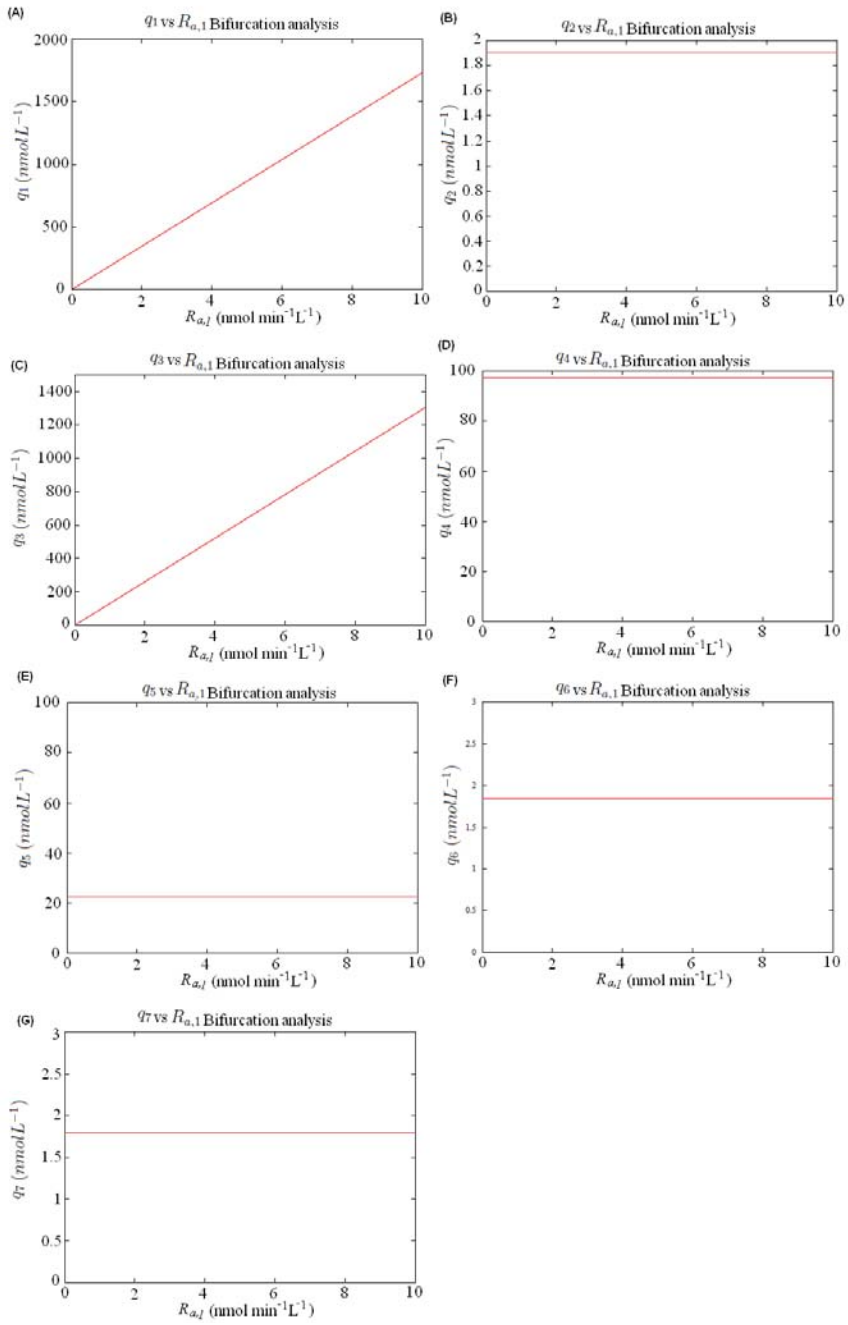

Figure 58: Bifurcation analysis for $\mathbf{q}$ variables against IGFBP (50kDa) production rate, $R_{a,1}$ in nmol min^{-1} L^{-1} (Boroujerdi et al. (1997) model). Bifurcation diagrams of (A) Free IGFBPs (50kDa) vs. $R_{a,1}$, (B) free IGF-1 in the plasma vs. $R_{a,1}$, (C) bound IGF-1/IGFBP (50kDa) vs. $R_{a,1}$, (D) free IGFBP-3 (150kDa) vs. $R_{a,1}$, (E) bound IGF-1/IGFBPs (50kDa) vs. $R_{a,1}$, (F) free IGF-1 in interstitial fluid vs. $R_{a,1}$ and (G) Receptor bound IGF-1 vs. $R_{a,1}$.

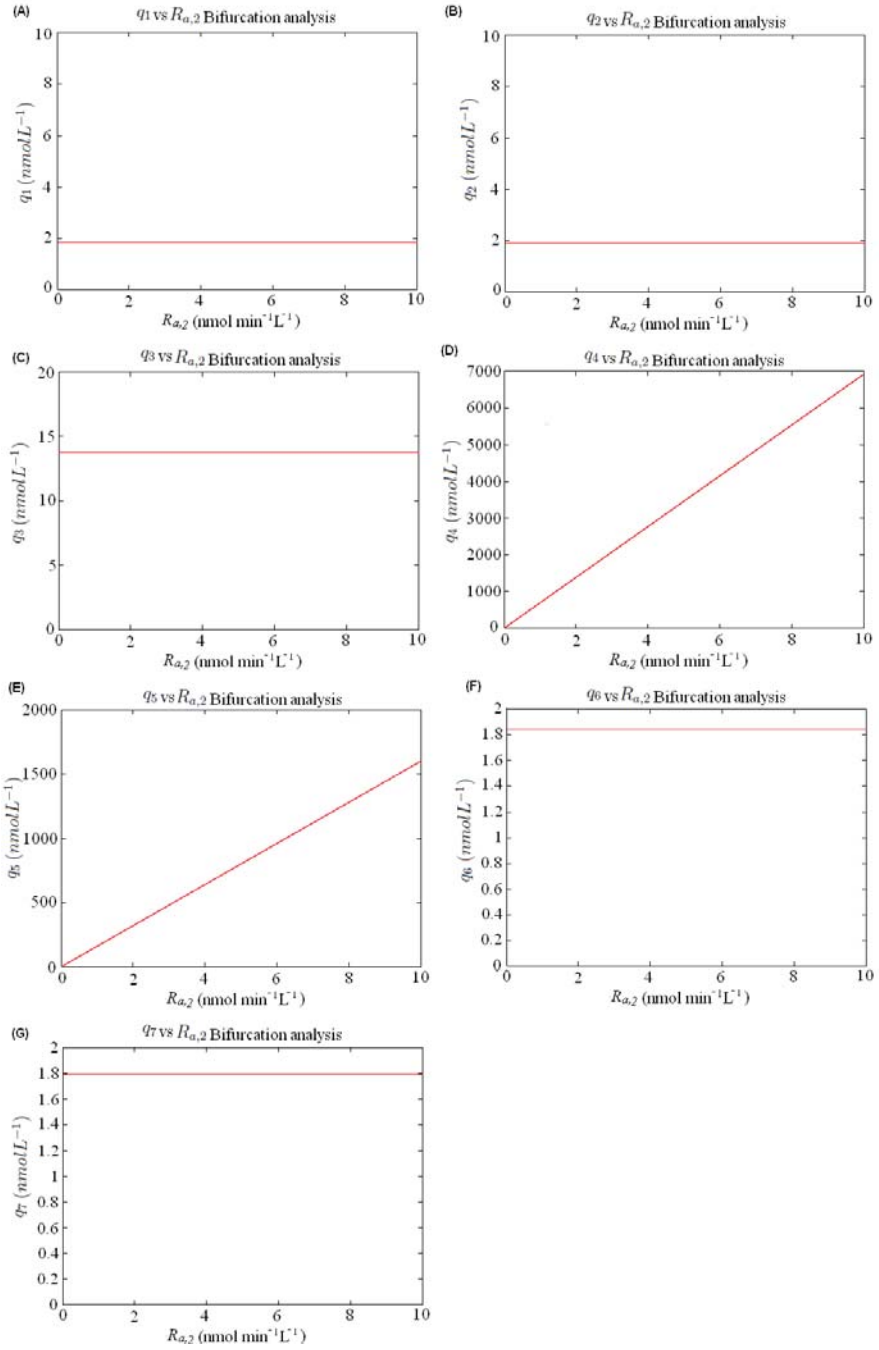

Figure 59: Bifurcation analysis for **q** variables against IGFBP-3 (150kDa) production rate, $R_{a,2}$ in nmol min^{-1} L^{-1} (Boroujerdi et al. (1997) model). Bifurcation diagrams of (A) Free IGFBPs (50kDa) vs. $R_{a,2}$, (B) free IGF-1 in the plasma vs. $R_{a,2}$, (C) bound IGF-1/IGFBP (50kDa) vs. $R_{a,2}$, (D) free IGFBP-3 (150kDa) vs. $R_{a,2}$, (E) bound IGF-1/IGFBPs (50kDa) vs. $R_{a,2}$, (F) free IGF-1 in interstitial fluid vs. $R_{a,2}$ and (G) Receptor bound IGF-1 vs. $R_{a,2}$.

B.2.2 Boroujerdi et al. (1997) Model ($-k_{02}q_2$ added) Bifurcation Diagrams

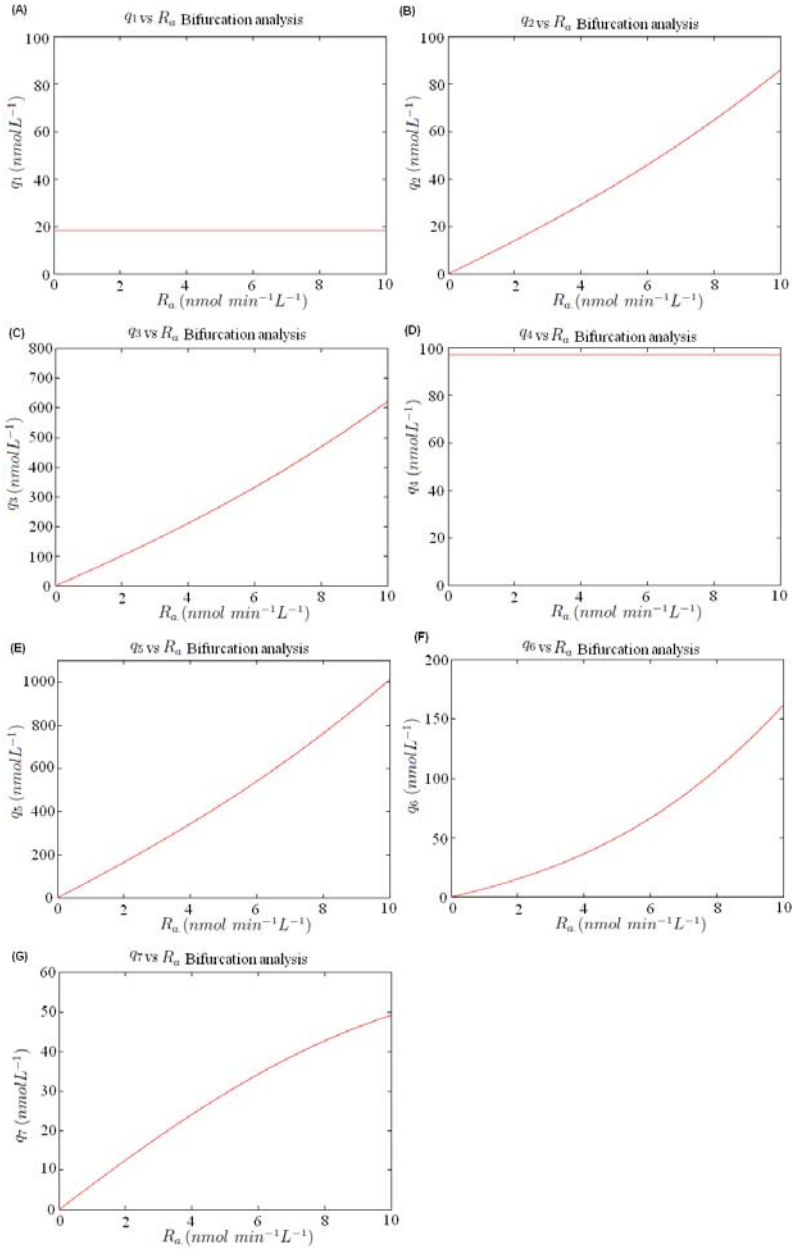

Figure 60: Bifurcation analysis for $\mathbf{q}$ variables against IGF-1 production rate, R_a in nmol min^{-1} L^{-1} (Boroujerdi et al. (1997) model with -$k_{02}q_2$ term). Bifurcation diagrams of (A) Free IGFBPs (50kDa) vs. R_a, (B) free IGF-1 in the plasma vs. R_a, (C) bound IGF-1/IGFBP (50kDa) vs. R_a, (D) free IGFBP-3 (150kDa) vs. R_a, (E) bound IGF-1/IGFBPs (50kDa) vs. R_a, (F) free IGF-1 in interstitial fluid vs. R_a and (G) Receptor bound IGF-1 vs. R_a.

B.2.3 *In Vivo* Model Bifurcation Diagrams

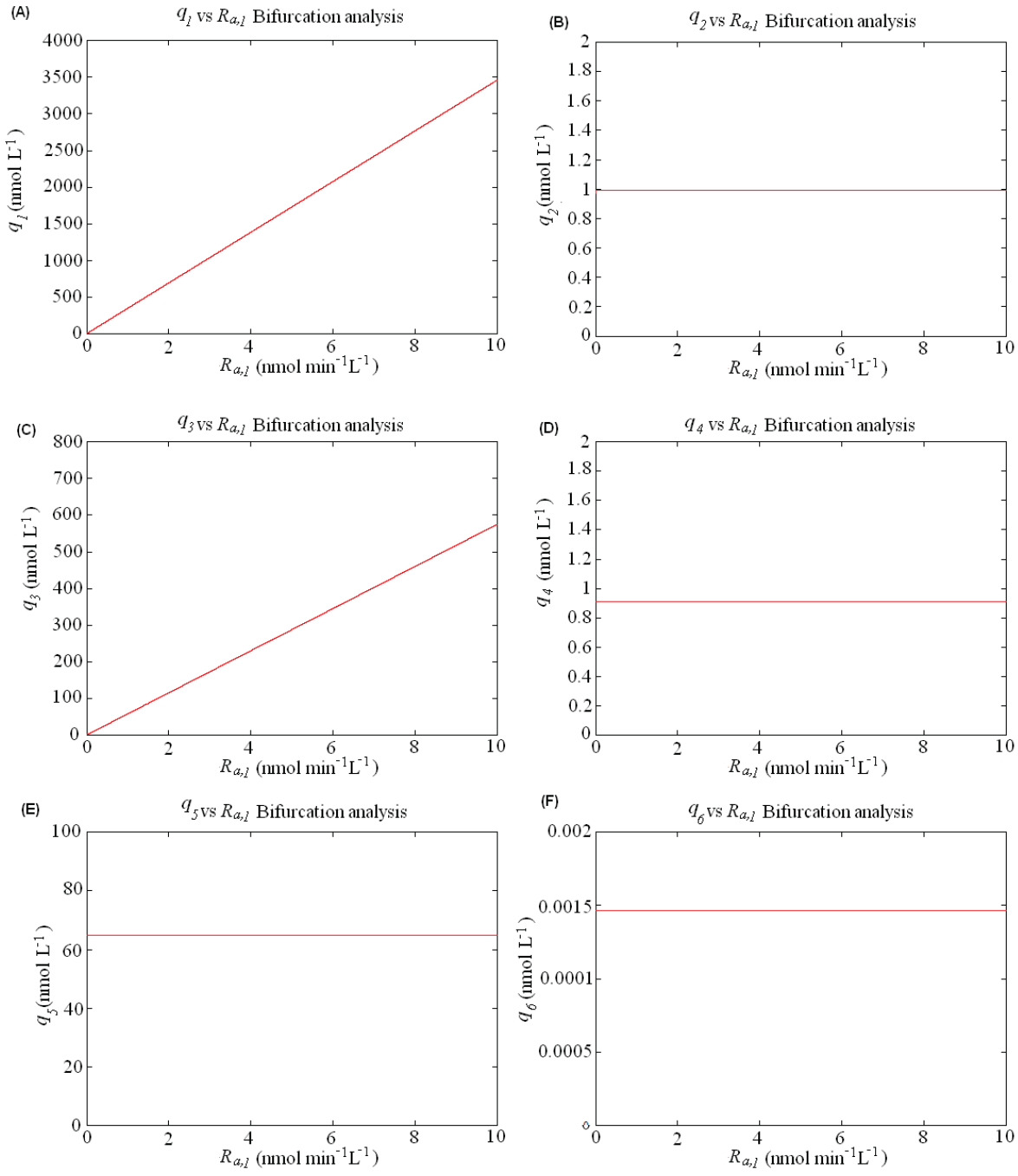

Figure 61: Bifurcation analysis for **q** variables against IGFBP production rate, $R_{a,1}$ in nmol min^{-1} L^{-1} (*In Vivo* Model). Bifurcation diagrams of (A) Free IGFBPs vs. $R_{a,1}$, (B) free IGF-1 vs. $R_{a,1}$, (C) bound IGF-1/IGFBPs vs. $R_{a,1}$, (D) receptor bound IGF-1 (150kDa) vs. $R_{a,1}$, (E) free IGF-1 receptors vs. $R_{a,1}$ and (F) free CGP vs. $R_{a,1}$.

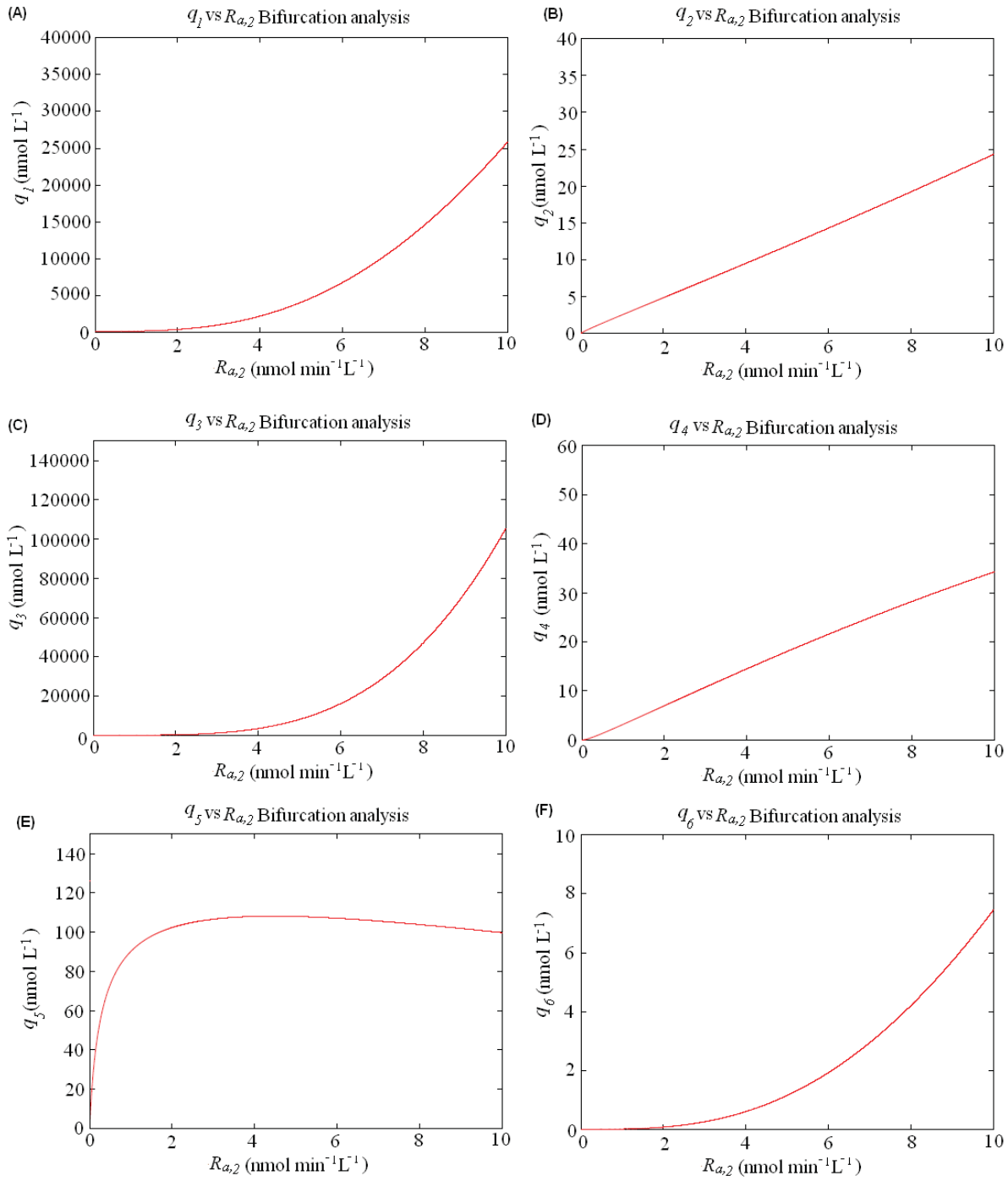

Figure 62: Bifurcation analysis for **q** variables against IGF-1 production rate, $R_{a,2}$ in nmol min^{-1} L^{-1} (*In Vivo* Model). Bifurcation diagrams of (A) Free IGFBPs vs. $R_{a,2}$, (B) free IGF-1 vs. $R_{a,2}$, (C) bound IGF-1/IGFBPs vs. $R_{a,2}$, (D) receptor bound IGF-2 (150kDa) vs. $R_{a,2}$, (E) free IGF-1 receptors vs. $R_{a,2}$ and (F) free CGP vs. $R_{a,2}$.

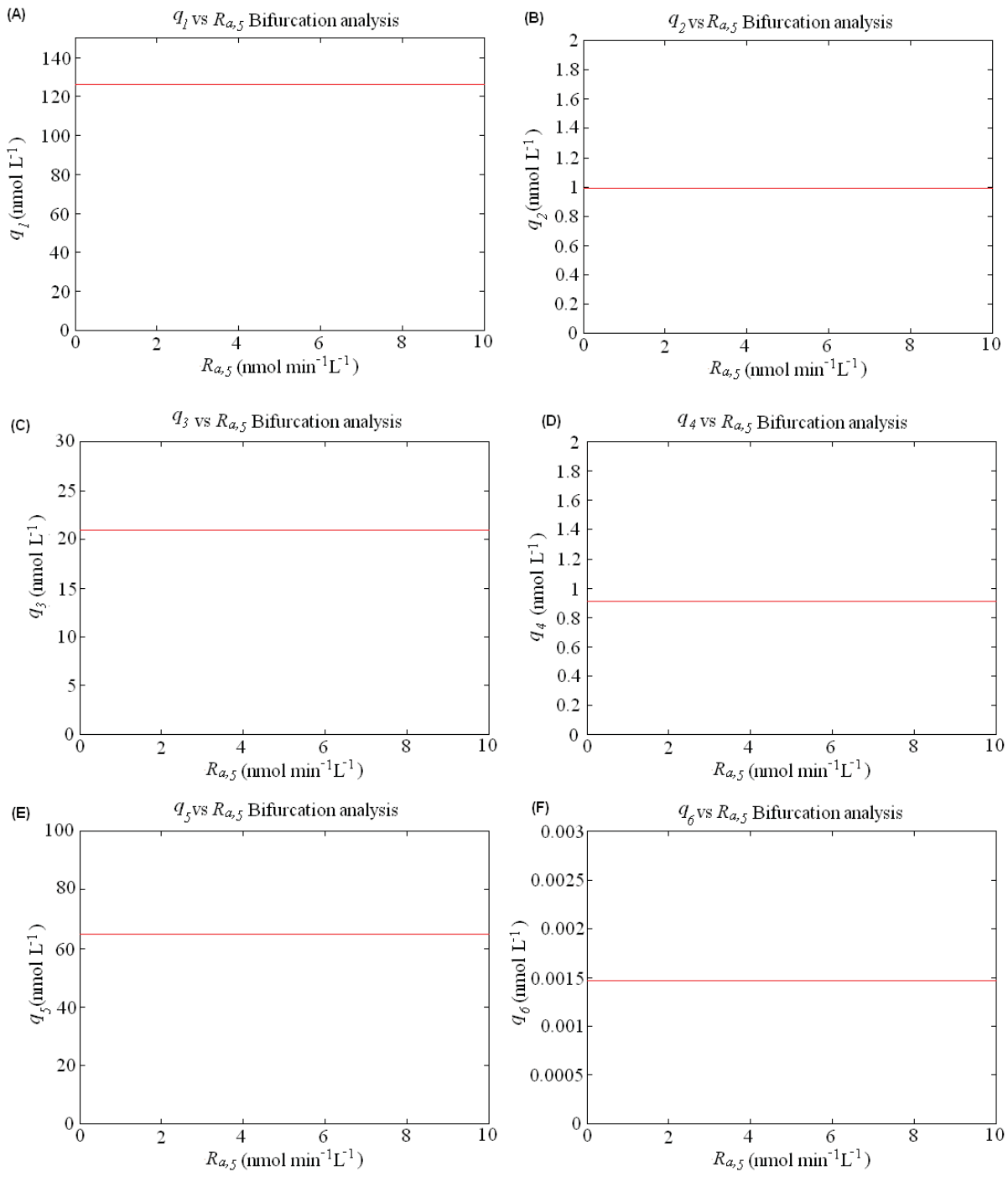

Figure 63: Bifurcation analysis for **q** variables against receptor production rate, $R_{a,5}$ in nmol min^{-1} L^{-1} (*In Vivo* Model). Bifurcation diagrams of (A) Free IGFBPs vs. $R_{a,5}$, (B) free IGF-1 vs. $R_{a,5}$, (C) bound IGF-1/IGFBPs vs. $R_{a,5}$, (D) receptor bound IGF-2 (150kDa) vs. $R_{a,5}$, (E) free IGF-1 receptors vs. $R_{a,5}$ and (F) free CGP vs. $R_{a,5}$.

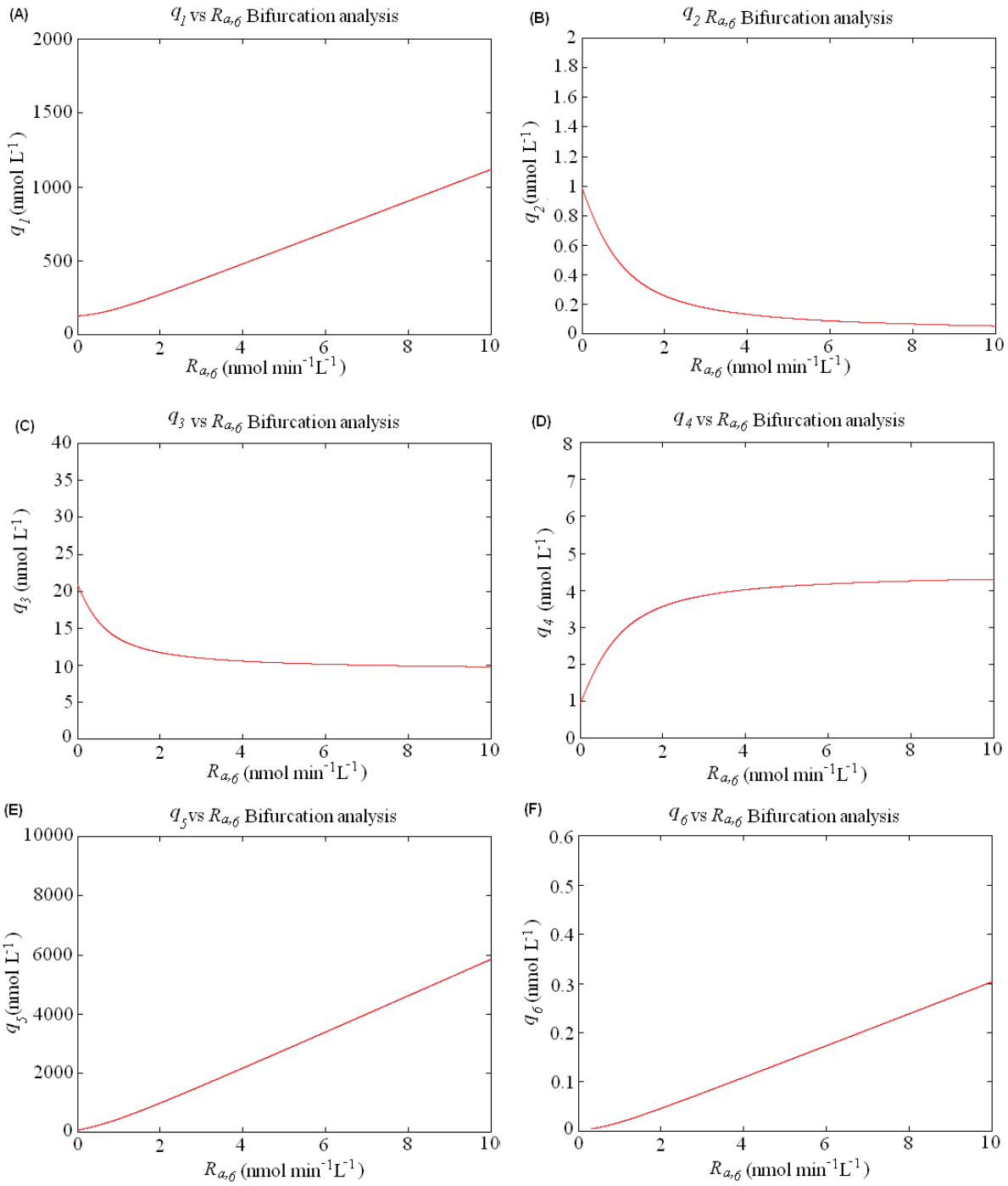

Figure 64: Bifurcation analysis for **q** variables against CGP production/infusion rate, $R_{a,6}$ in nmol min^{-1} L^{-1} (*In Vivo* Model). Bifurcation diagrams of (A) Free IGFBPs vs. $R_{a,6}$, (B) free IGF-1 vs. $R_{a,6}$, (C) bound IGF-1/IGFBPs vs. $R_{a,6}$, (D) receptor bound IGF-2 (150kDa) vs. $R_{a,6}$, (E) free IGF-1 receptors vs. $R_{a,6}$ and (F) free CGP vs. $R_{a,6}$.

C Basic Mathematical Background of Methods used in this Research:

C.1 Introduction

The models in this research used nonlinear ordinary differential equations and therefore needed numerical methods to solve them. The equations involved mass action kinetics. To estimate parameter values, model calibration against *in vitro* data was done. This was done using a gradient based, simplex method. Some calibration methodology was also used to calculate the variance covariance matrix to give an estimate of uncertainty. A bifurcation analysis was performed on some of the simpler models (two of which resulted in Hopf bifurcations). The coefficient of determination was calculated to determine how well the models fit the data. A brief explanation of the methods used are listed in this chapter.

C.2 Ordinary Differential Equations

Differential equations can be ordinary or partial, both of which can be either linear or nonlinear. Linear refers to equations whereby the unknown function and its derivatives appear to the first power, if this is not the case they are nonlinear. Partial differential equations (PDE's) are differential equations where the unknown function is a function of multiple independent variables and the equation involves its partial derivatives. These can be further classified as elliptic, hyperbolic, parabolic or mixed type.

Here we discuss ordinary differential equations (ODE's) and ways of finding solutions. An ordinary differential equation is an equation which shows the relationship between a function of one independent variable, say $\boldsymbol{q}(t)$, its derivatives of various orders $\boldsymbol{q}'(t)$, $\boldsymbol{q}''(t)$, etc. and the independent variable time, t. The order of the equation is determined by the highest derivative in the equation. We will focus on first-order systems of differential equations which are of the form:

$$\boldsymbol{F}(t, \boldsymbol{q}, \boldsymbol{q}') = 0,$$

where t is the independent variable time, $\boldsymbol{q}$ is a vector of functions $\boldsymbol{q}$=(q_1, q_2, q_3, etc.) and $\boldsymbol{q}'$ is a vector of its derivatives $\boldsymbol{q}'$=(q_1', q_2', etc.).

To find a solution to this equation we use the initial condition:

$$\boldsymbol{q}(0)=\boldsymbol{a}$$

where $\boldsymbol{a}$ is a vector of initial values.

There are several special types of first order ODEs for which solution techniques are known (i.e. separable, linear, homogeneous and exact equations), however, we focus on the case whereby the solutions must be approximated through numerical integration.

Numerical integration is used when other techniques are not possible or are too complicated to find a solution to the system of equations. Numerical integration refers to the use of approximating methods such as Eulers method, Improved Eulers method, Simpson's rule, Trapezoidal rule, Runge-Kutta method etc. To make things easier, these methods can be implemented through software such as MATLAB® (2009) or XPPaut (2002). In most cases we use MATLAB's 'ode45' differential equation solver to employ the Runge-Kutta method. The most common Runge-Kutta method is the fourth order (RK4) method. This produces a vector consisting of a column of '**T**' values representing time points and a column of '**Q**' values representing each 'q' solution corresponding to the time points in column **T**.

The equations used in RK4 to find an approximate solution to a first order differential equation ($q_1' = f(t, q_1)$, with $q_1(t_0) = q_{1,0}$) are the following:

$$q_{1,n+1}=q_{1,n} + h\tfrac{1}{6}(k_1 + 2k_2 + 2k_3 + k_4)$$
$$t_{n+1}=t_n + h$$

for n=0, 1, 2, 3, etc., h is the step size greater than zero and using:

$$k_1=f_{t_n,q_n}$$
$$k_2=f_{t_{(n+0.5)h},q_n+h0.5k_1}$$
$$k_3=f_{t_{(n+0.5)h},q_n+h0.5k_2}$$
$$k_4=f_{t_{(n+h)},q_n+hk_3}$$

XPPaut also has options to use different solvers, it is set to RK4 for replicating the Boroujerdi et al. (1997) model as it was mentioned in his article that this method was used.

C.3 Stability of the system

To view the steady state solutions of our equations we can often calculate the fixed points, or equilibria (long term solutions) by setting our differential equations equal to zero:

$$\mathrm{d}\boldsymbol{q}/\mathrm{d}t=0,$$

where $\boldsymbol{q}$=(q_1, q_2, etc.). Then solve for each q variable. This is not always possible so other methods must be employed to find the equilibrium (e.g. using numerical integration and running it for a long period of time). This can be done using MATLAB or XPPaut.

Once we have these equlibria we need to look into what is happening near them, to do this we find the eigenvectors and eigenvalues. First we compute the Jacobian matrix, which is a matrix of all the first order partial derivatives of our system (Edelstein-Keshet, 2005):

$$\mathbf{A}=\begin{pmatrix} \frac{\partial q_1}{\partial q_1} & \frac{\partial q_1}{\partial q_2} & . & . & . \\ \frac{\partial q_2}{\partial q_1} & \frac{\partial q_2}{\partial q_2} & . & . & . \\ . & & . & & \\ . & & . & & \\ . & & . & & \end{pmatrix}$$

If $\mathbf{A}$ is the n x n Jacobian matrix and there exists a non-zero vector $\mathbf{v}$ such that: A$\mathbf{v}$=$\lambda\mathbf{v}$, then λ is an eigenvalue of $\mathbf{A}$ and the vector $\mathbf{v}$ is an eigenvector of $\mathbf{A}$ which corresponds to λ. To find these terms, the equation is rearranged to be:

$$(\mathbf{A}\text{-}\lambda\mathbf{I})\mathbf{v}=0,$$

where $\mathbf{I}$ is the n x n identity matrix. For $\mathbf{v}$ to be non-zero the matrix ($\mathbf{A}$-$\lambda\mathbf{I}$) must not be invertible, this means the determinant must be zero. This in turn leads to finding the determinant of ($\mathbf{A}$-$\lambda\mathbf{I}$) which is the characteristic polynomial of $\mathbf{A}$. From here the roots of this polynomial are to be obtained to yield the eigenvalue, λ. The eigenvectors can be found by substituting this λ into the original equation and solving for $\mathbf{v}$, for each eigenvalue.

Near the equilibrium point, the system resembles a linearised system. We can therefore

look at the local behaviour near an equilibrium point and then put all the information together to get a better idea of the overall behaviours in the system (Blanchard, Devaney, & Hall, 2006). The behaviour of the system found from this, is only applicable to initial conditions near that equilibrium point.

Eigenvalues show us the stability of the equilibrium point, while the eigenvectors can show the direction of the flow around it, locally. If all the eigenvalues are negative it indicates that the equilibrium point is a sink and is stable (flow near it moves towards it). If one or more eigenvalues are positive, then the system is not stable and the equilibrium solution is either a saddle or a source. If the eigenvalue is complex then the system will be oscillatory. If all the eigenvalues are purely imaginary then the the equilibrium solution is called a center.

We use the eigenvalues and eigenvectors to obtain a better picture of the system's long term behaviour (often using phase portraits).

C.4 Explanation of Bifurcations

A bifurcation analysis can be performed to predict what kind of behaviour is occurring in the parameter space. This was done for the previous Boroujerdi et al. (1997) and the new *in vivo* model. A bifurcation analysis is where we look at a qualitative change in the solution of the dynamical system, as the model's parameter changes. A qualitative change in the system can include a change in stability, the number of equilibrium points or the appearance or disappearance of periodic orbits, as a parameter is altered. There are many different types of bifurcations.

One particular example of bifurcations seen in this research is a Hopf bifurcation. This appears in the new *in vivo* model for conditions which were not biologically relevant but were interesting mathematically.

When performing a bifurcation analysis it is easier to plot the parameter being changed along the x-axis and have the equilibrium solution value plotted along the y-axis. Both MATLAB and XPPaut are capable of showing a bifurcation diagram. The bifurcations produced in this thesis are all obtained using the AUTO interface from XPPaut.

An example of this happening can be seen in Figures 65-67, where the bifurcation process starts with a stable spiral equilibrium (negative complex eigenvalues), moves

through the bifurcation point (zero amplitude periodic orbits with purely imaginary eigenvalues) and then ends up with an unstable spiral equilibrium (at least one positive complex eigenvalue), surrounded by a limit cycle after which eventually oscillates at a constant amplitude (Strogratz, 1994).

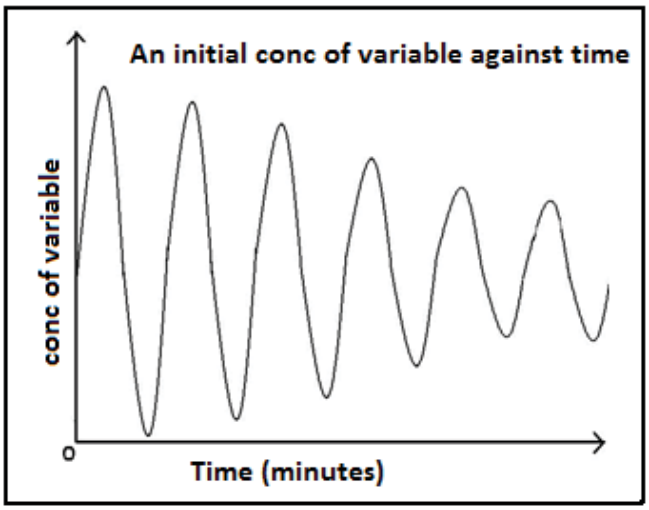

Figure 65: Example of a stable spiral equilibrium, before the Hopf bifurcation point at R_a=1 nmol min^{-1} (negative complex eigenvalue)

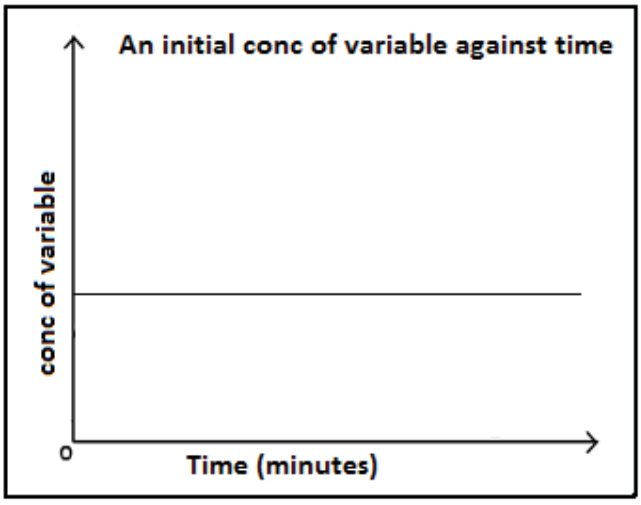

Figure 66: Example of a Hopf bifurcation at the bifurcation point with zero amplitude at R_a=5 nmol min^{-1} (purely imaginary eigenvalues)

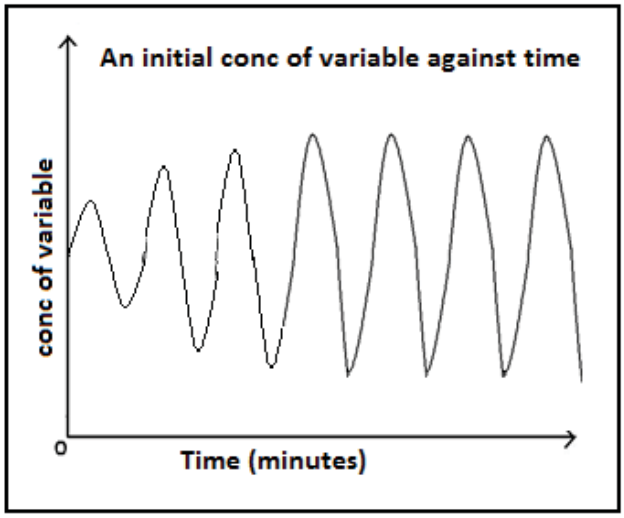

Figure 67: Example of an unstable spiral equilibrium, after Hopf bifurcation point at R_a=10 nmol min^{-1}(positive complex eigenvalue). The amplitude increases until it reaches a constant amplitude (reaches the limit cycle).

These pictures can be put together to produce a bifurcation diagram showing the Hopf occurring (see Figure 68).

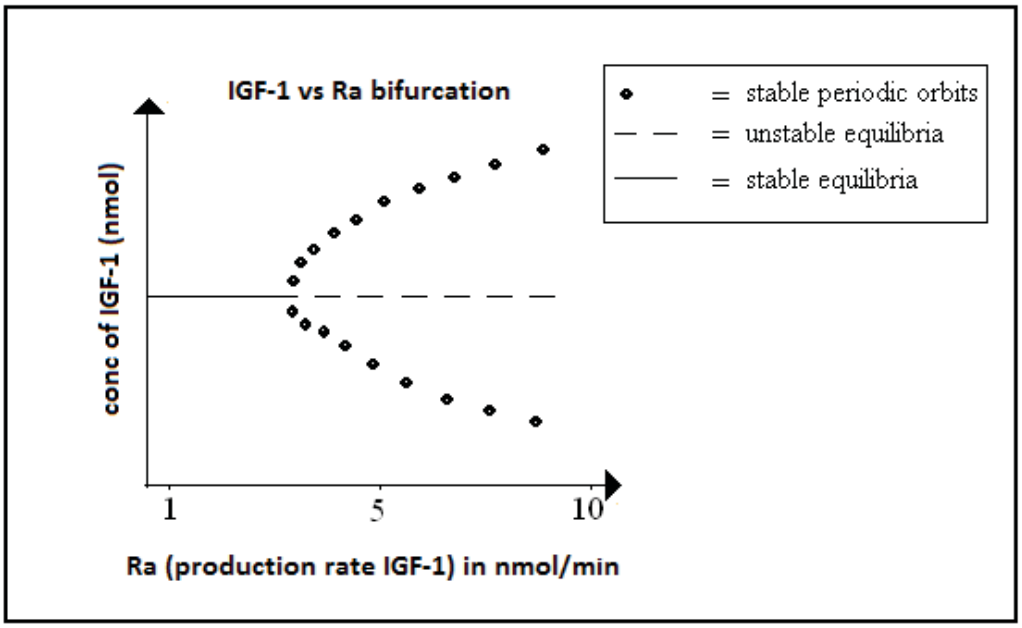

Figure 68: Example of a Hopf bifurcation diagram

There are a number of bifurcations which occur in systems, this is just one example.

C.5 Law of Mass Action and Mass Action Kinetics

The Law of Mass Action describes "the rate at which chemicals, whether large macromolecules or simple ions, collide and interact to form different chemical combinations" (p. 1 Keener & Sneyd, 2009). This law is used to simulate competitive binding reactions in mathematical models. A reaction whereby substrates A and B, combine to make substrate C and C dissociates to make A and B (reversible reaction) can be written as:

$$[\mathrm{A}]+[\mathrm{B}] \underset{k_-}{\overset{k_+}{\rightleftharpoons}} [\mathrm{C}]$$

Using the law of mass action this can be represented by the equations:

$$\begin{aligned}
\tfrac{d[A]}{dt} &= k_-[C] - k_+[A][B] \\
\tfrac{d[B]}{dt} &= k_-[C] - k_+[A][B] \\
\tfrac{d[C]}{dt} &= k_+[A][B] - k_-[C]
\end{aligned}$$

Here k_+ and k_- represent the forward and reverse rate constants respectively. This is seen in some of the *in vivo* and *in vitro* model equations.

At equilibrium there is no change to the concentration, this can be represented by the equilibrium constant, K_{eq}, which is the ratio of k_-/k_+ (Keener & Sneyd, 2009).
The law of mass action uses the assumption that when a substrate reacts with an enzyme, the reaction velocity increases linearly as the substrate concentration increases. In reality the reaction rate reaches a maximum level at high concentrations of the substrate. The Michaelis and Menten (1913) model accounts for this problem in the law of mass action. The equation they came up with demonstrates how an enzyme (E) combines with a substrate (S) to from a complex (C), then breaks down into the product (P) and the enzyme (E), (Klipp, Herwig, Kowald, Wierling, & Lehrac, 2005):

$$\begin{aligned}
\tfrac{d[S]}{dt} &= k_{-1}[C] - k_{+1}[S][E] \\
\tfrac{d[E]}{dt} &= (k_{-1} + k_{+2})[C] - k_{+1}[S][E] \\
\tfrac{d[C]}{dt} &= k_{+1}[S][E] - (k_{-1} + k_{+2})[C] \\
\tfrac{d[P]}{dt} &= k_{+2}[C]
\end{aligned}$$

If these equations are analysed using the equilibrium approximation ($k_{-1} >> k_2$), which assumes that the substrate is in instantaneous equilibrium with the complex, the re-

sulting Michaelis-Menten equation is:

$$V=\frac{V_{max}[S]}{K1+[S]},$$

where V is the reaction rate, $K1 = \frac{k_{-1}}{k_{+1}}$, [S] is substrate concentration and V_{max} is the maximum reaction velocity (when all the enzyme is complexed with the substrate).

If these equations are analysed using the quasi-steady-state approximation, an analysis proposed by Briggs and Haldane (1925) which uses the assumption that $\frac{d[C]}{dt}$ is approximately zero, the resulting equation for the reaction rate is:

$$V=\frac{V_{max}[S]}{Km+[S]}, \text{ where } Km = \frac{k_{-1}+k_{+2}}{k_{+1}}$$

Reactions do not have to be reversible, for example in the case of IGF-1 binding to receptors, once IGF-1 is bound to these receptors, the product is internalised and leaves the system.

Another behaviour which can occur in a reaction is cooperativity. This is used to describe the activity occurring when one enzyme is capable of binding to more than one substrate. Once bound to a substrate, the rate of any other binding is affected. The Hill equation was developed to represent the case of positive cooperativity:

$$V = \frac{V_{max}S^n}{K_m^n+S^n}, \text{ n}> 1.$$

This equation has a sigmoidal shape and is often used to describe the degree of cooperativity in non Michaelis-Menten kinetics. However in this research it is employed purely for its sigmoidal shape.

C.6 Nonlinear Least Squares

The first step to using nonlinear least squares is to create a model which will represent the biology accurately. There will be data to compare the model outcomes after substituting in estimated parameter values. It is often helpful to produce a graph of the equations to be able to visually compare the data. The parameters which will be fitted or kept constant must be chosen and good initial estimates for the fitting parameters need to be selected. The ability of the model to fit the data is calculated by the sum of squares error (SSE). This is the sum of squared distances between each data point and that predicted from the model. The formula for this is:

$$SSE = \sum((data - predictedvalue)^2) \tag{84}$$

The goal of non-linear least squares is to obtain parameter values that minimise the SSE. This is done using local or global optimisation methods. When using local optimisation methods it is useful to look at changing the initial parameters to see if better fits can be obtained (multi-search).

In our model we use differential equations and numerically integrate them, after substituting in our estimated parameter values. Then we compare the resulting graphs with the data plots. We minimise the SSE using the simplex method (Fminsearch in MATLAB) until convergence. Using the final sum of squares value we can then calculate the calibration R^2 value to see how much of the data variance the model explains. To do this the mean of each data set must be calculated and subtracted from each data point, squared and then summed up:

$$SStot = \sum((data - mean)^2), \tag{85}$$

$$R^2 = 1 - \frac{SSE}{SStot}, \tag{86}$$

where SSE is calculated from the nonlinear regression program (see Equation 74 above). The R^2 value is a number between -∞ and 1 and the closer this is to 1, the better the model fits the data. A value of one indicates that the estimated curve lies identically over the data. Generally a value above 0.4 is acceptable.

For the optimisation routine to converge to the global minima, we need the initial estimated parameters to be close enough to the global solution. The closer these values are to the global solution the quicker the model will converge and the more likely it is that it will reach the global solution rather than a local minimum sum of squares value. See Figure 69 below, (Motulsky & Christopoulos, 2009).

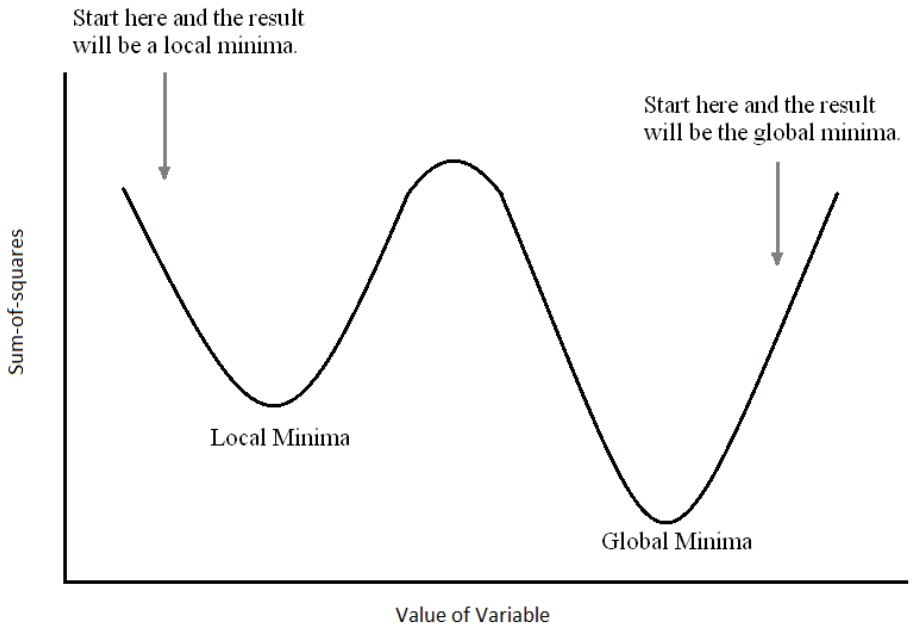

Figure 69: Example of a local minimum compared to a global Minimum

If there is uncertainty as to the range of the initial parameter values then it is best to plot a graph of the model for estimated values and change these values before re-plotting until you find the graph that fits the data best. Another way of getting a good initial estimate for the parameters is to work your way up from a simple model to a more complicated model. The simple model, perhaps one with less compartments, will be the starting value for the more complicated model.

If the model does not fit the data there are a few things that need to be taken into consideration. Firstly, depending on whether the replicated data from the experiment is independent or not will determine whether it is wise to use purely the raw data or to use averaged values from the data in the model. For the case of independent replicates

in data, each data point should be used and it is best to not average any of the values when calculating the sum of squares error. This is because all the replicated data can be influenced by random factors individually whereas there is no influence as a group. Values that come from *in vitro* experiments usually have independent replicates, we use this assumption about our data (replicate one from one experiment is not related to replicate one from another experiment). When we calculate the sum of squares error we use every individual data point and do not take an average of any of the replicates so that the standard errors are not increased or decreased.

When the replicated data points are not independent it is better to take an averaged value to use instead of every data point. In this case, the replicates as a group, can be influenced by random factors. Secondly, depending on how scattered the data is determines whether the model needs to have a weighting scheme or not. This is determined by how much scatter there is around the data sets. If the scatter is about the same throughout all the data then there is no need for a weighting scheme. For example if there are two treatments and the first has data points around the same value, while the second has values much more spread out, the program will favour fitting the spread out values and neglect the close values. This will potentially result in biased parameter estimates (heteroscedestic residuals). In this case there would be a need for a weighted least squares program. In our model the variance does not change with time or IGF-1/CGP treatment we, therefore do not use a weighted least squares scheme.

There are a multitude of localisation methods that could be used, all of which would give qualitatively the same results. The gradient based 'simplex' optimisation method was implemented through the use of a MATLAB function 'Fminsearch' in our models. Fminsearch finds a local minima of the function **f** of several variables, given the initial guess **x0**. This built in function uses the 'simplex' method and performs model fitting or least squares by minimising the sum of squares residuals. Once the code is set up it is just a matter of waiting for the iterative process to converge to a solution. Some common problems with using this are; the length of time it takes for the code to converge to a solution, getting negative parameter estimates when they are restricted to be positive only, and the SSE value fluctuating between increasing and decreasing values. If the parameters are very large it can make the program run slow. A way of avoiding this is by taking the log of each parameter value to get all parameters with less variation. Since Fminsearch is an unconstrained method it does not exclude negative

values. There are a number of ways we can restrict it to only positive numbers. If we convert all the unknown fitting parameters (excluding any initial **q** values) to be the exponential of their value we can ensure that they remain positive. ie P=exp(param), where P=old parameters and param=new parameters. This results in the exp(param) term being positive only. However, by taking the exponential of the parameters you change the distribution properties of the estimate from normal to log normal. Another way of restricting the parameter values to the positive region is by taking the absolute value of the parameter after each iteration, Param=abs(Param) in MATLAB.

Another use of nonlinear regression is to determine which equation is best to use in a model. In the case whereby you have a few choices of equations which could represent how a reaction takes place and you want to choose the equation which will fit closest to the shape of the data curve, you could use nonlinear regression. The data used in this model measured the cell absorbance levels and we looked at three equations which could fit this process. For each equation, a treatment value was substituted in and an estimated value for parameters in each of the three equations was obtained. This was done through using nonlinear regression. Once this was done for all three equations, the R^2 value was found and then the variance-covariance matrix was calculated.

C.7 Variance-Covariance Matrix

The term variance refers to the measure of variability in the data set. Or in other words, it is the sum of the deviation from the mean, squared. This can be written as:

$$\text{Var(X)}= \frac{\sum (X_i-\hat{X})^2}{N},$$

where N is the number of data values, $\hat{X}$ is the mean value and X_i is the ith data point

Covariance describes the level of correlation between two data sets. This can be positive if they vary together in the same direction or negative if they move in opposite directions. If the covariance is zero this means there is no linear dependence between the two variables (i.e. they are independent). The covariance can be written as (Pollard, 1977):

$$\text{Cov(X,Y)}=\frac{\sum (X_i-\hat{X})(Y_i-\hat{Y})}{N},$$

where N, $\hat{x}$ and x_i have the same meaning with respect to the first set of data, $\hat{Y}$ is the mean value of the second data set and Y_i is the ith data point in the second data set.

The variance-covariance matrix is a matrix consisting of variances along the diagonal and covariances on the off-diagonal elements. To find the variance-covariance matrix you first obtain your estimated parameter values ($\hat{\beta}$) from running Fminsearch to minimise the SSE for the model. Next you find the solution of the equation by substituting the estimated parameters and setting the t value to represent the concentration of IGF-1 in each of the treatments. The estimated error variance is calculated by subtracting the data values from each solution value, squaring it then dividing by the number of data points minus the number of model parameters. The formula for calculating the variance-covariance matrix, for $\hat{\beta}$, is (Fox & Weisberg, 2011):

$$\hat{V}(\hat{\beta}) = s^2(F'F)^{-1},$$

where s^2 is the estimated error variance, $\hat{\beta}$ is a vector of the estimated model parameters and F=$\text{F}_{i,j}$, which is the partial derivative of the estimating function with respect to each parameter:

$$F_{ij} = \frac{\partial f(\hat{\beta},x_i')}{\partial \hat{\beta}_j},$$

where f is the nonlinear function which is fitted to data.